RESEARCH ARTICLE

Multi-verse Optimizer with Rosenbrock and Diffusion Mechanisms for Multilevel Threshold Image Segmentation from COVID-19 Chest X-Ray Images

Yan Han[1] · Weibin Chen[1] · Ali Asghar Heidari[2] · Huiling Chen[1]

Abstract

Coronavirus Disease 2019 (COVID-19) is the most severe epidemic that is prevalent all over the world. How quickly and accurately identifying COVID-19 is of great significance to controlling the spread speed of the epidemic. Moreover, it is essential to accurately and rapidly identify COVID-19 lesions by analyzing Chest X-ray images. As we all know, image segmentation is a critical stage in image processing and analysis. To achieve better image segmentation results, this paper proposes to improve the multi-verse optimizer algorithm using the Rosenbrock method and diffusion mechanism named RDMVO. Then utilizes RDMVO to calculate the maximum Kapur's entropy for multilevel threshold image segmentation. This image segmentation scheme is called RDMVO-MIS. We ran two sets of experiments to test the performance of RDMVO and RDMVO-MIS. First, RDMVO was compared with other excellent peers on IEEE CEC2017 to test the performance of RDMVO on benchmark functions. Second, the image segmentation experiment was carried out using RDMVO-MIS, and some meta-heuristic algorithms were selected as comparisons. The test image dataset includes Berkeley images and COVID-19 Chest X-ray images. The experimental results verify that RDMVO is highly competitive in benchmark functions and image segmentation experiments compared with other meta-heuristic algorithms.

Keywords COVID-19 · Multilevel threshold image segmentation · Kapur's entropy · Multi-verse optimizer · Meta-heuristic algorithm · Bionic algorithm

1 Introduction

Coronavirus Disease 2019 (COVID-19) is currently the world's most severe epidemic, posing a global public health problem and challenge. Diagnostic COVID-19 early and accurately is essential to controlling the spread of the epidemic.

The most popular diagnostic method in biochemical is Real-Time Polymerase Chain Reaction (RT-PCR), which is currently the most popular diagnostic method against COVID-19 [1]. Although RT-PCR has a lower cost, it is time-consuming and may produce false positives [2]. In radiology, analyzing Chest CT and X-ray images of COVID-19 is also a key technology. Studies have shown that Chest CT scans are more sensitive than RT-PCR in the early detection of COVID-19 infection [3, 4]. When RT-PCR is negative, Chest CT image analysis is critical for diagnosing COVID-19. However, it is impossible to use CT on a large scale as CT is an expensive and unsafe test. The American College of Radiology (ACR) warns that the CT disinfection necessary following screening COVID-19 individuals potentially cause radiological service availability to be disrupted, and recommends that portable chest radiography be explored to minimize the likelihood of cross-infection [5]. Also, a positive X-ray test may not require CT if COVID-19 is suspected at a clinical high [6]. Therefore, Chest X-ray image testing is a feasible solution for the early diagnosis and control of COVID-19.

✉ Weibin Chen
  sun@wzu.edu.cn

✉ Huiling Chen
  chenhuiling.jlu@gmail.com

  Yan Han
  21451943006@stu.wzu.edu.cn

  Ali Asghar Heidari
  as_heidari@ut.ac.ir

1 Department of Computer Science and Artificial Intelligence, Wenzhou University, Wenzhou 325035, China

2 School of Surveying and Geospatial Engineering, College of Engineering, University of Tehran, Tehran, Iran

Artificial intelligence (AI), which is concerned with imitating human reasoning in computation, has made tremendous advances in a variety of fields [7, 8]. AI-assisted healthcare systems have lately attracted interest, with the aim of producing diagnostic technologies and clinical decision-making more instantaneous, self-sufficient, and efficient [9–11]. As we all know, image segmentation is crucial in computer image processing and analysis, and Multilevel threshold Image Segmentation (MIS) is a simple and efficient image segmentation technique [12]. Medical images are a particular class of images, their feature space is usually more complex, and more attention is paid to the accuracy and efficiency of image segmentation[13]. In recent years, many research results have been published on applying the Meta-Heuristic Algorithm (MHA) to optimize MIS on medical images [14–16]. The advantages of MHA in medical image segmentation are becoming more and more prominent. Since the outbreak of COVID-19, many scholars have conducted much research on MIS based on the MHA [13, 17–23]. These results indicate that the advantages of using MHA to optimize the segmentation of COVID-19 Chest X-ray Images (COVID-19-CXIs) are apparent. However, to achieve better segmentation results and improve the diagnostic quality of COVID-19, more research is still needed to propose better MHAs and segmentation schemes. As a result, this paper focuses on studying the MIS based on the MHA and proposes a high-performance scheme to segment COVID-19-CXIs.

Image segmentation is the process of dividing an image into different areas based on specific rules. These areas do not intersect, and each region has a universal consistency. Formally, it can be defined as follows: if $g(x, y)$ is the set of all pixels, where (x, y) denotes the spatial coordinate, then segmentation is a partitioning of the set g into a set of connected subsets $(g_1, g_2 \ldots g_n)$. These subsets satisfy the following conditions [24]:

- g_i is a connected region, $1 \leq i \leq n$.
- $\bigcup_{i=1}^{n} g_i = g$.
- $g_i \cap g_j = \varnothing, 1 \leq x \leq n, 1 \leq y \leq n, i \neq j$.
- g_i satisfies certain rules.

Image segmentation can be achieved using a variety of techniques. Pal [12] provided an overview of image segmentation methods, which include: gray-level thresholding [25–28], iterative pixel classification [29–31], surface-based segmentation [32, 33], segmentation of color images [34], edge detection [35], methods based on fuzzy set theory [36]. In addition, Pham et al. [37] divided these methods into eight categories: thresholding approaches, region growing approaches, classifiers, clustering approaches, Markov Random Field (MRF) models, artificial neural networks, deformable models, and atlas-guided approaches. Regardless of classification,

thresholding is an old, simple, and popular image segmentation technique [12]. Thresholding is classified as Bilevel threshold Image Segmentation (BIS) or MIS based on the number of thresholds. BIS is the process of dividing the image into two regions: the object and the background. When multiple thresholds are chosen, the image can be divided into several objects and backgrounds, a process known as MIS. MIS is used in the majority of real-world scenes.

There are many ways of MIS, such as histogram shape-based [38, 39], clustering-based [25, 40], similarity-based [41, 42], entropy-based [28], etc. Among these, the MIS based on entropy is widely used due to its ease of implementation and accurate results. For example, Kapur's entropy [28], fuzzy entropy [43], Tsallis entropy [44], etc. Kapur proposed Kapur's entropy image segmentation in 1985. The essence of Kapur's entropy image segmentation is to determine a set of segmentation thresholds to maximize Kapur's entropy. Determining a set of segmentation thresholds is the key to Kapur's entropy image segmentation. The traditional exhaustive method is time-consuming and ineffective [17, 18]. Determining the threshold is equivalent to solving a constrained optimization problem, precisely what the MHA is designed to solve.

The MHA is an iterative algorithm that uses the advantageous different data distribution of particle swarms. This new search method solves complex problems faster than traditional optimization analysis algorithms and is more adaptable. Therefore, many researchers were highly concerned about the MHA soon after it was first proposed. Various excellent MHAs have been continuously proposed, including Multi-Verse Optimizer (MVO) [45], Whale Optimization Algorithm (WOA)[46], Grey Wolf Optimization (GWO)[46], Harris Hawk Optimization (HHO) [47], Bat Algorithm (BA)[46], Particle Swarm Optimization (PSO) [48], Hunger Games Search (HGS) [49], Colony Predation Algorithm (CPA) [50], Slime Mould Algorithm (SMA) [51], Harris Hawks Optimization (HHO) [47], Weighted Mean of Vectors (INFO) [52], Runge Kutta Optimizer (RUN) [53], etc. They are widely used to solve optimization problems in many fields, such as image segmentation [54, 55], optimization of machine learning model [56], economic emission dispatch problem [57], medical diagnosis [58, 59], scheduling problems [60–62], plant disease recognition [63], practical engineering problems [64, 65], solar cell parameter Identification [66], feature selection [67, 68], bankruptcy prediction [69, 70], expensive optimization problems [71, 72], combination optimization problems [73], and multi-objective problem [74, 75]. There have also been numerous achievements in image segmentation.

Li et al. [76] improved the barnacle mating optimizer using a logistic model and chaotic mapping, and a multilevel color image segmentation algorithm was applied combined with Masi entropy. Li et al. [77] improved the pollination algorithm

used for Tsallis entropy image segmentation. Li et al. [78] proposed a Modified Artificial Bee Colony (MABC) optimizer and solved the MIS problem. In 2021, Li et al. [79] used an improved coyote optimization algorithm to achieve fuzzy MIS. Houssein et al. [80] improved manta ray foraging optimization for MIS. Khairuzzaman [81] applied the GWO to Otsu MIS in 2017. Further, many studies based on Kapur's entropy have also been published. Akay [82] applied PSO and Artificial Bee Colony (ABC) to Kapur's entropy MIS, respectively, and compared the performance, Bhandari et al. [83] applied the Cuckoo Search (CS) algorithm and Wind Driven Optimization (WDO) to Kapur's entropy MIS respectively in 2014, in the second year, they improved the ABC and combined using Kapur, Otsu, and Tsallis functions respectively for satellite image segmentation [84].

In 2016, Mirjalili et al. [45] proposed a new MHA called MVO. MVO, like other MHAs, suffers from slow convergence and is prone to falling into local optimum. However, it has a miracle that the structure is simple and the parameters are few. Since MVO was proposed in 2016, it has drawn the concentration of many scholars. In recent years, research results on MVO have been published continuously. In 2016, Faris et al. [85] proposed to use MVO to train the Multi-Layer Perceptron (MLP) neural network. PSO, Differential Evolution (DE), Firefly (FF), and CS were experimentally compared and then compared with two traditional gradient-based training methods (BP and LM algorithms). The experimental results showed that the MVO algorithm to retrain the MLP neural network is competitive. In 2017, Faris et al. [86] applied MVO to the machine learning algorithm in the paper. They proposed using MVO to optimize the Support Vector Machine (SVM) parameters and select the optimal features. The experimental results showed that MVO is used. The MVO algorithm can efficiently feature the number and improve the accuracy of predictions. Ewees et al. [87] proposed the Chaotic MVO (CMVO) algorithm in the paper. The CMVO algorithm combines the chaotic map based on the MVO algorithm, which effectively improves the algorithm's performance and was successfully used to solve the problem of feature selection. Mirjalili et al. [88] proposed a Multi-Objective MVO (MOMVO) for solving problems in a multi-objective search space. Fathy et al. [89] applied MVO to determine the optimal parameter selection for Proton Exchange Membrane Fuel Cells (PEMFCs) under specific operating conditions. Yilmaz et al. [90] proposed a hybrid algorithm, IMVOSA, mixing MVO, and the simulated annealing algorithm. In the paper [91], MVO was improved, called the enhanced version of MVO EMVO. EMVO was used as a task scheduler in the cloud computing environment. Experiments showed that it could effectively improve resource utilization and minimize manufacturing time. Pothiraj et al. [92] used MVO to optimize 3D IC floor planning.

It is clear that it can improve MVO and apply it to real-world problems. However, as far as the author knows, there has not been much MVO research in the direction of Kapur's entropy MIS. Considering all this, this paper improves the shortcomings of MVO and applies it to COVID-19-CXI segmentation.

This paper proposes the RDMVO algorithm to address the shortcomings of MVO. RDMVO is based on MVO and incorporates the Rosenbrock Method (RM) and the Diffusion Mechanism (DM). To test the performance of RDMVO. This paper first selected IEEE CEC2017 [93] as benchmark functions and used the Wilcoxon signed-rank test [94] and the Friedman test [95] to compare some mainstream MHAs. The experimental results show that RDMVO effectively improves the global search and local search capabilities of MVO and the convergence speed and accuracy of most test functions. The comprehensive performance is better than other MHAs involved in the experiment. Then, at different threshold levels, RDMVO was applied to Kapur's entropy MIS experiment and compared to some MHAs. Using the Peak Signal-To-Noise Ratio (PSNR) [96], Structural Similarity Index (SSIM) [97], and Feature Similarity Index (FSIM) [98], three indicators for image segmentation effect evaluation, the results show that RDMVO's performance is satisfactory. At the same time, Berkeley images (BKIs) and the COVID-19-CXIs were selected for the test images. The BKIs are widely used in image processing. It is used to test the comprehensive performance of RDMVO in MIS. COVID-19-CXIs are some of the Chest X-rays of patients with confirmed COVID-19. It is also the problem to be solved in this paper. The MIS experimental effects are all satisfactory. In addition, to clarify the generality of the algorithm, we use the Friedman test, and the test results also show that RDMVO is statistically significant. The main contributions of this paper are as follows:

- An improved MVO algorithm is proposed, called RDMVO, which significantly enhances the convergence speed, accuracy, and ability to jump out of the local optimum of MVO.
- The performance comparison experiment of RDMVO and some mainstream MHAs were conducted on IEEE CEC2017. The experimental data reveal that RDMVO's performance is better than the other MHA's.
- A novel MIS scheme (RDMVO-MIS) is proposed. Kapur's entropy is used as the objective function, RDMVO determines the threshold, and the image segmentation experiment was successfully carried out on BKIs and COVID-19-CXIs.
- MIS comparison experiments with some MHAs were carried out. The effect and generality of Kapur's entropy MIS based on RDMVO are the best.

The remaining work is scheduled as follows in this paper: in Sect. 2, the work is related to image segmentation and improved Kapur's entropy image segmentation method. In Sect. 3, the original MVO algorithm is presented. In Sect. 4, this paper mainly describes the proposed RDMVO algorithm. In Sect. 5, comparative experiments on benchmark functions and image segmentation experimentations are run to verify RDMVO's and RDMVO-MIS's performance. Section 6 gives a discussion. Finally, in Sect. 7, conclusions and the direction of future work are summarized.

2 Multilevel Threshold Image Segmentation

Thresholding is the most commonly used image segmentation method. In essence, thresholding is to select an attribute to divide the gray value of an image into two or more sets. Thresholding is commonly performed based on the histogram generated by the image's gray level. The image is not disturbed by noise in an ideal situation, the histogram of the segmented image has two or more peaks, the threshold is set at the trough, and the image can be divided into multiple objects and backgrounds as needed. In a real picture, however, the image will be disturbed by various noises, and the gray value of the image is not the correct data. The histogram is disturbed by noise, there is no peak on the histogram, or there may be multiple peaks. Image segmentation results with thresholds on the troughs will be poor or incorrect. In this case, many threshold determination methods have been proposed [99–101]. To evaluate the threshold selection results, Pun [102] proposed the concept of entropy in 1980 and determined the optimal threshold by calculating the threshold corresponding to the maximum entropy. Kapur then proposed an improved threshold segmentation method based on maximum entropy based on Pun in 1985, which is simple to calculate and has a good segmentation effect.

The traditional calculation of Kapur's entropy is based on the image's one-dimensional gray value, which has poor anti-noise interference ability. Buades et al. [103] proposed non-local means 2D histogram in 2005. This technology can effectively reduce noise interference and has a good segmentation effect when the image is polluted by noise. Kapur's entropy MIS used in this paper is based on non-local means 2D histogram. The specific process is to obtain the grayscale image corresponding to the original image and then perform non-local mean noise reduction processing on the grayscale image. The obtained image is called the NLM image. Then non-local means 2D histogram is obtained according to the grayscale and NLM images. Perform the maximum Kapur's entropy calculation based on the 2D histogram, then obtain a set of thresholds corresponding to the maximum Kapur's entropy, and finally perform image segmentation according to the thresholds.

Figure 1 shows an image segmentation example in this paper. The specific related content is introduced in the following. In addition, three mainstream image segmentation evaluation methods used in this paper will also be introduced one by one.

2.1 Kapur's Entropy

Kapur's entropy MIS is based on the gray value of the image. We define the gray value of the image to be stored in 8 bits, and the gray value ranges from 0 to 255. Let L=256, n_i represents the number of pixels whose gray value is i, then the Kapur's entropy H is defined according to the following formula:

$$N = \sum_{i=0}^{L-1} n_i \tag{1}$$

$$p_i = \frac{n_i}{N} \tag{2}$$

$$H = - \sum_{i=0}^{L-1} p_i ln p_i \tag{3}$$

where p_i is the probability of occurrence of gray value i, H is Kapur's entropy. For BIS, images are divided into two subclasses, C_0 and C_1. $C_0 = \{1, 2, 3 \ldots t_1 - 1\}$, $C_1 = \{t_1, \ldots L - 1\}$, the Kapur's entropy H_C is described according to the following formula:

$$H_C = H_{C_0} + H_{c_1} \tag{4}$$

$$H_{C_0} = - \sum_{j=0}^{t_1-1} \frac{p_j}{\omega_0} ln \frac{p_j}{\omega_0} \tag{5}$$

$$\omega_0 = \sum_{n=0}^{t_1-1} p_n \tag{6}$$

$$H_{C_1} = - \sum_{j=t_1}^{L-1} \frac{p_j}{\omega_1} ln \frac{p_j}{\omega_1} \tag{7}$$

$$\omega_1 = \sum_{n=t_1}^{L-1} p_n \tag{8}$$

$$t^\star = argMax(H_c) \tag{9}$$

where $t^\star$ is the split point set when H_c takes the maximum value, it is also the determined threshold. Similar to BIS, for MIS, suppose the image gray value is divided into m subsets, $C_0 = \{1, 2, 3 \ldots t_1 - 1\}$, $C_1 = \{t_1, \ldots t_2 - 1\}$,

Fig. 1 Image segmentation
example in this paper

Input image

Grayscale image

No-local mean filter

NLM image

2D-histogram

Optimal threshold

Segmented grayscale image

Segmented jet colormap
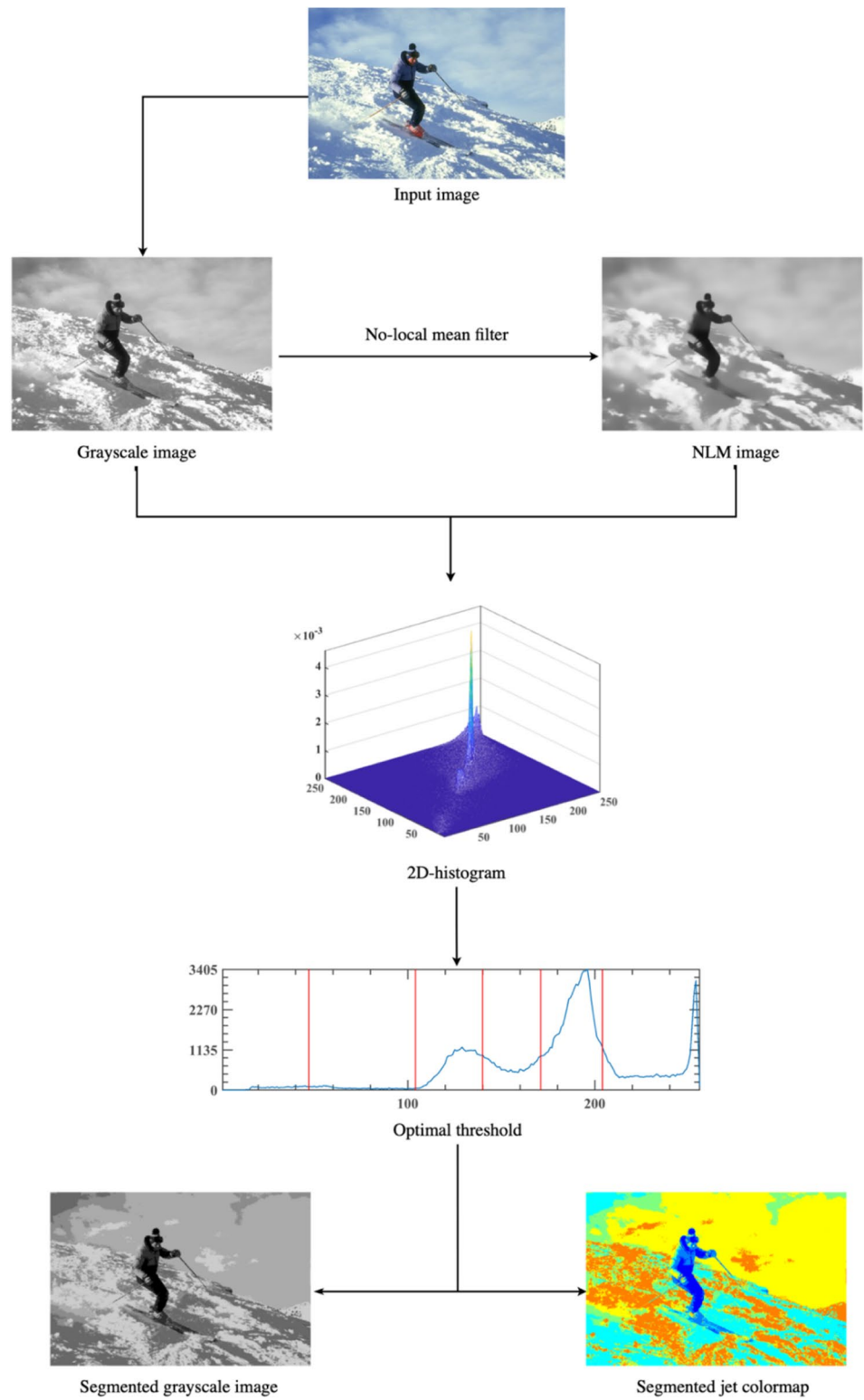
$C_2 = \{t_2, \ldots t_3 - 1\}, \ldots, C_{m-1} = \{t_{m-1}, \ldots L - 1\}$, the Kapur's entropy is described according to the following formula:

$$H_C = \sum_{i=0}^{m-1} H_{C_i} \tag{10}$$

$$H_{C_i} = - \sum_{j=t_i}^{t_{i+1}-1} \frac{p_j}{\omega_i} ln \frac{p_j}{\omega_i} \tag{11}$$

$$\omega_i = \sum_{n=t_i}^{t_{i+1}-1} p_j \tag{12}$$

$$t^\star = argMax(H_c) \tag{13}$$

2.2 Non-local Means 2D Histogram

Buades et al. [103] proposed non-local means 2D histogram in 2005; this innovative technology uses redundant information for denoising and maintaining the maximum detailed features of the image. Assuming that the original image is O, the non-local mean denoised image is N, and the gray value of the pixels p in the image O is denoted as $O(p)$, then after non-local mean filtering, the gray value $N(p)$ of pixels p can be obtained by the following formula:

$$N(p) = \frac{\sum_{q \epsilon O} O(q) \omega(p,q)}{\sum_{q \epsilon O} \omega(p,q)} \tag{14}$$

$$\omega(q,p) = exp^{-\frac{|\mu(p)-\mu(q)|^2}{\partial^2}} \tag{15}$$

$$\mu(p) = \frac{\sum_{i \epsilon O(p)} O(i)}{m \times m} \tag{16}$$

$$\mu(q) = \frac{\sum_{i \epsilon O(q)} O(i)}{m \times m} \tag{17}$$

where $\omega(q,p)$ is the weight of pixel p and q, and $L(p)$ and $L(q)$ are local images and centered on pixel p and q, respectively, and the size is $m \times m$. $\mu(p)$ and $\mu(q)$ are the local mean of pixel p and q, respectively, and the mean of $L(p)$ and $L(q)$. ∂ is the standard deviation.

So far, there are corresponding grayscale image O and image N filtered by non-local mean. Combining them, the abscissa is the gray value corresponding to the pixel of the original image O, and the ordinate is the gray value corresponding to the image N filtered by the non-local mean. Then we can get a 2D view of the 2D histogram, shown in Fig. 2. The non-local means 2D histogram according to the following formula:

$$P_{ij} = \frac{h_{ij}}{m \times n} \tag{18}$$
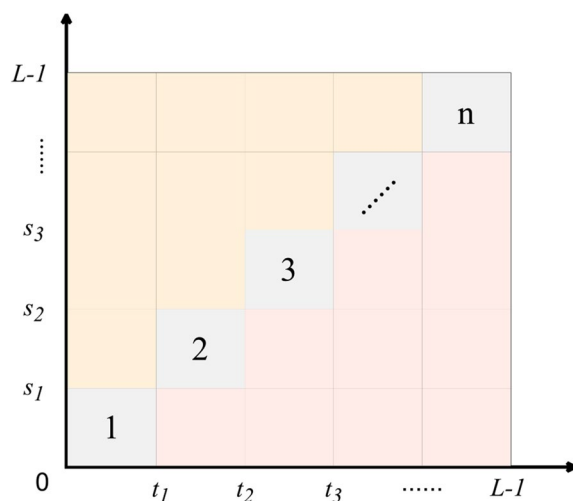
Fig. 2 2D view of the 2D histogram

where i refers to the value of image $O(x, y)$ pixels, j refers to the value of image $N(x, y)$ pixels, and $h(i, j)$ denotes the number of times the point (i, j) appears on the gray value vector (s, t), the total number of pixels in this image is $m \times n$.

2.3 Kapur's Entropy-based 2D Histogram

A 2D view histogram based on the above 2D histogram is given in Fig. 2. The main diagonal of the 2D histogram contains adequate image information. This paper calculates Kapur's entropy as the objective function and Kapur's entropy of the subregions on the main diagonal using Eq. (19). The optimal solution found by in $\{t, t_2 \ldots t_n - 1\}$ is the optimal threshold.

$$H(s,t) = - \sum_{i=0}^{s_1} \sum_{j=0}^{t_1} \frac{P_{ij}}{P_1} ln \frac{P_{ij}}{P_1} - \sum_{i=s_1+1}^{s_2} \sum_{j=t_1+1}^{t_2} \frac{P_{ij}}{P_2} ln \frac{P_{ij}}{P_2} \cdots$$
$$- \sum_{i=s_{L-2}+1}^{s_{L-1}} \sum_{j=t_{L-2}+1}^{t_{L-1}} \frac{P_{ij}}{P_{L-1}} ln \frac{P_{ij}}{P_{L-1}} \tag{19}$$

And $P_1 = \sum_{i=0}^{s_1} \sum_{j=0}^{t_1} P_{ij}$, $P_2 = \sum_{i=s_1+1}^{s_2} \sum_{j=t_1+1}^{t_2} P_{ij}$, $P_{L-1} = \sum_{i=s_{L-2}+1}^{s_{L-1}} \sum_{j=t_{L-2}+1}^{t_{L-1}} P_{ij}$.

2.4 Image Segmentation Evaluation

We all know how important it is to conduct practical evaluations of image segmentation experiments. The evaluation of mathematical computations is a crucial juncture that requires benchmarking, sufficient data, and appropriate metrics for a credible evaluation [104–106]. Many methods for evaluating segmentation results have been proposed, each with advantages and disadvantages. The three most commonly used evaluation methods are PSNR [96], SSIM [97], and FSIM

[98]. As a result, they will be used to analyze the experimental results in this paper.

- PSNR. PSNR is a full-reference image quality evaluation index, and it is the most commonly used image quality assessment metric. PSNR relies on MSE to measure the degree of distortion of the image. The calculation of PSNR is expressed as follows [96]:

$$PSNR(f, G) = 10 \times log_{10} \frac{L}{MSE(f,G)} \tag{20}$$

$$MSE(f, G) = \frac{\sum_{i=0}^{M-1} \sum_{j=0}^{N-1} [f(i,j) - G(i,j)]^2}{M \times N} \tag{21}$$

M and N are the numbers of rows and columns of the image, respectively, f represents the original image, and G represents the segmented image. $f(i,j)$ represents the pixel gray-scale value of the original image, and $G(i,j)$ is the pixel gray-scale value of the segmented image. L is the scale range of the image. For an 8-bit image, $L = 2^8 - 1 = 255$.

- SSIM. SSIM is a full-reference image quality evaluation index. Furthermore, it is a widely used image quality evaluation metric based on the assumption that the human eye extracts structured information from an image when viewing it. It calculates the brightness, contrast, and structure comparison functions of the image, respectively, then makes a comprehensive evaluation. Its calculation process is as follows [97]:

$$SSIM(x, y) = \frac{(2\mu_x \mu_y + C_1)(2\sigma_{xy} + c_2)}{\left(\mu_x^2 + \mu_y^2 + C_1\right)\left(\sigma_x^2 + \sigma_y^2 + C_2\right)} \tag{22}$$

where x represents the image block of the original image, y represents the image block of the segmented image. μ_x and μ_y are the means of the image block x and the image block y, respectively, and it reflect the brightness information of the image. σ_x and σ_y are the standard deviations of the image block x and the image block y, respectively, and it reflects the contrast information of the image. σ_{xy} is the correlation coefficient between the image block x and the image block y. And it reflects the structural similarity information of the image.

- FSIM. FSIM is a relatively new full reference image quality evaluation index. It is based on two major features, Phase Consistency (PC) and Gradient Magnitude (GM). The calculation of FSIM is expressed as follows [98]:

$$FSIM = \frac{\sum_{I \in \Omega} S_L(X) PC_m(X)}{\sum_{I \in \Omega} PC_m(X)} \tag{23}$$

$$S_L(X) = S_{PC}(X)^\alpha S_G(X)^\beta \tag{24}$$

$$PC_m(X) = \frac{E(X)}{(\epsilon + \sum_m A_n(X))} \tag{25}$$

$$S_{PC}(X) = \frac{2PC_1(X)PC_2(X) + T_1}{PC_1^2(X)PC_2^2(X) + T_1} \tag{26}$$

$$S_G(X) = \frac{2G_1(X)G_2(X) + T_2}{G_1^2(X)G_2^2(X) + T_2} \tag{27}$$

$$G = \sqrt{G_X^2 + G_Y^2} \tag{28}$$

FSIM is coupled by PC term and GM term, S_L refers to the similarity score, α and β take 1 by convention. $PC_m(X)$ is $Max(PC_1(X), PC_2(X))$, ϵ is a very small positive number, preventing a denominator of 0. T_1 and T_2 are a constant, $E(X)$ indicates the local energy, $A_n(X)$ is the amplitude value.

3 Overview of Original MVO

MVO's mathematical model and algorithm are based on the multi-verse theory of cosmology's three concepts of white holes, black holes, and wormholes. According to cosmological theory, white and black holes are two amazing celestial bodies, and their properties are diametrically opposed. White holes only eject matter and energy to the outside and are considered the main part of the universe. Black holes only absorb matter and energy in the universe. Wormholes are tunnels that connect parallel universes, bridging the gap between white and black holes, and allowing objects to move instantly between universes and time-spaces.

In the MVO algorithm, the concepts of white holes and black holes are modeled to represent the exploration process in the search space, and the wormhole model simulates the exploitation process. MVO proposes the concept of the expansion rate and believes that the universe is constantly changing, and objects in the multi-verse are constantly evolving to the most stable universe according to the expansion rate, white holes, black holes, and wormholes. The MVO algorithm specifies the following rules [45]:

- The greater the expansion rate, the greater the possibility of a white hole, and the lower the possibility of a black hole.
- A universe with a higher expansion rate sent matter through a white hole.
- Universes with lower expansion rates receive more matter through black holes.
- Regardless of the expansion rate, all objects in the universe can move randomly through wormholes toward the optimal universe.

Therefore, MVO starts by generating random universes. In each iteration, objects use white/black holes to move from universes with high expansion rates to other universes with low expansion rates. Furthermore, objects in any universe are randomly teleported to the best universe through a wormhole. Repeating these processes until the final criteria are met.

Based on the above theory, MVO first randomly generates a multi-verse:

$$X = \begin{bmatrix} X_1^1 & X_1^2 & \cdots & X_1^d \\ X_2^1 & X_2^2 & \cdots & X_2^d \\ \vdots & \vdots & \vdots & \vdots \\ X_n^1 & X_n^2 & \cdots & X_n^d \end{bmatrix} \tag{29}$$

where n represents the number of universes, each universe represents a candidate solution, d represents the amount of matter in each universe, and the matter in the universe represents the parameters in the solution. The update of the universe is based on the following formula:

$$X_i^j = \begin{cases} X_k^j, & r_1 < NI(X_i) \\ X_i^j, & r_1 \geq NI(X_i) \end{cases} \tag{30}$$

Among them, X_i is the ith universe, $NI(X_i)$ is the normalized expansion rate of the ith universe, X_i^j refers to the jth matter in the ith universe, and X_k^j is the jth substance of the kth universe, k is generated by the roulette selection mechanism, and r_1 is a random number of [0, 1]. As can be seen from these equations, the selection and determination of white holes are made by roulette, which is based on the normalized expansion rate. The lower the expansion rate, the more likely it is that an object will pass through the tunnel of a white hole. Beyond that, there could be wormholes in the universe that randomly alters objects in the universe, regardless of their expansion rate. The mechanism is expressed as follows:

$$X_i^j = \begin{cases} \begin{cases} X_{best}^j + TDR \times \left((ub - lb) \times r_4 + lb\right), & r_3 < 0.5 \\ X_{best}^j - TDR \times \left((ub - lb) \times r_4 + lb\right), & r_3 \geq 0.5 \end{cases} & r_2 < WEP \\ X_i^j, & r_2 \geq WEP \end{cases} \tag{31}$$

Among them, X_i^j refers to the jth substance in the ith universe, X_k^j is the jth substance in the kth universe, X_{best}^j is the jth substance in the current best universe, ub, lb is the upper and lower bounds of the variable, r_2, r_3, r_4 are random numbers of [0, 1], TDR is the travel distance rate, which defines that an object can be teleported by a wormhole to the currently obtained best universe around the distance rate, which increases in iterations. Moreover, WEP is the wormhole existence rate, which defines the probability that wormholes exist in the universe and increases linearly in iterations. The adaptive formulas of TDR and WEP are as follows:

$$WEP = min + l \times \left(\frac{max - min}{L} \right) \tag{32}$$

$$TDR = 1 - \left(\frac{l^{1/p}}{L^{1/p}} \right) \tag{33}$$

where min is the minimum value, max is the maximum value, l represents the current iteration number, and L represents the maximum iteration number. Where p defines the development precision in iterations. The higher p is, the faster and more accurate the local search is. Algorithm 1 shows the pseudo-code of MVO.

Algorithm 1 Pseudo-code of MVO

Initialize the population $X_i(i = 1,2,...,n)$, the maximum number of iterations T, the problem dimension dim, and other related parameters.
While $(t \leq T)$
  For $i = 1:n$
    Evaluate the inflation rates.
    Find the best Universe X_{best}.
  End For
  Update WEP by Eq. (32)
  Update TDR by Eq. (33)
  Normalized inflation rates $NI(X_i)$
  For $i = 1:n$
    For $j = 1:dim$
      Generate r_2, r_3, r_4.
      If r1 < NI (X_i)
      Then
        Roulette wheel selection generate white hole
        Update X_i^j by Eq. (30)
      End If
      If r_2 < WEP
      Then
        Update X_i^j by Eq. (31)
      End If
    End For
  End For
  $t = t + 1$;
End While
Return **the solution of the question**
End

---

4 Proposed RDMVO

4.1 Rosenbrock Method (RM)

RM is a local search method proposed by Rosenbrock [107] in 1960. It can adapt to the search direction and size and conduct multiple searches until a relatively optimal solution is found in a specific limited area. Regarding the determination of the search size, RM will first determine a random number ε as the search size and then determine whether a better solution is obtained under the search size through calculation and comparison. If a better solution is obtained, the next search size is $\varepsilon \times \alpha$ and$\alpha > 1$, otherwise the next search size is $\varepsilon \times \beta$ and $0 < \beta < 1$. Regarding the determination of the search direction, RM refers to the orthonormal basis of the n-dimensional space rather than experimenting in a single direction.

The basic RM is effective for unimodal functions, and it is not easy to jump out of the local optimum for multimodal functions. The basic RM was modified in 2011 by Kang et al. [108] to solve this problem. Li et al. [109] applied RM modified to the HHO in 2021 and proved the mechanism's performance. The modified RM is used to enhance MVO's performance in this paper. Algorithm 2 shows the pseudo-code of modified RM.

Algorithm 2 The pseudo-code of modified RM

Initialize the initial orthonormal basis $d_i (i = 1,2,...,n)$, the step size adjustment factors α and β, and the termination parameter $\varepsilon_1, \varepsilon_2, N, k_1, k_2$.
Initialize the step size $\delta_i (i = 1,2,...,n)$ using Eq, and let $x_k = x_0$.
Repeat
  $x = x_k; k_1 = 0; z = x$
  Repeat
    For ($i = 1,2,...,n$)
      $y = x + d_i \delta_i$
      If (y is better than x)
        $x = y$
        $\delta_i = \alpha \delta_i (\alpha > 1)$
      Else
        $\delta_i = \beta \delta_i (-1 < \beta < 0)$
      End If
    End For
    If ($[abs(f(z) - f(x))/(abs(f(x)) + \varepsilon_1)] < \varepsilon_2$)
      $k_2 = k_2 + 1$
    Else
      $k_2 = 0$
    End If
    $k_1 = k_1 + 1$
  Until ($k_1 \geqslant N$)
  If ($f(x) < f(x_k)$)
    $x_k = x$
    Update the orthonormal basis d_i
  End If
Until (($\delta_{min} < \varepsilon_1) or (k_2 \geqslant 2N)$)

Eq refers to $\delta_i = \sqrt[2]{\frac{\sum_{k=1}^{n}(x_{ki} - avgx_i)}{n}} + \varepsilon_1, i = 1, 2 \dots d$. and $avgx_i = \frac{\sum_{k=1}^{n} x_{ki}}{n}$. Where n is the number of prospect particles, $avgx_i$ refers to the average of the prospect particles in the *ith* dimension, x_{ki} refers to the value of the *kth* prospect particles in the *ith* dimension. $\varepsilon_1 = 1.0e^{-150}$ is a very small variable for preventing the initial value from being 0.

4.2 Diffusion Mechanism (DM)

The DM is mentioned in Literature [110, 111], which effectively alleviates the optimum local problem and dramatically improves the possibility of finding the global optimum. The diffusion process refers to the random diffusion of new particles around the original agent at different locations. There are two main methods for generating new particles: Levy flight and Gaussian distribution [111]. They are applied based on Eqs. (4.1) and (4.2), respectively.

$$x_i^q = x_i + \alpha_i^q \otimes Levy(\lambda) \qquad (34)$$

$$x_i^q = x_i + \beta \times Gaussian(P_i, |BP|) - (\gamma \times BP - \gamma_1 \times P_i) \qquad (35)$$

In Eq. (34), x_i refers to the original agent, and q refers to the number of new particles obtained after diffusion. α is a variable used to control the convergence speed. The symbol $\otimes$ refers to the Hadamard multiplications. In Eq. (35), likewise, x_i refers to the original agent, and q refers to the number of new particles obtained after diffusion. β is equal to $(log(t))/t$, and t is the number of iterations. γ and γ_1 are random numbers between [0, 1], and BP is the best position of new particles so far. $Gaussian(P_i, |BP|)$ is the Gaussian distribution, and the mean and standard deviation are P_i and $|BP|$, respectively.

In this paper, reference paper [112], We use the mathematical model of the DM as follows:

$$X_i = Gaussian(Bestposition, \varepsilon, m) + \sigma \times (Bestposition - X_i) \qquad (36)$$

where $Gaussian(Bestposition, \varepsilon, m)$ means to generate a random matrix that obeys Gaussian distribution. $Bestposition$ and ε represent the mean and standard deviation, respectively, and m is a vector that determines the form of the generated matrix. $Bestposition$ denotes the position of the global optimal solution. σ is a random number between [0, 1]. The calculation of ε is expressed as follows:

$$\varepsilon = \frac{log(t)}{t} \times |X_i - Bestposition| \qquad (37)$$

The RDMVO algorithm introduces the RM and the DM into the standard MVO algorithm, enhancing the global search ability and local exploration ability of the MVO algorithm and effectively improving the convergence speed and accuracy. Algorithm 3 shows the pseudo-code of RDMVO. The flowchart of RDMVO is shown in Fig. 3.

Algorithm 3 Pseudo-code of RDMVO

Initialize the population $X_i (i = 1,2,...,n)$, the maximum number of iterations T, the problem dimension dim, and other related parameters.
While ($t \leq T$)
  For $i = 1:n$
    Evaluate the inflation rates.
    Find the best Universe X_{best}.
  End For
  Update WEP by Eq. (32)
  Update TDR by Eq. (33)
  Normalized inflation rates $NI(X_i)$
  For $i = 1:n$
    For $j = 1:dim$
      Generate r_1, r_2, r_3.
      If $r1 < NI(X_i)$
      Then
        Roulette wheel selection generate white hole
        Update X_i^j by Eq. (30)
      End If
      If $r_2 < WEP$
      Then
        Update X_i^j by Eq. (31)
      End If
    End For
    Carry out the Rosenbrock method
  End For
  Carry out the diffusion mechanism
  $t = t + 1;$
End While
Return *the solution of the question*
End

Fig. 3 Flowchart of RDMVO
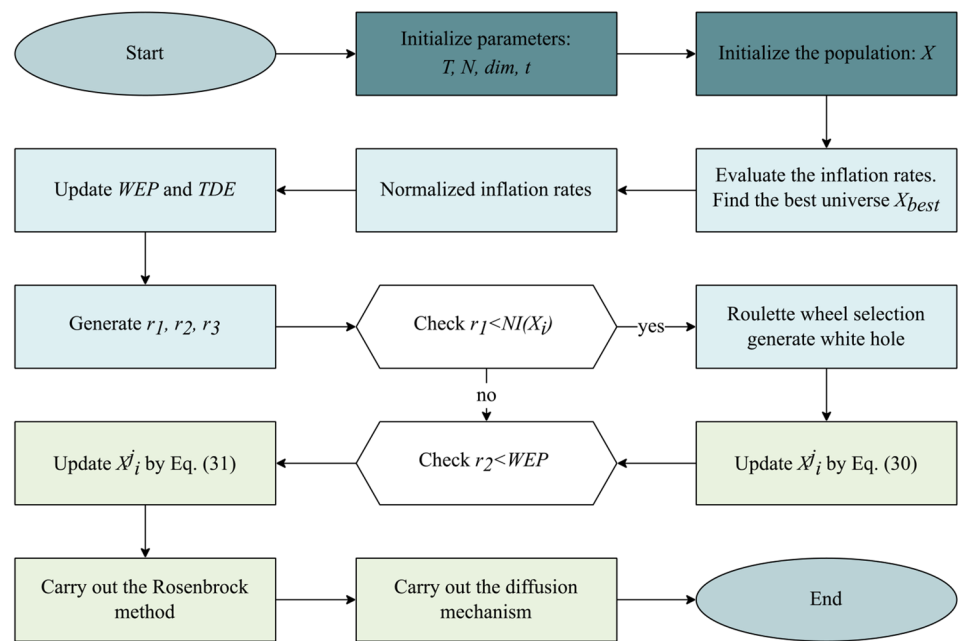
4.3 Algorithm Complexity Analysis

Figure 3 shows the main process of RDMVO. The time complexity of RDMVO is mainly determined by the initialization, the RM, the DM, and the iterative updates of MVO. In addition, the parameters also affect the algorithm complexity. These parameters are mainly: the algorithm's maximum number of iterations (T), the dimension (d) and the population size (N). Therefore, the main time complexity of RDMVO is $O(RDMVO) = O(initialization) + O(fitness\ evaluation) + O(MVO\ iterative\ updates) + O(RM) + O(DM) \approx O(n \times d) + O(T \times n) + O(n \times d) + O(n \times d) + O(n)$.

5 Experimental Results and Analysis

A series of experiments were pushed to verify RDMVO's performance. To begin, we choose the IEEE CEC2017 as benchmark functions. On IEEE CEC2017, we selected some contemporary mainstream MHAs to conduct an algorithm comparison experiment. The experimental data show that RDMVO has apparent convergence speed and accuracy advantages. Also, we conducted parametric experiments on IEEE CEC2017 to choose a better p. Furthermore, we applied RDMVO in conjunction with Kapur's entropy to segment BKIs and COVID-19-CXIs, compared the performance with some mainstream MHAs, and selected PSNR, SSIM, and FSIM as evaluation indicators. The experimental results are also positive. The following section will briefly introduce these experimental procedures and results. In addition, this paper uses MATLAB coding. All experiments were performed on the same computer. Computer parameters and coding software versions are given in Table 14.

5.1 Experiment on IEEE CEC2017 Benchmark Functions

The IEEE CEC2017 benchmark functions and related parameter settings are first introduced in this section. The parameter set includes two parts, the first part is the setting of public parameters, and the second part is the parameters of the algorithm participating in the experiment. Common parameters mean that to ensure the experiment's fairness, as per other computational science works [113], and the differences in the algorithm itself, other parameters must be unified during the experiment. The settings of public parameters are shown in Table 1. Where N is the number of particles in the population, D is the dimension of the problem, *MaxFEs* is the Maximum number of evaluations, F is the number of independent runs of the experiment, and we set F to 30 to reduce the influence of randomness on the experimental results. In addition, the relevant parameter settings of the MHA involved in this experiment are given in Table 16.

Then, we analyzed the experimental results from multiple perspectives. The first is the mean and standard deviation. To reduce the experimental error, we ran the experiment 30 times independently and recorded the minimum value of the test function obtained by each relevant algorithm. Thus, we

Table 1 Unified parameter settings

N	D	*MaxFEs*	F
30	30	300,000	30

would get 30 on each test function result for each algorithm. We computed the mean and standard deviation of these values and recorded Avg and Std, respectively. Furthermore, use Avg and Std to evaluate the algorithm's performance. We expect them to be as small as possible, and the minimum value is shown in bold in the relevant tables. In addition, to verify whether the experimental results are statistically significant, we applied nonparametric statistical tests with a significance level of 0.05, Wilcoxon signed-rank test, and Friedman test to the experimental results.

The symbol "±/=" in the related table is the result summary of the Wilcoxon signed-rank test, and ARV represents the mean value of the Friedman test results of the overall test function of the algorithm.

5.1.1 Benchmark Functions

IEEE CEC2017 [93] is the relatively new test function set used to test the performance of the MHA, which can better measure the superiority of algorithm improvement strategies. The test function of IEEE CEC2017 is shown in Table 15. F1 to F3 are unimodal functions, F4 to F10 are simple multimodal functions, F11 to F20 are hybrid functions, and F21 to F30 are composition functions.

5.1.2 Influence of Two Mechanisms

In Sect. 4, we propose using DM and RM to enhance the performance of the MVO algorithm. Experiments must be carried out to determine whether these two mechanisms are effective. We added a single mechanism to MVO, named RDMVO1, RDMVO2, in addition to the original algorithm MVO and the new algorithm RDMVO, for a total of four algorithms. Table 2 contains a detailed description of each algorithm. The letter Y means that the mechanism is included, while the letter N means no such mechanism exists. For the convenience of description, RDMVO1, RDMVO2, and MVO are called variants of RDMVO. We used IEEE CEC2017 to experiment with these four algorithms, and the experimental results are shown in Tables 17, 18, and Fig. 4.

The ARV indicator after the Friedman test in Table 17 (The best results are bolded) shows that the RDMVO has the best overall ranking across all test functions; RDMVO outperformed the other variants. The "±/=" indicators also show that RDMVO outperforms its variants on most test functions, especially the original MVO, which outperforms its original

MVO in 27 out of 30 test functions. In general, the experimental results demonstrate that the combination of RM and DM improves the performance of MVO the most.

Table 18 shows the *P* values of the experimental results via the Wilcoxon signed-rank test with 5% significance, and *P* values ⩾ 0.05 are shown in boldface. As can be seen from the *P* values in Table 18, RDMVO and RDMVO2 are statistically different in each test function, RDMVO and MVO are statistically different in each test function except for F9 and F17.

Figure 4 is the convergence curve of RDMVO and its variants on some test functions. As shown in Fig. 4, the convergence speed and accuracy of the variant RDMVO2 are worse than those of the original algorithm MVO. RDMVO2 only adds DM to the MVO, which means that only adding DM has not affected the improvement of MVO or had a negative effect. When comparing the variants RDMVO1 and MVO, the convergence accuracy of RDMVO1 is significantly improved, as is the convergence speed. That is, RM speeds up the overall global search speed of MVO and effectively enhances the ability of MVO to jump out of the local optimum. Finally, we compared RDMVO and RDMVO1, and the convergence rate of RDMVO1 was further enhanced under the action of DM. From the above analysis, it can be concluded that the combined action of the RM and DM have the most powerful effect on MVO: effectively enhancing MVO's global search ability and local exploration ability, improving the problem that MVO is easy to fall into local optimum, and improving the search accuracy of MVO.

5.1.3 Parameter Test

In Sect. 3, the MVO algorithm is introduced in detail. The *TDR* in Eq. (31) directly affects the algorithm's development efficiency and accuracy. *p* in Eq. (33) is the only parameter that affects *TDR*. In RDMVO, it is necessary to determine an appropriate *p*. So, this section selected multiple *p* to conduct experiments on IEEE CEC2017. For the convenience of description, the algorithm name in this section is RDMVO- *p* {*x*}, representing that the *p* in RDMVO is set to *x*. Table 3 shows the Friedman test rankings when *p* is 4, 5, 6, and 7, respectively. From Table 3, it can be seen that the performance of RDMVO is relatively best when *p* is 6 if we set *p* to any of 4, 5, 6, and 7. Accordingly, we have set the *p* at 6 in the subsequent experiments in this paper.

5.1.4 Comparison with Other Algorithms

In this part, RDMVO was mainly compared with DE [46], WOA, GWO, HHO [47], BA [46], PSO [46], and MVO [45], seven mainstream MHAs on IEEE CEC 2017. All the algorithms involved were compared under the same conditions,

Table 2 Results of the combination of mechanisms

mechanism	RDMVO	RDMVO1	RDMVO2	MVO
RM	Y	Y	N	N
DF	Y	N	Y	N
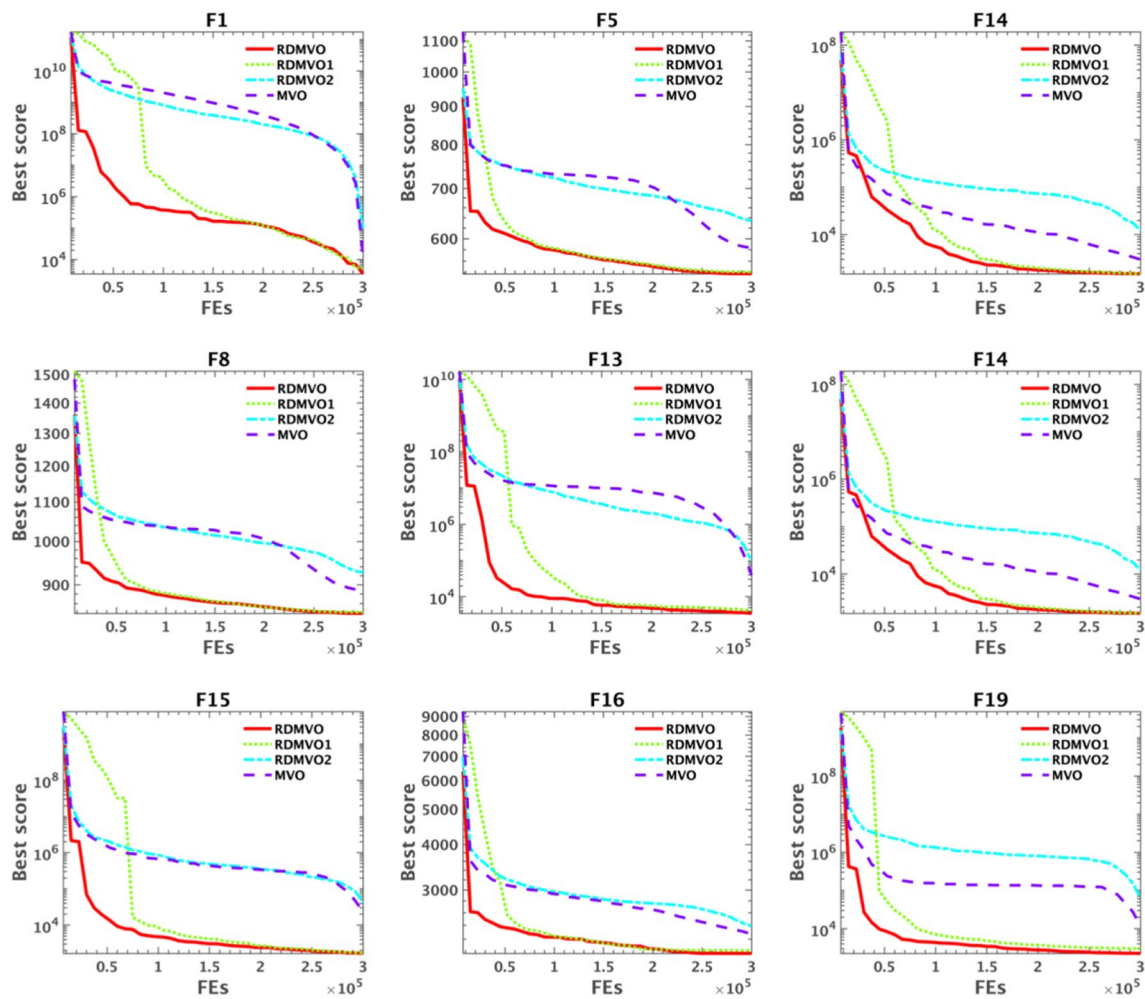
Fig. 4 Convergence curves of 9 benchmark functions

and the experimental results are shown in Tables 4, 19, 20, and Fig. 9.

Table 19 displays the performance of RDMVO and 7 other MHAs on benchmark functions, and the best results are bolded. The "±/=" indicators in Table 19 show that RDMVO outperforms other competitors in most test functions. RDMVO outperforms the efficient algorithm DE on 20 test functions and the traditional algorithm PSO on up to 28. RDMVO outperforms the original algorithm MVO in 26 test functions, with two being equal to MVO and two being weaker. According to the ARV metric after the Friedman test, RDMVO has the highest overall ranking among all tested functions, followed by the DE algorithm.

For further detailed analysis, the Friedman test ranking of all algorithms on the benchmark functions is shown in Table 4. It is clear to find that RDMVO scored first place in F5, F7, F8, F10, F12, F16, F17, F18, F19, F20, F21, and F22, and second place in F1, F4, F6, F9, F11, F13, F14, F15, F23, F24, F26, F27, F28, F29, and F30. This shows that RDMVO

has excellent performance on multimodal functions and performs well on some Hybrid Functions and Composition Functions.

Table 20 shows the *P* values of the experimental results via the Wilcoxon signed-rank test with 5% significance, and *P* values ≥ 0.05 are shown in boldface. As can be seen from the *P* values in Table 20, RDMVO and HHO, BA are statistically different on each test function, and RDMVO and MVO are statistically different on each test function except F9. In most cases, RDMVO was statistically significantly different from its competitors.

To visually better see the difference, the convergence curve on some test functions (F5, F7, F8, F10, F16, F18, F19, F20, F22) is given in Fig. 9. The convergence speed and accuracy of RDMVO and other competitors are compared. RDMVO has a faster convergence trend than other algorithms, achieving good convergence results early in the algorithm iteration.

Table 3 Friedman test ranking on the benchmark functions

F	RDMVO-$p\{4\}$	RDMVO-$p[114]$	RDMVO-$p\{6\}$	RDMVO-$p\{7\}$
F1	4	2	3	1
F2	4	3	2	1
F3	1	3	2	4
F4	4	2	3	1
F5	3	2	4	1
F6	4	1	2	3
F7	4	3	1	2
F8	2	4	1	3
F9	2	3	1	4
F10	4	3	2	1
F11	3	2	1	4
F12	1	3	2	4
F13	4	2	3	1
F14	3	1	2	4
F15	4	3	1	2
F16	4	2	1	3
F17	2	3	4	1
F18	3	2	4	1
F19	4	2	1	3
F20	3	2	1	4
F21	3	4	1	2
F22	2	1	4	3
F23	4	3	1	2
F24	1	2	3	4
F25	2	1	4	3
F26	3	2	1	4
F27	3	4	2	1
F28	2	3	1	4
F29	4	3	1	2
F30	3	4	2	1
Avg	3.0	2.5	2.03	2.47
Rank	4	3	1	2

5.2 Experiment on Image Segmentation

In this section, we applied RDMVO to image segmentation. First, RDMVO is combined with Kapur's entropy. Specifically, Kapur's entropy is used as a fitness function, and the position of the universe is used as a set of thresholds at a certain threshold level. Slightly adjust RDMVO logic to find the maximum value of Kapur's entropy. This is simple to accomplish. The image segmentation and evaluation are performed under the resulting set of thresholds. The specific experimental process is shown in Fig. 5.

In other AI-related publications, there are proposals for fair experimental comparisons of two or more computational approaches on a certain dataset, which need allocating

the same computer resources to each methodology [115–118]. Same as Sect. 5.1, to ensure the fairness of the experiment and compare the differences in the algorithms themselves, we set other experimental parameters uniformly. As shown in Table 5, where N is the number of particles in the population, T is the number of iterations, and we set the number of experiments F to 20, so each algorithm was run independently 20 times to reduce the influence of randomness on the experimental results. Table 16 shows the relevant parameter settings of the MHA used in this experiment.

We ran three sets of experiments. The first set was a mechanism comparison experiment on BKIs to verify the effectiveness of RM and DM; the second set was an algorithm comparison experiment on BKIs. We chose some MHAs that have been applied to image segmentation. Moreover, compare the image segmentation effects of RDMVO and these algorithms to determine whether the RDMVO algorithm is more advantageous; the third group conducted algorithm comparison experiments on COVID-19-CXIs, and the difference from the second group is that the test image set has been changed. In addition, considering the complexity of the actual situation, all our experiments set multiple threshold levels to verify the adaptability of the algorithm. Finally, we used the Friedman test to perform a statistical test on the results. Furthermore, use PSNR, SSIM, and FSIM as evaluation indicators. All experiments are set out in detail below.

5.2.1 Influence of the Two Mechanisms

As in Sect. 5.1.2, a mechanism comparison experiment on image segmentation was first performed. We selected nine complex representative images from the BKIs as the research objects, as shown in Fig. 10. Figure 11 depicts the grayscale, histogram, and 2D histograms of these images. The first column in Fig. 11 is the grayscale image, the second column is the histogram, and the third column is the 2D histogram. The experimental results are shown in Tables 6, 21, and Fig. 6.

Fitness is the maximum of Kapur's entropy obtained by segmentation, representing the amount of information in the segmented image. A suitable segmentation method will have a more significant amount of information. Simultaneously, with the improvement of the threshold level, the amount of information obtained by a suitable segmentation method will also increase. The fitness values of RDMVO and variant algorithms at different segmentation levels are given in Table 21. The bold shows the maximum fitness value obtained for each experimental image at each threshold level. In addition, Fig. 6 shows the maximum fitness of all images of RDMVO and variants under different thresholds. In Table 21, as the threshold level increases from 2 to 4, the fitness obtained by RDMVO and variant algorithms increases gradually. It can be observed more directly in Fig. 6. In Fig. 6, the abscissa is the different

Table 4 Friedman test ranking of all algorithms on the benchmark functions

F	RDMVO	DE	WOA	GWO	HHO	BA	PSO	MVO
F1	2	1	5	8	6	4	7	3
F2	3	6	7	8	4	1	5	2
F3	7	6	5	8	4	1	3	2
F4	2	5	7	8	6	1	3	4
F5	1	4	7	2	5	8	6	3
F6	2	1	7	3	6	8	5	4
F7	1	3	6	4	7	8	5	2
F8	1	4	7	3	6	8	5	2
F9	2	1	7	4	6	8	5	3
F10	1	6	8	2	4	5	7	3
F11	2	1	7	8	5	6	4	3
F12	1	2	7	8	5	3	6	4
F13	2	1	4	8	6	5	7	3
F14	2	1	8	7	5	4	6	3
F15	2	1	5	8	4	6	7	3
F16	1	2	7	3	6	8	5	4
F17	1	2	7	3	6	8	5	4
F18	1	5	8	6	7	3	4	2
F19	1	2	8	5	4	6	7	3
F20	1	2	7	3	5	8	6	4
F21	1	5	7	8	6	2	3	4
F22	1	4	7	3	6	8	5	2
F23	2	4	6	5	1	7	8	3
F24	2	8	4	6	1	5	3	7
F25	3	4	2	8	1	7	6	5
F26	2	7	3	5	1	8	4	6
F27	2	3	7	5	1	6	8	4
F28	2	8	3	6	1	5	4	7
F29	2	3	7	4	1	8	6	5
F30	2	3	8	5	1	6	7	4
Avg	1.83	3.5	6.27	5.47	4.23	5.7	5.4	3.6
Rank	1	2	8	6	4	7	5	3

Fig. 5 Flowchart of Kapur's entropy image segmentation based RDMVO
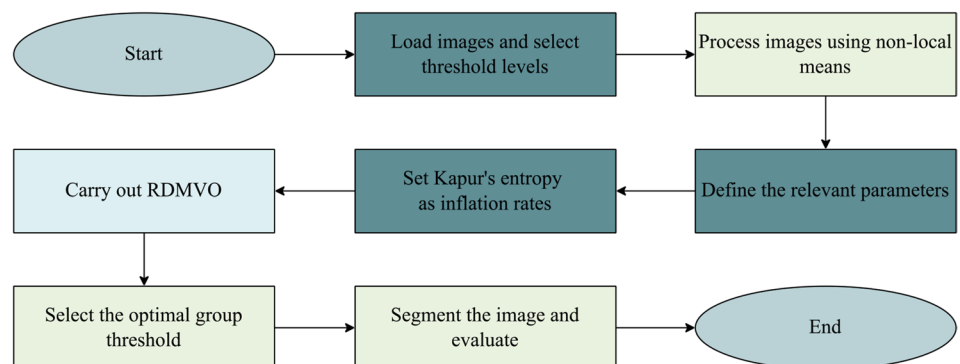
Table 5 Unified parameter settings

N	T	F
20	50	20

Table 6 Friedman test results for each algorithm on PSNR, FISM and SSIM

Thresholds	Index	Item	RDMVO	RDMVO1	RDMVO2	MVO
2	PSNR	Avg	**2.91**	2.89	2.13	2.07
		Rank	**1**	2	3	4
	FISM	Avg	2.85	**2.90**	2.16	2.08
		Rank	2	**1**	3	4
	SSIM	Avg	**2.78**	**2.78**	2.19	2.24
		Rank	**1**	**1**	4	3
3	PSNR	Avg	**3.07**	2.84	2.17	1.92
		Rank	**1**	2	3	4
	FISM	Avg	**2.96**	2.84	2.26	1.95
		Rank	**1**	2	3	4
	SSIM	Avg	**3.03**	2.91	2.18	1.88
		Rank	**1**	2	4	4
4	PSNR	Avg	**3.17**	3.05	2.08	1.70
		Rank	**1**	2	3	4
	FISM	Avg	**3.09**	3.04	2.14	1.73
		Rank	**1**	2	3	4
	SSIM	Avg	**3.10**	3.06	2.04	1.81
		Rank	**1**	2	3	4
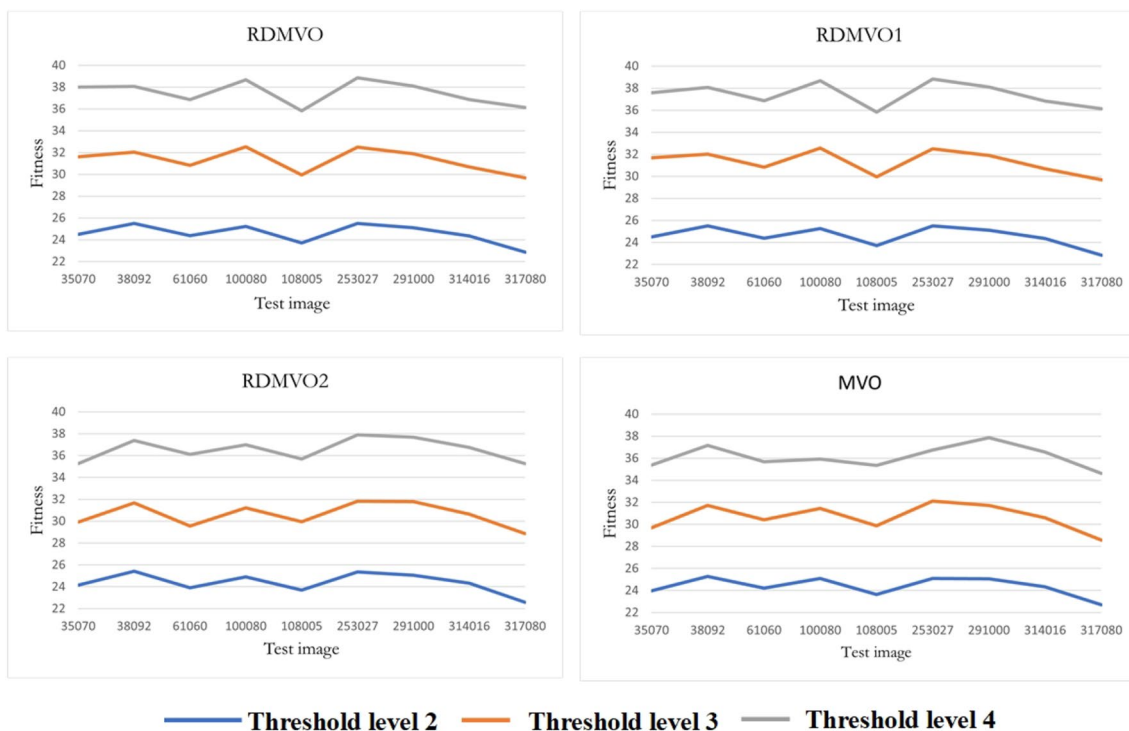
Fig. 6 Maximum fitness of RDMVO and variants at different thresholds

test images, the ordinate is the maximum fitness, and curves of different colors represent different threshold levels. It can be seen that the curve with a larger threshold level is always above the curve smaller than its threshold level. The above shows that RDMVO and variant algorithms are suitable for image segmentation on Kapur's entropy.

Table 6 shows three evaluation data of PSNR, FSIM, and SSIM of the segmentation results of RDMVO and variant algorithms and a more extended Friedman test. Among them, Avg is the average value of the relevant evaluations across all images. The larger the average value, the better the comprehensive result of image segmentation. Rank is the corresponding ranking. The best Avg and Rank values are bolded. RDMVO achieves top results for all three evaluations on experimental images at all threshold levels except the FSIM metric with a threshold level of 2.

In summary, RDMVO is more competitive in image segmentation experiments. That is, the introduced RM and DM have meaning.

5.2.2 Comparison with Other Algorithms on Berkeley

In this section, we compared some mainstream algorithms with the original algorithm MVO. These mainstream algorithms included ACOR, BA, WOA, SSA, DE, AVOA, CLPSO and HHO. Some MHAs have been successfully applied to image segmentation or some relatively new algorithms [18, 81, 119–125]. Nine test images are shown in Figs. 10 and 11. In addition, we set the threshold levels to 2, 3, 4, and 5 for experiments.

Table 22, 23, and 24 show three evaluation values of segmentation quality at different threshold levels, including the mean and standard deviation of PSNR, SSIM, and FSIM evaluations, respectively. The data are derived from the results of 20 independent runs of the experiment. Avg refers to the average value obtained by running the experiment independently 20 times. The higher the Avg, the better the corresponding evaluation result. The Std denotes the standard deviation from running the experiment independently 20 times. The smaller the Std, the more stable the algorithm. The most significant mean and standard deviation are bold in the table. From Tables 22, 23, and 24, we can see that RDMVO can achieve an enormous average value and obtain a minor standard deviation in most cases. This shows that RDMVO has better performance and is more stable than other competitors.

Further, Tables 22, 23, and 24 are also subjected to the Friedman test. Tables 7, 8, and 9 show the average test results.

PSNR measures the difference between the obtained segmented image and the original image, specifically the degree of distortion of the image. The higher the PSNR value, the closer the segmented image is to the original image. Table 22 shows the evaluation results of the PSNR of all algorithms. Table 22 shows that compared with other competitors, the RDMVO algorithm can obtain higher PSNR in most cases. Moreover, under the same test image, with the increase of the

Table 7 Overall Friedman test results for each algorithm on PSNR

Thresholds	Item	RDMVO	MVO	ACOR	BA	WOA	SSA	DE	AVOA	CLPSO	HHO
2	Avg	**7.07**	4.77	5.80	4.66	5.55	5.24	6.56	5.32	5.27	4.77
	rank	**1**	9	3	10	4	7	2	5	6	8
3	Avg	**6.90**	4.62	5.88	5.83	5.19	5.50	6.02	5.47	4.49	5.10
	rank	**1**	9	3	4	7	5	2	6	10	8
4	Avg	**7.18**	4.04	6.12	6.10	4.79	5.69	5.88	6.09	4.21	4.89
	rank	**1**	10	2	3	8	6	5	4	9	7
5	Avg	**7.52**	3.54	7.14	6.46	5.13	5.13	5.93	6.15	3.40	4.60
	rank	**1**	9	2	3	6	6	5	4	10	8

Table 8 Overall Friedman test results for each algorithm on SSIM

Thresholds	Item	RDMVO	MVO	ACOR	BA	WOA	SSA	DE	AVOA	CLPSO	HHO
2	Avg	**6.65**	4.74	5.79	4.91	5.52	5.44	6.35	5.22	5.24	5.15
	rank	**1**	10	3	9	4	5	2	7	6	8
3	Avg	**6.90**	4.64	5.76	5.39	5.77	5.39	5.89	5.20	4.65	5.41
	rank	**1**	10	4	6	3	7	2	8	9	5
4	Avg	**7.28**	4.36	6.42	5.54	5.05	5.67	5.90	5.68	4.32	4.78
	rank	**1**	9	2	6	7	5	3	4	10	8
5	Avg	**7.60**	3.65	7.17	6.42	5.07	5.03	5.67	5.92	3.73	4.73
	rank	**1**	10	2	3	6	7	5	4	9	8

Table 9 Overall Friedman test results for each algorithm on FISM

Thresholds	Item	RDMVO	MVO	ACOR	BA	WOA	SSA	DE	AVOA	CLPSO	HHO
2	Avg	**6.75**	4.78	5.72	5.24	5.04	5.41	5.83	5.47	5.58	5.19
	rank	**1**	10	3	7	9	6	2	5	4	8
3	Avg	**6.76**	4.84	5.93	5.72	5.47	5.42	5.70	5.57	4.35	5.24
	rank	**1**	9	2	3	6	7	4	5	10	8
4	Avg	**7.39**	4.13	6.42	5.71	5.06	5.74	5.96	5.74	4.12	4.74
	rank	**1**	9	2	6	7	5	3	4	10	8
5	Avg	**7.53**	3.52	6.99	6.51	5.21	5.21	5.79	5.96	3.71	4.58
	rank	**1**	10	2	3	7	6	5	4	9	8

threshold level, the PSNR gradually becomes larger, which indicates that the RDMVO segmentation result is more accurate. Table 7 is the average result of the Friedman test on Table 22, avg is the average result over all test images, and rank is the ranking of the average result. The best Avg and Rank values are bolded. After the Friedman test, RDMVO can achieve first place at all threshold levels. This means that the RDMVO segmentation method based on Kapur's entropy is statistically significant, indicating that RDMVO is better than other competitors.

SSIM evaluates the visual difference between the obtained segmented and original images. The larger the SSIM value, the closer the segmented image is to the original image visually. Table 23 shows the evaluation results of SSIM of all algorithms. It can be seen in Table 23 that compared with other competitors, the RDMVO algorithm can obtain higher SSIM in most cases. Moreover, under the same test image, as the threshold level increases, the SSIM gradually becomes larger, which indicates that the RDMVO segmentation result is more in line with human visual observation. Table 8 is the average result of the Friedman test in Table 23. The best results are bolded. After the Friedman test, RDMVO can also achieve first place at all threshold levels. Therefore, from the SSIM point of view, the RDMVO segmentation method based on Kapur's entropy is also more statistically significant.

FSIM is to evaluate the feature similarity between the obtained segmented image and the original image. The evaluation results of FSIM of all algorithms are given in Table 24. In Table 24, it can be seen that compared to other competitors, the same as the above evaluation indicators, the RDMVO algorithm can obtain higher FSIM in most cases. Moreover, under the same test result, as the threshold level increases, FSIM gradually becomes larger. Table 9 is the average result of the Friedman test in Table 24. The best results are bolded. Similarly, RDMVO can achieve first place at all threshold levels after the Friedman test. Therefore, from the FSIM point of view, the RDMVO algorithm is also the best.

In addition, Tables 25, 26, and 27 give the Friedman test results of different images under different thresholds for all algorithms. These data are the data basis of Tables 7, 8, and 9.

Figures 12, 13, 14 and 15 are the convergence information of all algorithms when the threshold levels are 2, 3, 4, and 5, respectively. The best value is the average fitness value obtained by running each algorithm 20 times independently, and the abscissa is the number of iterations. It can be seen from the figure that under all threshold levels, RDMVO can achieve the best convergence speed and the most prominent fitness. The performance of RDMVO is satisfactory. Especially the comparison effect of RDMVO and the original algorithm MVO. It is obvious that the convergence speed and optimal value of RDMVO have significant advantages. The performance of the RDMVO algorithm we propose dramatically improves.

Figure 16 shows the specific thresholds obtained by all related algorithms when the threshold level is 3 for image 35,070. Figure 17 shows the segmented images obtained by different algorithms when the threshold level is 3 for image 35070. Figure 18 is the segmentation image obtained using RDMVO when the thresholds are 2, 3, 4, and 5. The first column has a threshold level of 2, the second column has a threshold level of 3, the third column has a threshold level of 4, and the fourth column has a threshold level of 5. Obviously, as the threshold level increases, the segmentation effect is better.

5.2.3 Comparison with Other Algorithms on COVID-19

Testing for COVID-19, we selected nine medical images. These are the X-ray images of nine patients with COVID-19, clinically recorded between January 21 and March 10, 2020, at a tertiary-level A hospital in eastern China. Our study was approved by the Ethics Committee of the Affiliated Yueqing Hospital of Wenzhou Medical University (Yueqing, China; protocol number 202000002) and complied with the Helsinki declaration. Except for the different test image sets, the experimental parameters and procedures are the same as in
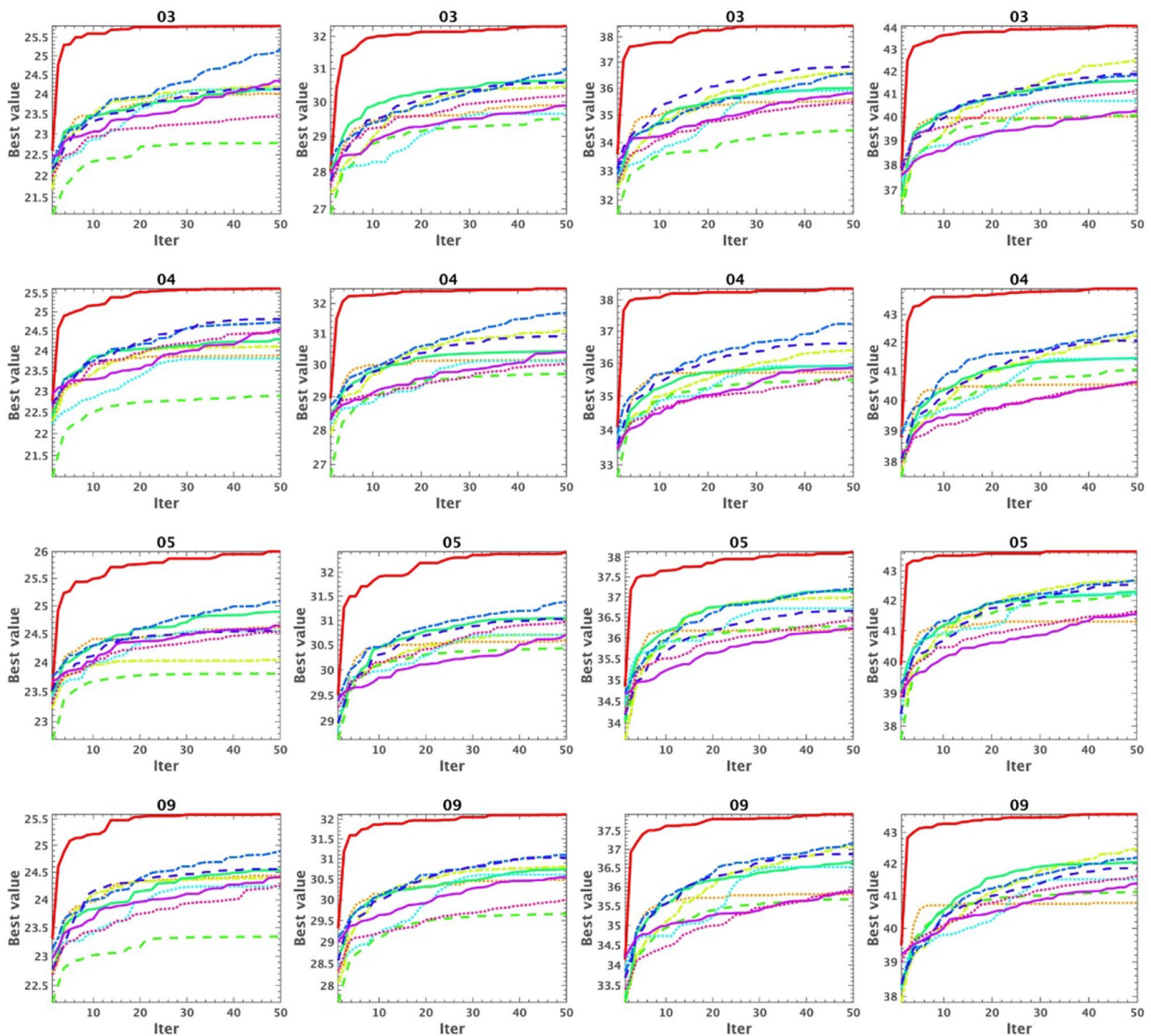
Fig. 7 Kapur's entropy convergence curve of all algorithms at different thresholds

Sect. 5.2.3. Below we give the specific experimental results without further explanation. For the specific analysis of the results, please refer to Sect. 5.2.3. Figure 19 is the original test image, and Figure 20 is the grayscale image, grayscale value histogram, and 2D histogram corresponding to the original image.

Figure 7 is a graph of fitness convergence curves in all images corresponding to all algorithms. From a longitudinal perspective, there are 4 columns corresponding to different thresholds. The first column has a threshold level of 2, the

second column has a threshold level of 3, the third column has a threshold level of 4, and the fourth column has a threshold level of 5. It can be seen from the figure that with different thresholds, the convergence speed of RDMVO can be the fastest, and the maximum fitness value can be obtained at the same time. From the horizontal view, there are 9 lines corresponding to different test images, from top to bottom, corresponding to the test images 03, 04, 05, 09, 12, 15, 20, 21, and 25. As can be seen from the figure, for all the test images, the performance of RDMVO far exceeds that of
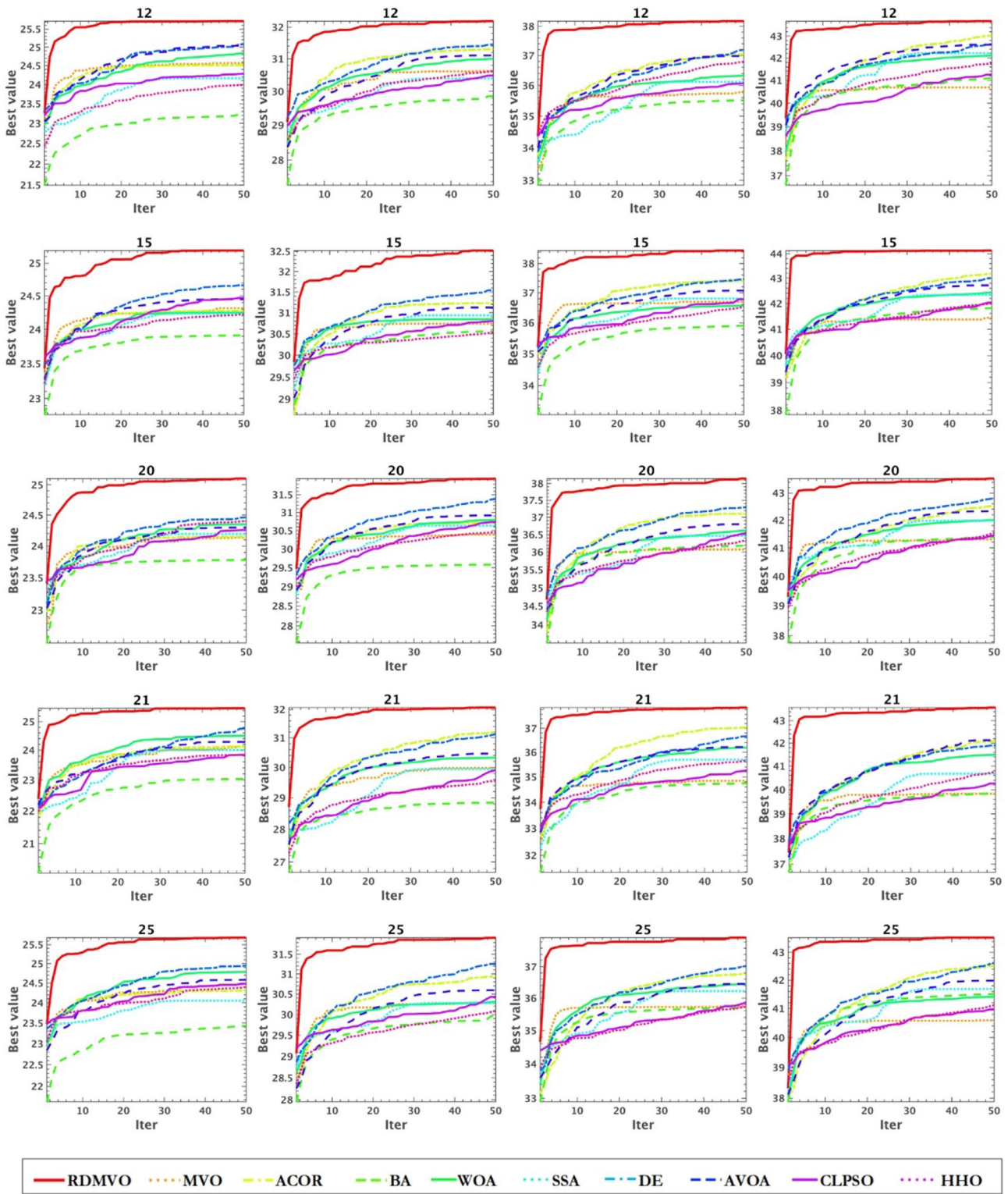
Fig. 7 (continued)

Table 10 The result of the Wilcoxon signed-rank test with 5% significance at different thresholds

±/=	2			3			4			5		
	PSNR	SSIM	FSIM	PSNR	SSIM	FSIM	PSNR	SSIM	FSIM	PSNR	SSIM	FSIM
RDMVO	~	~	~	~	~	~	~	~	~	~	~	~
MVO	6/2/1	7/0/2	6/0/3	9/0/0	8/0/1	8/0/1	8/0/1	5/0/4	4/0/5	9/0/0	3/0/6	5/0/4
ACOR	5/3/1	8/0/1	7/0/2	6/1/2	6/0/3	6/0/3	4/0/5	3/0/6	6/0/3	2/0/7	2/0/7	0/0/9
BA	6/3/0	8/0/1	8/0/1	6/0/3	8/0/1	8/0/1	6/0/3	6/0/3	7/0/2	1/0/8	2/0/7	3/0/6
WOA	6/2/1	6/0/3	6/0/3	6/0/3	5/0/4	7/0/2	7/0/2	3/0/6	6/0/3	6/0/3	1/0/8	2/0/7
SSA	5/2/2	6/0/3	6/0/3	7/0/2	7/0/2	7/0/2	9/0/0	3/0/6	5/0/4	3/0/6	4/0/5	3/0/6
DE	3/2/4	7/1/1	4/1/4	3/0/6	5/0/4	7/0/2	5/0/4	3/0/6	5/0/4	5/0/4	2/1/6	3/0/6
AVOA	4/2/3	8/1/0	8/1/0	6/0/3	7/0/2	8/0/1	4/0/5	3/0/6	4/0/5	3/0/6	2/0/7	3/0/6
CLPSO	5/2/2	6/0/3	6/0/3	7/0/2	6/0/3	7/0/2	7/0/2	4/0/5	5/0/4	8/0/1	5/0/4	7/0/2
HHO	6/0/3	7/0/2	7/0/2	9/0/0	7/0/2	8/0/1	8/0/1	3/0/6	5/0/4	8/0/1	4/1/4	4/0/5

Table 11 PSNR, SSIM, FISM results of all algorithms at different thresholds

Thresholds	Index	Item	RDMVO	MVO	ACOR	BA	WOA	SSA	DE	AVOA	CLPSO	HHO
2	PSNR	Avg	**6.33**	4.83	6.04	5.80	4.56	5.42	6.21	6.31	5.07	4.44
		rank	**1**	8	4	5	9	6	3	2	7	10
	SSIM	Avg	**7.81**	4.91	5.03	4.38	5.58	5.14	6.13	5.34	5.54	5.13
		rank	**1**	9	8	10	3	6	2	5	4	7
	FISM	Avg	**7.81**	4.91	5.03	4.38	5.58	5.14	6.13	5.34	5.54	5.13
		rank	**1**	9	8	10	3	6	2	5	4	7
3	PSNR	Avg	**7.65**	4.16	6.09	5.91	4.77	5.23	6.69	5.93	4.89	3.69
		rank	**1**	9	3	5	8	6	2	4	7	10
	SSIM	Avg	**7.82**	4.96	5.48	4.72	5.44	4.92	5.86	5.09	5.51	5.19
		rank	**1**	8	4	10	5	9	2	7	3	6
	FISM	Avg	**7.82**	4.96	5.48	4.72	5.44	4.92	5.86	5.09	5.51	5.19
		rank	**1**	8	4	10	5	9	2	7	3	6
4	PSNR	Avg	**7.74**	4.49	6.56	5.87	4.73	5.13	5.86	5.99	4.50	4.13
		rank	**1**	9	2	4	7	6	5	3	8	10
	SSIM	Avg	**6.94**	5.12	5.54	4.87	5.25	5.53	5.73	5.61	5.19	5.21
		rank	**1**	9	4	10	6	5	2	3	8	7
	FISM	Avg	**6.94**	5.12	5.54	4.87	5.25	5.53	5.73	5.61	5.19	5.21
		rank	**1**	9	4	10	6	5	2	3	8	7
5	PSNR	Avg	**7.45**	3.82	6.56	6.71	4.73	5.41	5.85	6.02	4.25	4.19
		rank	**1**	10	3	2	7	6	5	4	8	9
	SSIM	Avg	**6.50**	4.65	6.02	5.59	5.62	5.21	5.71	5.69	4.64	5.37
		rank	**1**	9	2	6	5	8	3	4	10	7
	FISM	Avg	**6.50**	4.65	6.02	5.59	5.62	5.21	5.71	5.69	4.64	5.37
		rank	**1**	9	2	6	5	8	3	4	10	7

other competitors at different threshold levels. We know that selecting the threshold level generally depends on the actual practical needs. That is to say, the adaptability of RDMVO is greater.

Table 10 shows the results of PSNR, SSIM, and FISM of different algorithms after the Wilcoxon signed-rank test with 5% significance at different threshold levels. The "+" denotes the number by which RDMVO is better than other algorithms. "-" means that RDMVO is worse than the number of other
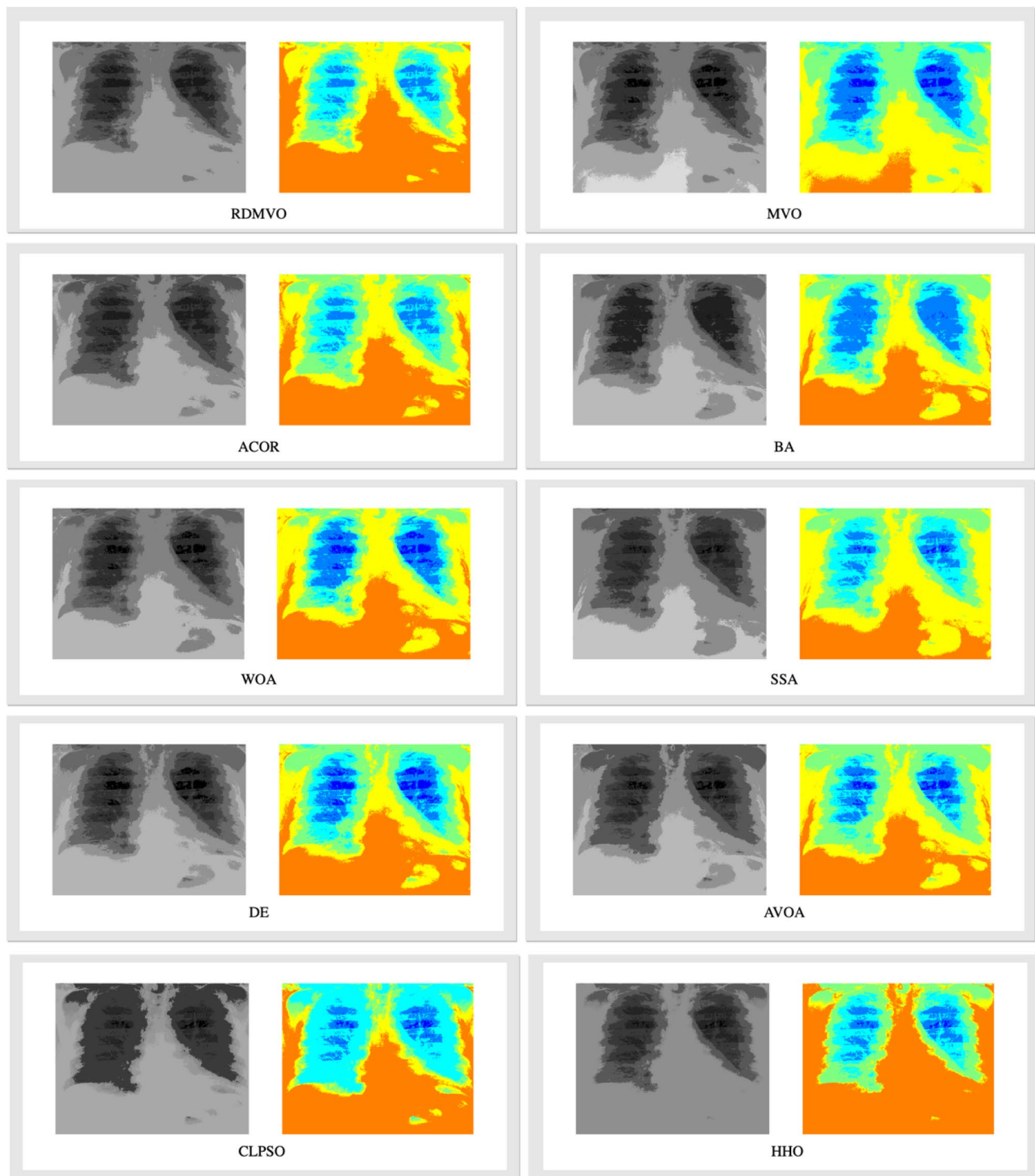
Fig. 8 The grayscale image and jet colormap image obtained by all algorithms on image 03

Table 12 PSNR, SSIM, FSIM mean of all algorithms on image 03

Index	RDMVO	MVO	ACOR	BA	WOA	SSA	DE	AVOA	CLPSO	HHO
PSNR	**19.37**	16.51	19.26	19.14	17.23	18.79	18.43	18.40	16.93	16.58
SSIM	**0.72**	0.65	0.70	0.68	0.69	0.66	0.68	0.67	0.69	0.69
FISM	**0.78**	0.74	0.77	0.76	0.77	0.75	0.76	0.76	0.75	0.76

Table 13 PSNR, SSIM, FSIM standard deviation of all algorithms on image 03

Index	RDMVO	MVO	ACOR	BA	WOA	SSA	DE	AVOA	CLPSO	HHO
PSNR	**0.96**	2.21	1.76	2.23	2.65	1.16	1.52	2.01	1.70	1.91
SSIM	**0.01**	0.08	0.04	0.04	0.06	0.04	0.04	0.07	0.05	0.07
FISM	**0.02**	0.04	0.03	0.04	0.04	**0.02**	0.03	0.03	0.04	0.04

algorithms. "=" represents the number of RDMVO that is not significantly different from other algorithms. When the threshold level is 3, 4, and 5, and any PSNR, SSIM, and FSIM are used as evaluation indicators, RDMVO outperforms other algorithms on all images. Except that there is one image on which RDMVO performance is weaker than ACOR when the threshold level is 3 and the PSNR metric; there is one image on which RDMVO performance is weaker than DE when the threshold level is 5, and under the SSIM metric. When the threshold level is 2 and the PSNR metric is used, the performance of RDMVO is weaker than other algorithms on more images, but RDMVO performs better than the comparison algorithm in more images when compared to the number of "+" and "−".

Table 11 contains the average results of the three indicators PSNR, SSIM, and FSIM of all algorithms under different threshold levels after the Friedman test, and the optimal data are bolded. It can be seen in Table 11 that under the Friedman test, RDMVO is the first at all threshold levels on all images. The thresholds obtained by all algorithms at all threshold levels of the test images are given in Table 28.

Furthermore, we analyze the test image 03 at a threshold level of 5, and Fig. 8, Tables 12, and 3 are the experimental results of image 03. Figure 8 compares the grayscale and jet colormap images obtained by all algorithms based on Kapur's entropy to segment the test image. Table 12 shows the mean values of PSNR, SSIM, and FSIM obtained by running 20 segmentation experiments independently for all algorithms, and the optimal data are bolded. Table 13 shows the standard deviations of PSNR, SSIM, and FSIM obtained by running 20 segmentation experiments independently for all algorithms, and the optimal data are bolded. It can be seen that the mean of RDMVO is the largest, and the standard deviation is the smallest. The all-around performance of the RDMVO algorithm is consistent with the overall performance in picture 03.

6 Discussions

This paper proposes an innovative algorithm RDMVO based on the MVO. Moreover, designs an image segmentation scheme RDMVO-MIS that is Kapur's entropy

MIS based on RDMVO to segment COVID-19-CXIs quickly and accurately. Then, a series of experiments were carried out to validate three aspects: the general performance of RDMVO, the feasibility of RDMVO-MIS, and the performance of RDMVO-MIS for BKIs and COVID-19-CXIs.

RDMVO introduces two mechanisms based on MVO, RM and DM. The impact of introducing the two mechanisms is demonstrated in the mechanism comparison experiment on IEEE CEC2017. The combined RM and DM can significantly enhance MVO's ability to jump out of the local optimum and improve MVO's solution accuracy. According to the convergence curves on some test functions, the RM mainly improves MVO's ability to jump out of the local optimum. Only adding DM has no effect on improving MVO or has a negative effect, but the action of DM in the MVO improved by RM can further improve the convergence speed. In conclusion, combining RM and DM to improve MVO performance makes sense.

Then, in the performance comparison experiment on IEEE CEC2017 with some mainstream MHAs, RDMVO performed admirably, ranking first among all related experimental algorithms. RDMVO outperforms other algorithms, particularly in multimodal and hybrid functions. Although RDMVO performs well in composition functions compared to other excellent algorithms such as HHO, but there is still much room for improvement.

Further, MIS experiments on the BKIs prove that RDMVO-MIS is feasible. Compared with other MHAs, RDMVO has better performance. RDMVO consistently outperforms other MHAs in terms of the convergence speed on Kapur's entropy function, the obtained maximum Kapur's entropy, and the algorithm's stability. Moreover, RDMVO outperforms other MHAs in the three most commonly used image segmentation evaluation indicators, PSNR, SSIM, and FSIM. Finally, we implemented RDMVO-MIS to segment COVID-19-CXIs and compared it with other MHAs. RDMVO also has the best performance and segmentation effect. In addition, the experiment's threshold levels were set to 2, 3, 4, and 5, respectively. The threshold level selection in this paper is relatively small compared to these papers [13, 19–23]. This is mainly based

on considering studies supplementing segmentation horizons with small thresholds. At the same time, it should be noted that RDMVO's performance at high threshold levels has not been validated, and this is also something to consider for future works.

In summary, RDMVO has the best performance in all experiments, so it also can be applied to many other fields in the future, such as human activity recognition [126], information retrieval services [127–129], power flow optimization [130], location-based services [131, 132], endoscope imaging [106], image dehazing [113], image-to-image translation [133], autism spectrum disorder classification [134], disease identification and diagnosis [135, 136], dynamic module detection [137, 138], and pharmacoinformatic data mining [139, 140]. Different from the paper [17], the author only verified the COVID-19-CXI segmentation performance of the improved algorithm and did not verify the improved algorithm itself, and the performance of the improved algorithm universality is difficult to confirm. In this paper, in addition to COVID-19-CXI segmentation experiments, we also comprehensively tested the performance of RDMVO on the IEEE CEC2017 benchmark functions and BKIs. Moreover, the performance of RDMVO is satisfactory. As a result, it is highly recommended that managers try RDMVO when managers need to segment other types of images rather than COVID-19-CXIs. Of course, the parameters used in this paper are unsuitable for all problems as every problem has its character. The managers should adjust the parameters according to the specific problem to achieve maximum performance. In addition, according to the previous analysis of the time complexity of RDMVO, the dimension of the problem will directly affect the RDMVO's running time. When using RDMVO, whether the time cost caused by the dimension is acceptable is also a problem that managers should consider for some high-dimensional problems.

7 Conclusions and Future Works

As COVID-19 spreads throughout the world, its diagnosis is vital. Chest X-ray image analysis and diagnosis are considered effective means. Experts and scholars worldwide have invested a lot of energy and time in improving the efficiency of COVID-19-CXI analysis. To better improve the effect of image segmentation, a novel improved MVO variant, namely RDMVO, was proposed and successfully applied to MIS and segmented COVID-19-CXIs. Experimental results show that our proposed RDMVO enhances MVO's ability to explore globally and jump out of local optimum. Moreover, it outperforms most MHAs on 2D Kapur's entropy MIS.

There is much work to be done in the future. First, MHA is a class of algorithms based on probability and randomness, although MHAs are widely used in various fields. However, the results of mathematical proof of MHAs are currently relatively lacking. Rigorous mathematical proofs are of great significance for the development of MHAs. More research is needed to provide rigorous mathematical proofs in the future, whether MVO, RDMVO, or other MHAs. Second, our experiments on RDMVO are only on MIS of BKIs and COVID-19-CXIs. Although, the images of different diseases have different characteristics. However, considering they all belong to medical images, we can still try to use RDMVO for image segmentation of other diseases. In addition, MHAs have already produced many research results in feature selection and engineering optimization. So, using RDMVO for feature selection and engineering optimization is also the future research direction. The most important and urgent work is to apply RDMVO to the actual COVID-19 diagnosis as soon as possible to help overcome COVID-19 and restore the regular operation of human social life.

Appendix 1

See Tables 14, 15, 16, 17, 18, 19, 20, 21, 22, 23, 24, 25, 26, 27 and 28.

Table 14 The experimental environment

Component	Description
Hardware	
CPU	Intel(R) Xeon(R) Silver 4208 CPU
Frequency	2.10 GHz
RAM	128 GB
Software	
Operating system	Windows Server 2019 Standard
Language	MATLAB R2021b

Table 15 Summary of the IEEE CEC2017's test function

	No	Functions	$Fi^* = Fi(x^*)$
Unimodal functions	F1	Shifted and rotated bent cigar function	100
	F2	Shifted and rotated sum of different power function*	200
	F3	Shifted and rotated Zakharov function	300
Simple multimodal functions	F4	Shifted and rotated Rosenbrock's function	400
	F5	Shifted and rotated Rastrigin's function	500
	F6	Shifted and rotated expanded Scaffer's F6 function	600
	F7	Shifted function and rotated Lunacek Bi_Rastrigin function	700
	F8	Shifted and rotated non-continuous Rastrigin's function	800
	F9	Shifted and rotated levy function	900
	F10	Shifted and rotated Schwefel's function	1000
Hybrid functions	F11	Hybrid function 1 ($N=3$)	1100
	F12	Hybrid function 2 ($N=3$)	1200
	F13	Hybrid function 3 ($N=3$)	1300
	F14	Hybrid function 4 ($N=4$)	1400
	F15	Hybrid function 5 ($N=4$)	1500
	F16	Hybrid function 6 ($N=4$)	1600
	F17	Hybrid function 6 ($N=5$)	1700
	F18	Hybrid function 6 ($N=5$)	1800
	F19	Hybrid function 6 ($N=5$)	1900
	F20	Hybrid function 6 ($N=6$)	2000
Composition functions	F21	Composition function 1 ($N=3$)	2100
	F22	Composition function 2 ($N=3$)	2200
	F23	Composition function 3 ($N=4$)	2300
	F24	Composition function 4 ($N=4$)	2400
	F25	Composition function 5 ($N=5$)	2500
	F26	Composition function 6 ($N=5$)	2600
	F27	Composition function 7 ($N=6$)	2700
	F28	Composition function 8 ($N=6$)	2800
	F29	Composition function 9 ($N=3$)	2900
	F30	Composition function 10 ($N=3$)	3000

Table 16 Parameter settings of MHAs

Algorithms	Parameters
RDMVO	Random numbers: [0, 1]; WEP_Max = 1; WEP_Min = 0.2; $p=6$; $\alpha=50$; $\beta=0.5$; $\varepsilon_1=1.0e-150$; $\varepsilon_2=1.0e-4$
DE	Random numbers: [0, 1]; $pCR=0.2$; β_min $=0.2$; β_max $=0.8$
WOA	Random numbers: [0, 1]; $b=1$
GWO	Random numbers:[0, 1];
HHO	Random numbers:[0, 1];
BA	Random numbers: [0, 1]; Qmin $=0$; Qmax $=2$
PSO	Random numbers: [0, 1]; wMin $=0.2$; $wMax=0.9$; $V_{max}=6$; $c_1=c_2=2$,
MVO	Random numbers: [0, 1]; WEP_Max = 1; WEP_Min = 0.2; $p=6$;
ACOR	Random numbers: [0, 1]; $k=10$; $q=0.5$; ibslo $=1$
BA	Random numbers: [0, 1]; $Q_{min}=10$; $q=0$; $Q_{max}=2$
SSA	Random numbers: [0, 1];
AVOA	Random numbers: [0, 1]; $p_1=0.6$; $p_2=0.4$; $p_3=0.6$; $\alpha=0.8$; $\beta=0.2$; $\gamma=2.5$
CLPSO	Random numbers: [0, 1]; $c=1.49445$; $m=5$

Table 17 Results of various MVOs on benchmark functions

	F1		F2		F3	
	Avg	Std	Avg	Std	Avg	Std
RDMVO	**3.52216E+03**	**2.16086E+03**	2.01056E+07	3.58194E+07	2.99529E+04	1.27045E+04
RDMVO1	5.36825E+03	3.40813E+03	3.66486E+07	9.41885E+07	2.34604E+04	7.99239E+03
RDMVO2	9.96456E+04	3.40223E+04	1.53803E+09	2.52701E+09	3.15771E+02	1.30613E+01
MVO	1.20971E+04	8.46127E+03	**2.24726E+04**	**4.02444E+04**	3.00335E+02	**1.42561E−01**
	F4		F5		F6	
	Avg	Std	Avg	Std	Avg	Std
RDMVO	**4.43074E+02**	2.93757E+01	**5.38822E+02**	1.13336E+01	**6.00024E+02**	**1.91788E−02**
RDMVO1	4.55494E+02	**2.18639E+01**	5.41807E+02	**1.08893E+01**	6.00078E+02	3.09370E−02
RDMVO2	5.06337E+02	3.64757E+01	6.33908E+02	3.15240E+01	6.23038E+02	1.22608E+01
MVO	4.76937E+02	3.13117E+01	5.83897E+02	2.08705E+01	6.06992E+02	5.85744E+00
	F7		F8		F9	
	Avg	Std	Avg	Std	Avg	Std
RDMVO	7.78889E+02	**1.23482E+01**	8.39638E+02	8.96948E+00	**1.20255E+03**	**1.88130E+02**
RDMVO1	**7.72719E+02**	2.03709E+01	8.41994E+02	**8.08209E+00**	1.21321E+03	3.57943E+02
RDMVO2	8.44531E+02	3.28816E+01	9.27589E+02	3.20199E+01	3.03321E+03	1.28479E+03
MVO	8.27538E+02	3.12606E+01	8.88264E+02	2.94009E+01	1.49066E+03	1.02455E+03
	F10		F11		F12	
	Avg	Std	Avg	Std	Avg	Std
RDMVO	2.48344E+03	**3.60935E+02**	**1.18836E+03**	3.59272E+01	**1.49287E+04**	**7.88316E+03**
RDMVO1	**2.38127E+03**	4.34005E+02	1.19283E+03	**3.35782E+01**	1.73343E+04	9.48553E+03
RDMVO2	4.18031E+03	6.39912E+02	1.31982E+03	6.13139E+01	4.70404E+07	2.86233E+07
MVO	4.02425E+03	6.29522E+02	1.28372E+03	7.04304E+01	1.88196E+07	7.78369E+06
	F13		F14		F15	
	Avg	Std	Avg	Std	Avg	Std
RDMVO	**3.47785E+03**	**1.47378E+03**	**1.48776E+03**	**2.81709E+01**	**1.65909E+03**	**8.74304E+01**
RDMVO1	4.29678E+03	2.06085E+03	1.50251E+03	4.13463E+01	1.72054E+03	1.43405E+02
RDMVO2	9.65440E+04	7.38168E+04	1.21563E+04	1.69885E+04	4.16655E+04	2.98014E+04
MVO	4.01327E+04	2.74837E+04	2.98424E+03	2.02294E+03	2.34422E+04	2.20367E+04
	F16		F17		F18	
	Avg	Std	Avg	Std	Avg	Std
RDMVO	**2.01027E+03**	1.84047E+02	**1.95012E+03**	9.87602E+01	4.18752E+04	1.60643E+04
RDMVO1	2.04825E+03	**1.76655E+02**	1.95052E+03	**8.08303E+01**	**3.74583E+04**	**1.54693E+04**
RDMVO2	2.39253E+03	2.22611E+02	2.14715E+03	2.41870E+02	1.47898E+05	9.11794E+04
MVO	2.27230E+03	2.05818E+02	2.00857E+03	1.43634E+02	7.84931E+04	5.30928E+04
	F19		F20		F21	
	Avg	Std	Avg	Std	Avg	Std
RDMVO	**2.25206E+03**	**4.43134E+02**	2.16673E+03	**8.96756E+01**	**2.20084E+03**	6.06842E+01
RDMVO1	3.01467E+03	1.52023E+03	**2.14583E+03**	9.92398E+01	2.20564E+03	5.64452E+01
RDMVO2	6.38847E+04	6.74997E+04	2.46581E+03	1.32376E+02	2.23907E+03	**2.68183E+01**
MVO	1.16750E+04	8.49502E+03	2.40696E+03	1.32810E+02	2.22007E+03	3.97257E+01

Table 17 (continued)

	F22		F23		F24	
	Avg	Std	Avg	Std	Avg	Std
RDMVO	**2.30152E+03**	5.66318E+01	2.58617E+03	1.41918E+02	**2.60000E+03**	1.41390E−03
RDMVO1	2.30180E+03	5.65020E+01	2.82571E+03	1.17784E+01	3.27788E+03	2.80990E+02
RDMVO2	2.34558E+03	**2.61685E+01**	**2.50000E+03**	**2.24123E−04**	2.60000E+03	**9.09515E−04**
MVO	2.32194E+03	3.51128E+01	2.86340E+03	2.67210E+01	3.38712E+03	1.49914E+02
	F25		F26		F27	
	Avg	Std	Avg	Std	Avg	Std
RDMVO	2.74301E+03	8.09932E+01	**2.80002E+03**	2.54534E−02	3.31923E+03	2.06888E+02
RDMVO1	2.90071E+03	4.34421E+00	4.78012E+03	5.20596E+02	3.43501E+03	3.74899E+01
RDMVO2	**2.70002E+03**	**1.04326E−02**	2.80002E+03	**1.37499E−02**	**2.90001E+03**	**8.91362E−03**
MVO	2.92217E+03	2.69368E+01	5.00033E+03	6.25395E+02	3.61761E+03	9.69221E+01
	F28		F29		F30	
	Avg	Std	Avg	Std	Avg	Std
RDMVO	3.10473E+03	8.05144E+01	3.24673E+03	1.40087E+02	1.35060E+04	8.04964E+03
RDMVO1	3.22548E+03	3.65494E+02	3.34434E+03	9.85103E+01	1.49292E+04	7.47301E+03
RDMVO2	**3.00003E+03**	**1.94344E−02**	**3.10005E+03**	**4.07222E−02**	**7.95035E+03**	**3.66100E+03**
MVO	3.88072E+03	9.39678E+02	3.70185E+03	1.73430E+02	1.22238E+06	1.13571E+06

	Comprehensive indicator	
	±/=	ARV
RDMVO	~	1.47
RDMVO1	12/1/17	2.2
RDMVO2	23/7/0	3.2
MVO	26/2/2	3.13

Table 18 P-values of the Wilcoxon signed-rank test with 5% significance of experimental results for various MVOs on benchmark functions (P values ≥ 0.05 are shown in bold face)

	F1	F2	F3	F4	F5	F6
RDMVO1	6.42421E−03	**5.99936E−01**	3.00099E−02	8.72967E−03	**1.58855E−01**	6.98378E−06
RDMVO2	1.73440E−06	1.02463E−05	1.73440E−06	1.73440E−06	1.73440E−06	1.73440E−06
MVO	2.35342E−06	1.73440E−06	1.73440E−06	2.41180E−04	1.73440E−06	1.73440E−06
	F7	F8	F9	F10	F11	F12
RDMVO1	**4.79947E−01**	**3.49346E−01**	**3.93334E−01**	**4.28430E−01**	**6.88359E−01**	**2.89477E−01**
RDMVO2	1.73440E−06	1.73440E−06	1.92092E−06	1.73440E−06	2.35342E−06	1.73440E−06
MVO	3.18168E−06	2.60333E−06	**8.61213E−01**	1.92092E−06	1.02463E−05	1.73440E−06
	F13	F14	F15	F16	F17	F18
RDMVO1	**7.52133E−02**	**8.97178E−02**	**5.44625E−02**	**3.08615E−01**	**9.75387E−01**	**3.18491E−01**
RDMVO2	1.73440E−06	1.73440E−06	1.73440E−06	8.46608E−06	1.70877E−03	6.33914E−06
MVO	1.73440E−06	1.73440E−06	1.73440E−06	1.60464E−04	**6.87136E−02**	6.15641E−04
	F19	F20	F21	F22	F23	F24
RDMVO1	1.85190E−02	**1.77907E−01**	6.42421E−03	**1.58855E−01**	5.75165E−06	2.60333E−06
RDMVO2	1.92092E−06	2.35342E−06	3.16034E−02	4.49189E−02	1.92092E−06	2.18267E−02
MVO	1.73440E−06	2.60333E−06	1.63945E−05	1.73440E−06	1.92092E−06	1.73440E−06
	F25	F26	F27	F28	F29	F30
RDMVO1	5.75165E−06	1.73440E−06	1.75184E−02	2.95746E−03	9.84214E−03	**4.04835E−01**
RDMVO2	1.04444E−02	3.85424E−03	1.92092E−06	2.35342E−06	3.18168E−06	2.41470E−03
MVO	2.12664E−06	1.73440E−06	1.73440E−06	3.51524E−06	1.73440E−06	1.73440E−06

Table19 Results of RDMVO and other 7 MHAs on benchmark functions

	F1		F2		F3	
	Avg	Std	Avg	Std	Avg	Std
RDMVO	4.02138E+03	4.06951E+03	2.30823E+07	3.91837E+07	2.89987E+04	1.23424E+04
DE	**3.70467E+02**	**9.60612E+02**	1.43610E+25	2.87458E+25	2.13184E+04	5.31169E+03
WOA	2.97158E+06	2.33187E+06	2.65565E+28	1.40440E+29	1.28673E+04	5.36911E+03
GWO	3.38307E+09	2.49601E+09	2.22874E+30	1.20894E+31	3.12212E+04	9.92300E+03
HHO	1.30412E+07	2.54876E+06	3.13137E+11	7.55891E+11	2.43298E+03	9.09738E+02
BA	4.66611E+05	2.77345E+05	**2.00000E+02**	**0.00000E+00**	3.00128E+02	1.24515E-01
PSO	1.47288E+08	1.25526E+07	2.26183E+12	2.86128E+12	6.29200E+02	3.42396E+01
MVO	9.37734E+03	4.43501E+03	4.31356E+04	8.07790E+04	3.00341E+02	1.53330E-01

	F4		F5		F6	
	Avg	Std	Avg	Std	Avg	Std
RDMVO	4.57617E+02	**1.93380E+01**	**5.42184E+02**	1.56177E+01	6.00025E+02	1.85273E-02
DE	4.95109E+02	2.85747E+01	6.11481E+02	**1.07040E+01**	**6.00000E+02**	**2.11111E-14**
WOA	5.99870E+02	5.43622E+01	6.94874E+02	5.86816E+01	6.64529E+02	1.20403E+01
GWO	6.46366E+02	8.40865E+01	5.80156E+02	1.92027E+01	6.06743E+02	3.23581E+00
HHO	5.55599E+02	4.36980E+01	6.70822E+02	1.86131E+01	6.53084E+02	5.27759E+00
BA	**4.21748E+02**	3.20948E+01	7.39132E+02	5.12912E+01	6.69468E+02	1.39624E+01
PSO	4.71333E+02	3.59286E+01	6.93436E+02	2.56765E+01	6.38141E+02	1.21386E+01
MVO	4.88020E+02	3.59895E+01	5.89885E+02	2.46634E+01	6.08626E+02	8.29192E+00

	F7		F8		F9	
	Avg	Std	Avg	Std	Avg	Std
RDMVO	**7.77896E+02**	1.46429E+01	**8.39376E+02**	**7.49107E+00**	1.27090E+03	3.24529E+02
DE	8.41752E+02	**8.96678E+00**	9.10297E+02	9.34993E+00	**9.00000E+02**	**4.22222E-14**
WOA	1.29355E+03	9.40547E+01	1.09898E+03	7.77537E+01	8.24000E+03	2.51454E+03
GWO	8.85227E+02	5.26068E+01	8.87998E+02	2.03857E+01	2.20782E+03	6.55977E+02
HHO	1.31710E+03	1.10867E+02	1.07150E+03	3.60865E+01	7.63653E+03	1.05658E+03
BA	1.71270E+03	2.16832E+02	1.16137E+03	8.08038E+01	1.50402E+04	5.64531E+03
PSO	9.21056E+02	1.66604E+01	1.05558E+03	2.96124E+01	6.57845E+03	2.45242E+03
MVO	8.24787E+02	3.20899E+01	8.80779E+02	1.82736E+01	2.14689E+03	1.89031E+03

	F10		F11		F12	
	Avg	Std	Avg	Std	Avg	Std
RDMVO	**2.45437E+03**	3.09342E+02	1.18704E+03	3.02544E+01	**1.65868E+04**	**8.05749E+03**
DE	5.57030E+03	**2.75497E+02**	**1.15275E+03**	**9.39094E+00**	2.24675E+04	6.75457E+04
WOA	5.81397E+03	8.45079E+02	1.49194E+03	1.23355E+02	9.02730E+07	5.92647E+07
GWO	3.95617E+03	4.65445E+02	3.43308E+03	4.66371E+03	2.26853E+08	5.33443E+08
HHO	4.90248E+03	7.74130E+02	1.37938E+03	9.44323E+01	5.86437E+07	4.28432E+07
BA	5.33920E+03	7.20697E+02	1.47342E+03	1.27237E+02	7.81989E+06	6.07085E+06
PSO	5.57882E+03	5.48232E+02	1.37259E+03	6.12185E+01	8.69731E+07	3.39637E+07
MVO	4.04593E+03	6.10725E+02	1.29703E+03	6.25929E+01	2.10806E+07	1.12538E+07

	F13		F14		F15	
	Avg	Std	Avg	Std	Avg	Std
RDMVO	4.04836E+03	1.86362E+03	1.47750E+03	1.74360E+01	1.65141E+03	8.67070E+01
DE	**1.35442E+03**	**4.89314E+01**	**1.46360E+03**	**6.30802E+00**	**1.55076E+03**	**1.35311E+01**
WOA	9.45249E+04	8.76834E+04	3.18256E+05	1.53658E+05	4.65758E+04	4.07490E+04
GWO	7.32248E+06	1.56219E+07	9.70620E+04	1.24886E+05	9.80837E+06	3.63578E+07

Table19 (continued)

	F13		F14		F15	
	Avg	Std	Avg	Std	Avg	Std
HHO	2.80350E+05	1.99420E+05	2.94984E+04	2.38531E+04	4.29453E+04	2.68229E+04
BA	2.17148E+05	1.24910E+05	1.42126E+04	7.12012E+03	1.11810E+05	6.36655E+04
PSO	2.76646E+06	6.30056E+05	3.11301E+04	2.07255E+04	2.80770E+05	1.20357E+05
MVO	4.24015E+04	6.71448E+04	2.53289E+03	1.21512E+03	2.77791E+04	2.55218E+04
	F16		F17		F18	
	Avg	Std	Avg	Std	Avg	Std
RDMVO	**1.99172E+03**	1.64458E+02	**1.93755E+03**	1.03596E+02	**3.36402E+04**	**1.55814E+04**
DE	1.99345E+03	**1.18172E+02**	1.96331E+03	**4.25767E+01**	3.53007E+05	1.77778E+05
WOA	3.26916E+03	4.38657E+02	2.58769E+03	2.83882E+02	4.71052E+06	3.35633E+06
GWO	2.21827E+03	2.21284E+02	1.97710E+03	9.62840E+01	3.90790E+05	5.45155E+05
HHO	2.96596E+03	3.22874E+02	2.54620E+03	2.80672E+02	1.20170E+06	1.00181E+06
BA	3.32127E+03	3.44411E+02	2.81707E+03	2.87639E+02	7.62698E+04	4.92508E+04
PSO	2.73125E+03	3.16145E+02	2.41930E+03	2.87985E+02	8.65127E+04	3.15629E+04
MVO	2.29014E+03	2.44395E+02	2.06146E+03	1.24286E+02	7.21009E+04	4.39903E+04
	F19		F20		F21	
	Avg	Std	Avg	Std	Avg	Std
RDMVO	**3.25972E+03**	**2.16919E+03**	**2.17018E+03**	8.79943E+01	**2.13540E+03**	3.28592E+01
DE	5.46048E+03	2.77980E+03	2.21362E+03	**3.54927E+01**	2.20897E+03	**2.53790E+01**
WOA	4.88701E+05	5.98777E+05	2.75371E+03	1.86291E+02	2.27972E+03	3.07227E+01
GWO	3.17677E+05	1.49479E+06	2.38099E+03	1.21833E+02	2.33060E+03	9.79596E+01
HHO	1.87062E+05	1.50353E+05	2.68339E+03	1.49434E+02	2.25461E+03	3.94566E+01
BA	3.29251E+05	1.72434E+05	2.86708E+03	2.91482E+02	2.16595E+03	4.53294E+01
PSO	3.84063E+05	1.84811E+05	2.70647E+03	1.14300E+02	2.18554E+03	3.43250E+01
MVO	1.52817E+04	1.06315E+04	2.41647E+03	1.26273E+02	2.18717E+03	2.76730E+01
	F22		F23		F24	
	Avg	Std	Avg	Std	Avg	Std
RDMVO	**2.23943E+03**	1.16197E+01	2.62803E+03	1.59352E+02	2.60000E+03	1.23381E-03
DE	2.31250E+03	**1.00770E+01**	2.87187E+03	1.35061E+01	3.39846E+03	7.06307E+00
WOA	2.43868E+03	5.13164E+01	3.18330E+03	1.49534E+02	2.85340E+03	4.67879E+02
GWO	2.30913E+03	3.89652E+01	2.88320E+03	4.35181E+01	3.25862E+03	2.58487E+02
HHO	2.42466E+03	2.44984E+01	**2.50000E+03**	**0.00000E+00**	**2.60000E+03**	**0.00000E+00**
BA	2.50228E+03	6.08308E+01	3.56539E+03	3.16109E+02	2.92018E+03	5.80362E+02
PSO	2.42407E+03	2.76902E+01	4.50893E+03	5.17560E+02	2.66686E+03	3.72565E+00
MVO	2.27964E+03	2.42688E+01	2.86716E+03	2.13295E+01	3.38285E+03	1.88611E+02
	F25		F26		F27	
	Avg	Std	Avg	Std	Avg	Std
RDMVO	2.79582E+03	1.01307E+02	2.80001E+03	1.05154E-02	3.21057E+03	2.63521E+02
DE	2.91401E+03	1.31297E+01	5.35205E+03	1.37704E+02	3.43604E+03	1.76542E+01
WOA	2.71478E+03	8.09464E+01	3.52340E+03	1.89130E+03	3.94894E+03	1.70437E+02
GWO	3.18453E+03	8.81748E+01	4.66915E+03	1.24788E+03	3.71750E+03	1.49292E+02
HHO	**2.70000E+03**	**0.00000E+00**	**2.80000E+03**	**0.00000E+00**	**2.90000E+03**	**0.00000E+00**
BA	3.02137E+03	3.49925E+01	5.97692E+03	3.79893E+03	3.88138E+03	1.74093E+02
PSO	2.94651E+03	3.11603E+01	3.55804E+03	7.82562E+02	4.74821E+03	8.79335E+02
MVO	2.91528E+03	2.16476E+01	4.97979E+03	7.69209E+02	3.60387E+03	1.13808E+02

Table19 (continued)

	F28		F29		F30	
	Avg	Std	Avg	Std	Avg	Std
RDMVO	3.11550E+03	7.34960E+01	3.27329E+03	1.08483E+02	1.57119E+04	9.64417E+03
DE	3.78676E+03	6.98813E+02	3.46824E+03	8.41194E+01	6.21766E+04	2.41279E+04
WOA	3.17829E+03	5.21666E+02	4.30934E+03	2.75527E+02	2.85978E+06	2.80092E+06
GWO	3.65661E+03	2.54061E+02	3.52465E+03	1.48120E+02	1.36363E+06	2.26689E+06
HHO	**3.00000E+03**	**0.00000E+00**	**3.10000E+03**	**0.00000E+00**	**3.20000E+03**	**0.00000E+00**
BA	3.52824E+03	6.93383E+02	4.62973E+03	3.53961E+02	1.45572E+06	1.15291E+06
PSO	3.28486E+03	5.44507E+01	4.02817E+03	2.19700E+02	2.69856E+06	1.36461E+06
MVO	3.76307E+03	8.81012E+02	3.65270E+03	1.52213E+02	1.14746E+06	8.02509E+05

	Comprehensive Indicator		
	±/=	ARV	Rank
RDMVO	~	1.83	1
DE	20/8/2	3.5	2
WOA	26/2/2	6.27	8
GWO	28/0/2	5.47	6
HHO	21/9/0	4.23	4
BA	27/3/0	5.7	7
PSO	28/1/1	5.4	5
MVO	26/2/2	3.6	3

Table 20 *P* values of the Wilcoxon signed-rank test with 5% significance of experimental results for RDMVO and other 7 MHAs on benchmark functions

	F1	F2	F3	F4	F5	F6
DE	1.23808E−05	1.73440E−06	9.84214E−03	2.16302E−05	1.73440E−06	1.73440E−06
WOA	1.73440E−06	1.73440E−06	3.18168E−06	1.73440E−06	1.73440E−06	1.73440E−06
GWO	1.73440E−06	1.73440E−06	**3.82034E−01**	1.73440E−06	2.87860E−06	1.73440E−06
HHO	1.73440E−06	1.73440E−06	1.73440E−06	1.73440E−06	1.73440E−06	1.73440E−06
BA	1.73440E−06	1.73440E−06	1.73440E−06	1.48393E−03	1.73440E−06	1.73440E−06
PSO	1.73440E−06	1.73440E−06	1.73440E−06	**6.88359E−01**	1.73440E−06	1.73440E−06
MVO	2.61343E−04	1.23808E−05	1.73440E−06	8.91873E−05	4.28569E−06	1.73440E−06
	F7	F8	F9	F10	F11	F12
DE	1.73440E−06	1.73440E−06	1.73440E−06	1.73440E−06	1.49356E−05	6.83586E−03
WOA	1.73440E−06	1.73440E−06	1.73440E−06	1.73440E−06	1.73440E−06	1.73440E−06
GWO	1.73440E−06	1.73440E−06	4.28569E−06	1.92092E−06	1.73440E−06	1.73440E−06
HHO	1.73440E−06	1.73440E−06	1.73440E−06	1.73440E−06	2.12664E−06	1.73440E−06
BA	1.73440E−06	1.73440E−06	1.73440E−06	1.73440E−06	1.73440E−06	1.73440E−06
PSO	1.73440E−06	1.73440E−06	2.35342E−06	1.73440E−06	1.73440E−06	1.73440E−06
MVO	5.21649E−06	1.73440E−06	**2.89477E−01**	1.73440E−06	2.60333E−06	1.73440E−06
	F13	F14	F15	F16	F17	F18
DE	1.73440E−06	8.94430E−04	3.88218E−06	**9.09931E−01**	**7.52133E−02**	1.73440E−06
WOA	1.73440E−06	1.73440E−06	1.73440E−06	1.73440E−06	1.92092E−06	1.73440E−06
GWO	1.73440E−06	1.73440E−06	1.73440E−06	5.30699E−05	**1.41390E−01**	4.72920E−06
HHO	1.73440E−06	1.73440E−06	1.73440E−06	1.73440E−06	1.92092E−06	1.73440E−06
BA	1.73440E−06	1.73440E−06	1.73440E−06	1.73440E−06	1.73440E−06	4.89690E−04
PSO	1.73440E−06	1.73440E−06	1.73440E−06	1.92092E−06	4.72920E−06	3.18168E−06
MVO	1.73440E−06	1.73440E−06	1.73440E−06	5.30699E−05	2.10526E−03	1.47728E−04
	F19	F20	F21	F22	F23	F24
DE	1.03568E−03	1.85190E−02	1.73440E−06	1.73440E−06	1.92092E−06	1.73440E−06
WOA	1.73440E−06	1.73440E−06	1.73440E−06	1.73440E−06	1.73440E−06	**3.70935E−01**
GWO	2.35342E−06	4.28569E−06	1.73440E−06	1.73440E−06	1.92092E−06	2.35342E−06
HHO	1.73440E−06	1.73440E−06	1.92092E−06	1.73440E−06	1.73440E−06	1.73440E−06
BA	1.73440E−06	1.73440E−06	1.24526E−02	1.73440E−06	1.73440E−06	1.73440E−06
PSO	1.73440E−06	1.73440E−06	3.40526E−05	1.73440E−06	1.73440E−06	1.73440E−06
MVO	2.37045E−05	4.28569E−06	6.98378E−06	2.87860E−06	1.73440E−06	1.73440E−06
	F25	F26	F27	F28	F29	F30
DE	2.87860E−06	1.73440E−06	4.19551E−04	1.73440E−06	2.87860E−06	1.73440E−06
WOA	3.11232E−05	1.47954E−02	1.73440E−06	**3.18491E−01**	1.73440E−06	7.69086E−06
GWO	1.73440E−06	5.30699E−05	1.73440E−06	1.73440E−06	2.87860E−06	1.73440E−06
HHO	1.73440E−06	1.73440E−06	1.73440E−06	1.73440E−06	1.73440E−06	1.73440E−06
BA	1.73440E−06	1.73440E−06	1.73440E−06	1.73440E−06	1.73440E−06	1.73440E−06
PSO	1.73440E−06	1.73440E−06	2.35342E−06	1.73440E−06	1.73440E−06	1.73440E−06
MVO	6.33914E−06	1.73440E−06	2.35342E−06	1.73440E−06	1.73440E−06	1.73440E−06

Table 21 The maximum fitness of combinatorial variants

Image	Thresholds	RDMVO	RDMVO1	RDMVO2	MVO
35070	2	**24.50020521**	**24.50020521**	24.16038019	23.95771111
	3	31.62484757	**31.68032015**	29.92649457	29.67929878
	4	**37.99096769**	37.60192008	35.26405088	35.36208612
38092	2	**25.49740767**	25.49735558	25.40865083	25.26465293
	3	32.0244545	**32.02531431**	31.67356148	31.72523597
	4	**38.06844885**	38.06664285	37.38185051	37.1659707
61060	2	**24.38674932**	**24.38674932**	23.90823716	24.2043071
	3	30.82591001	**30.83766353**	29.56627095	30.40616374
	4	**36.86230864**	36.85998578	36.10292269	35.67639678
100080	2	25.21720506	**25.26821172**	24.904261	25.10303361
	3	32.52113555	**32.54555546**	31.23230994	31.44966449
	4	**38.67393765**	38.67385625	36.97302928	35.92537722
108005	2	**23.69940604**	**23.69940604**	23.68551392	23.64983201
	3	**29.96229579**	**29.96229579**	29.94564818	29.87885301
	4	35.83732569	**35.83799862**	35.68677282	35.35814405
253027	2	**25.48654174**	25.48596609	25.36847788	25.09813118
	3	32.49228812	**32.49488628**	31.82286633	32.10355454
	4	**38.84857345**	38.84365632	37.88580233	36.74702973
291000	2	**25.09936552**	**25.09936552**	25.05896928	25.04948113
	3	31.89662919	**31.89704051**	31.80278711	31.71044423
	4	**38.09218105**	38.09074556	37.67382585	37.85488294
314016	2	**24.3397268**	**24.3397268**	24.33575855	24.32992203
	3	**30.67271529**	30.67267969	30.64488197	30.5919973
	4	**36.84559613**	36.84470406	36.73111368	36.56449912
317080	2	22.84722493	**22.85008789**	22.59330826	22.70301868
	3	29.67265318	**29.67692482**	28.87634834	28.56676689
	4	**36.13282835**	36.13134964	35.27896283	34.62224903

Table 22 Results for each algorithm on PSNR

Image	Thresholds	Item	RDMVO	MVO	ACOR	BA	WOA
35070	2	Avg	**1.67280E+01**	1.41717E+01	1.36596E+01	1.23798E+01	1.49069E+01
		Std	2.39321E+00	3.72565E+00	3.41117E+00	3.82471E+00	3.22318E+00
	3	Avg	**1.84386E+01**	1.64681E+01	1.76880E+01	1.69045E+01	1.66946E+01
		Std	1.40854E+00	2.80627E+00	**1.27414E+00**	2.81762E+00	3.98030E+00
	4	Avg	**2.01217E+01**	1.72420E+01	1.86473E+01	1.71161E+01	1.62363E+01
		Std	**1.12871E+00**	3.68308E+00	1.16767E+00	3.15653E+00	3.49683E+00
	5	Avg	**2.15629E+01**	1.81459E+01	1.94692E+01	1.90713E+01	1.92109E+01
		Std	**1.26996E+00**	3.75363E+00	1.50972E+00	3.27409E+00	3.87636E+00
			SSA	DE	AVOA	CLPSO	HHO
	2	Avg	1.38244E+01	1.66222E+01	1.35911E+01	1.57597E+01	1.32925E+01
		Std	4.00729E+00	**1.28800E+00**	3.78242E+00	2.45489E+00	3.68845E+00
	3	Avg	1.56150E+01	1.70572E+01	1.70063E+01	1.69639E+01	1.71906E+01
		Std	2.88820E+00	2.16299E+00	2.47791E+00	3.04369E+00	1.84738E+00
	4	Avg	1.80705E+01	1.91132E+01	1.87046E+01	1.76513E+01	1.92865E+01
		Std	1.81126E+00	1.18640E+00	2.05235E+00	3.89240E+00	2.42267E+00
	5	Avg	1.84807E+01	1.97540E+01	1.92050E+01	1.84599E+01	1.93759E+01
		Std	1.90513E+00	1.70004E+00	2.29163E+00	2.60772E+00	2.57780E+00
Image	Thresholds	Item	RDMVO	MVO	ACOR	BA	WOA
38092	2	Avg	**1.38148E+01**	1.29070E+01	1.28018E+01	1.26251E+01	1.29253E+01
		Std	**4.38269E−02**	8.88204E−01	6.94279E−01	1.01660E+00	3.06867E−01
	3	Avg	1.61943E+01	1.58467E+01	**1.63996E+01**	1.63027E+01	1.56209E+01
		Std	**1.16189E−01**	1.04572E+00	5.83986E−01	1.04229E+00	7.69615E−01
	4	Avg	1.83808E+01	1.67743E+01	**1.87080E+01**	1.80556E+01	1.80491E+01
		Std	**1.38939E−01**	1.80318E+00	3.57148E−01	2.17380E+00	9.49956E−01
	5	Avg	1.97300E+01	1.84424E+01	**2.02869E+01**	1.98788E+01	1.95353E+01
		Std	4.04505E−01	1.52018E+00	3.66163E−01	1.41325E+00	1.04294E+00
			SSA	DE	AVOA	CLPSO	HHO
	2	Avg	1.29471E+01	1.31969E+01	1.30242E+01	1.28184E+01	1.25146E+01
		Std	2.80085E−01	4.23497E−01	3.77426E−01	6.07335E−01	1.38990E+00
	3	Avg	1.60839E+01	1.63491E+01	1.62944E+01	1.56392E+01	1.56402E+01
		Std	8.43680E−01	6.15017E−01	6.05478E−01	1.13514E+00	7.09047E−01
	4	Avg	1.83728E+01	1.85734E+01	1.86409E+01	1.75506E+01	1.73203E+01
		Std	9.47994E−01	3.54888E−01	4.41919E−01	1.12129E+00	2.20875E+00
	5	Avg	1.98388E+01	2.00661E+01	2.00143E+01	1.87341E+01	1.89333E+01
		Std	8.34064E−01	**3.20859E−01**	4.14250E−01	1.00976E+00	1.61224E+00
Image	Thresholds	Item	RDMVO	MVO	ACOR	BA	WOA
61060	2	Avg	**1.60580E+01**	1.31222E+01	1.39769E+01	1.29992E+01	1.35202E+01
		Std	**4.03248E−01**	1.77599E+00	1.90140E+00	2.92237E+00	1.95824E+00
	3	Avg	**1.80594E+01**	1.50624E+01	1.50082E+01	1.53866E+01	1.51763E+01
		Std	**4.29967E−01**	2.04116E+00	1.25253E+00	2.45383E+00	1.64446E+00
	4	Avg	**1.87187E+01**	1.70826E+01	1.69167E+01	1.66415E+01	1.66021E+01
		Std	**6.20340E−01**	1.57855E+00	1.26390E+00	2.12000E+00	2.06828E+00
	5	Avg	**2.00089E+01**	1.75481E+01	1.88459E+01	1.87356E+01	1.79860E+01
		Std	**9.91382E−01**	1.98291E+00	1.63993E+00	1.28767E+00	1.59232E+00

Table 22 (continued)

			SSA	DE	AVOA	CLPSO	HHO
	2	Avg	1.36413E+01	1.43339E+01	1.36379E+01	1.35281E+01	1.24804E+01
		Std	1.62259E+00	1.84115E+00	1.56474E+00	1.80987E+00	2.35864E+00
	3	Avg	1.52699E+01	1.51358E+01	1.53692E+01	1.53899E+01	1.53266E+01
		Std	1.53935E+00	1.55119E+00	1.89073E+00	1.56799E+00	1.39254E+00
	4	Avg	1.77578E+01	1.71702E+01	1.72079E+01	1.68841E+01	1.62411E+01
		Std	1.27373E+00	1.11527E+00	1.97330E+00	1.61672E+00	2.03318E+00
	5	Avg	1.83556E+01	1.88181E+01	1.85665E+01	1.74877E+01	1.83416E+01
		Std	1.16861E+00	1.47001E+00	1.80142E+00	1.67664E+00	1.25823E+00
Image	Thresholds	Item	RDMVO	MVO	ACOR	BA	WOA
100080	2	Avg	**1.71337E+01**	1.38428E+01	1.55850E+01	1.37948E+01	1.54428E+01
		Std	**6.16427E−01**	3.36592E+00	1.61748E+00	2.21437E+00	3.13187E+00
	3	Avg	1.85834E+01	1.55172E+01	1.79167E+01	1.62454E+01	1.65668E+01
		Std	**9.23527E−01**	3.22760E+00	9.92578E−01	3.26761E+00	2.52816E+00
	4	Avg	2.02066E+01	1.82411E+01	**2.07741E+01**	1.73443E+01	1.77377E+01
		Std	**1.33248E+00**	3.50937E+00	1.33679E+00	3.72131E+00	3.28023E+00
	5	Avg	2.14528E+01	1.88055E+01	**2.16931E+01**	1.93972E+01	1.80553E+01
		Std	1.78239E+00	2.93918E+00	**1.44132E+00**	3.75909E+00	4.21904E+00
			SSA	DE	AVOA	CLPSO	HHO
	2	Avg	1.42374E+01	1.65923E+01	1.43858E+01	1.54275E+01	1.53195E+01
		Std	2.46523E+00	8.46991E−01	2.42637E+00	2.42564E+00	2.46819E+00
	3	Avg	1.63878E+01	**1.89251E+01**	1.68303E+01	1.72632E+01	1.76398E+01
		Std	2.92741E+00	1.10562E+00	2.60487E+00	2.70474E+00	2.06681E+00
	4	Avg	1.80018E+01	1.95615E+01	1.88973E+01	1.81542E+01	1.81453E+01
		Std	2.34488E+00	2.05362E+00	2.34042E+00	2.15504E+00	2.89297E+00
	5	Avg	1.94830E+01	2.08955E+01	2.01356E+01	1.88676E+01	1.96047E+01
		Std	2.51570E+00	1.50580E+00	2.32042E+00	2.51260E+00	3.16087E+00
Image	Thresholds	Item	RDMVO	MVO	ACOR	BA	WOA
108005	2	Avg	1.53483E+01	1.50415E+01	1.53374E+01	1.48677E+01	**1.54917E+01**
		Std	5.29095E−02	6.02887E−01	**3.32016E−02**	7.29528E−01	3.26451E−01
	3	Avg	1.68429E+01	1.73204E+01	1.72455E+01	1.72256E+01	1.72919E+01
		Std	**2.11830E−01**	1.14079E+00	5.75621E−01	1.28563E+00	6.76819E−01
	4	Avg	**2.02346E+01**	1.87556E+01	1.98567E+01	1.94612E+01	1.96594E+01
		Std	**6.72055E−02**	1.56946E+00	5.02153E−01	1.28552E+00	8.22650E−01
	5	Avg	**2.17752E+01**	2.03679E+01	2.14471E+01	2.10823E+01	2.10995E+01
		Std	**1.82398E−01**	1.41666E+00	4.87948E−01	8.94469E−01	6.53988E−01
			SSA	DE	AVOA	CLPSO	HHO
	2	Avg	1.53442E+01	1.53174E+01	1.52779E+01	1.52645E+01	1.52803E+01
		Std	2.27622E−01	1.29156E−01	1.65165E−01	6.75504E−01	4.10683E−01
	3	Avg	**1.76227E+01**	1.70271E+01	1.72020E+01	1.71027E+01	1.71583E+01
		Std	7.93173E−01	6.03002E−01	6.62297E−01	9.39202E−01	1.15316E+00
	4	Avg	1.96096E+01	1.98407E+01	2.00077E+01	1.89225E+01	1.91567E+01
		Std	7.39808E−01	5.24978E−01	5.06719E−01	1.23225E+00	1.63563E+00
	5	Avg	2.12017E+01	2.12473E+01	2.13640E+01	1.92179E+01	2.06911E+01
		Std	5.68664E−01	6.88499E−01	7.76764E−01	1.76491E+00	1.45997E+00
Image	Thresholds	Item	RDMVO	MVO	ACOR	BA	WOA

Table 22 (continued)

Image	Thresholds	Item	RDMVO	MVO	ACOR	BA	WOA
253027	2	Avg	1.35263E+01	1.26240E+01	**1.47376E+01**	1.43774E+01	1.34546E+01
		Std	**2.53357E−01**	2.76737E+00	1.22349E+00	1.54254E+00	2.03561E+00
	3	Avg	1.71723E+01	1.56420E+01	**1.73580E+01**	1.61864E+01	1.61792E+01
		Std	8.19773E−01	2.27663E+00	**5.25369E−01**	2.32060E+00	2.37431E+00
	4	Avg	**1.92281E+01**	1.78613E+01	1.89973E+01	1.85342E+01	1.83453E+01
		Std	**2.85648E−01**	1.47023E+00	9.24065E−01	2.02354E+00	1.71807E+00
	5	Avg	**2.07815E+01**	1.83833E+01	2.05214E+01	2.03059E+01	1.82778E+01
		Std	**3.33356E−01**	1.55265E+00	6.77426E−01	1.68354E+00	2.71910E+00
			SSA	DE	AVOA	CLPSO	HHO
	2	Avg	1.36916E+01	1.46537E+01	1.42559E+01	1.37139E+01	1.35945E+01
		Std	2.15376E+00	7.07903E−01	1.42448E+00	1.04515E+00	2.52958E+00
	3	Avg	1.65821E+01	1.73462E+01	1.53099E+01	1.59443E+01	1.64154E+01
		Std	1.87565E+00	7.33852E−01	2.40542E+00	1.85199E+00	1.37898E+00
	4	Avg	1.88607E+01	1.90047E+01	1.87517E+01	1.82892E+01	1.77869E+01
		Std	1.19806E+00	5.55966E−01	1.10679E+00	1.94209E+00	1.72912E+00
	5	Avg	1.97671E+01	2.03369E+01	1.99485E+01	1.91182E+01	1.93492E+01
		Std	1.65023E+00	7.05819E−01	1.05591E+00	1.51118E+00	1.40998E+00
Image	Thresholds	Item	RDMVO	MVO	ACOR	BA	WOA
291000	2	Avg	1.42354E+01	1.38730E+01	**1.43669E+01**	1.42045E+01	1.42943E+01
		Std	1.05092E−01	8.81088E−01	**1.03926E−01**	4.65296E−01	3.44132E−01
	3	Avg	1.69667E+01	1.64760E+01	**1.70016E+01**	1.69645E+01	1.64702E+01
		Std	1.43792E−01	7.50035E−01	**1.35091E−01**	2.14980E−01	1.24377E+00
	4	Avg	1.86500E+01	1.73628E+01	1.87020E+01	**1.89434E+01**	1.82076E+01
		Std	**1.64950E−01**	1.57243E+00	1.91627E−01	3.64913E−01	8.23084E−01
	5	Avg	2.02734E+01	1.85555E+01	**2.03454E+01**	2.01707E+01	1.94717E+01
		Std	2.70821E−01	1.35485E+00	**1.27184E−01**	6.54720E−01	8.25527E−01
			SSA	DE	AVOA	CLPSO	HHO
	2	Avg	1.41871E+01	1.42674E+01	1.43425E+01	1.40079E+01	1.38689E+01
		Std	3.10482E−01	1.30982E−01	2.14239E−01	4.32210E−01	6.44744E−01
	3	Avg	1.69177E+01	1.69442E+01	1.69408E+01	1.59056E+01	1.62196E+01
		Std	3.63749E−01	1.41582E−01	3.12029E−01	7.83532E−01	9.02026E−01
	4	Avg	1.82998E+01	1.86684E+01	1.87749E+01	1.76199E+01	1.78648E+01
		Std	5.38945E−01	1.91650E−01	3.95618E−01	1.21224E+00	7.72283E−01
	5	Avg	1.95931E+01	1.99874E+01	1.99491E+01	1.90403E+01	1.90915E+01
		Std	1.00934E+00	3.90546E−01	5.42652E−01	7.36728E−01	1.13066E+00
Image	Thresholds	Item	RDMVO	MVO	ACOR	BA	WOA
314016	2	Avg	**1.51056E+01**	1.48617E+01	1.50838E+01	1.38715E+01	1.47882E+01
		Std	**3.67831E−02**	2.41071E−01	5.30646E−02	2.38513E+00	3.63331E−01
	3	Avg	**1.79277E+01**	1.67874E+01	1.72290E+01	1.71833E+01	1.76021E+01
		Std	**3.91787E−02**	1.00842E+00	9.67863E−01	9.75058E−01	4.46821E−01
	4	Avg	**1.90471E+01**	1.77571E+01	1.89126E+01	1.88976E+01	1.84479E+01
		Std	**8.49912E−02**	1.22851E+00	2.26949E−01	7.03050E−01	8.15413E−01
	5	Avg	**2.09671E+01**	1.87197E+01	2.08492E+01	2.01641E+01	2.01543E+01
		Std	**1.10170E−01**	1.63707E+00	1.94306E−01	3.12275E+00	1.16782E+00

Table 22 (continued)

			SSA	DE	AVOA	CLPSO	HHO
	2	Avg	1.50361E+01	1.51051E+01	1.50346E+01	1.46842E+01	1.45396E+01
		Std	1.28510E−01	6.09725E−02	9.84233E−02	4.46605E−01	7.22943E−01
	3	Avg	1.71432E+01	1.76455E+01	1.73058E+01	1.66956E+01	1.75247E+01
		Std	8.79296E−01	4.73816E−01	8.60074E−01	1.29397E+00	4.98606E−01
	4	Avg	1.87611E+01	1.87804E+01	1.87676E+01	1.77033E+01	1.85466E+01
		Std	5.43718E−01	3.12183E−01	4.10680E−01	1.17145E+00	1.12807E+00
	5	Avg	1.99899E+01	2.02692E+01	2.04070E+01	1.92923E+01	1.97856E+01
		Std	9.31288E−01	5.71445E−01	9.59248E−01	1.32967E+00	1.15774E+00
Image	Thresholds	Item	RDMVO	MVO	ACOR	BA	WOA
317080	2	Avg	1.52162E+01	1.52310E+01	1.43408E+01	1.45323E+01	1.47119E+01
		Std	5.75741E−01	1.27003E+00	**4.23437E−01**	1.38355E+00	1.04174E+00
	3	Avg	1.83050E+01	1.76722E+01	1.73711E+01	1.79395E+01	1.81897E+01
		Std	1.61918E+00	1.46510E+00	**9.88610E−01**	1.34209E+00	1.42864E+00
	4	Avg	**2.09740E+01**	1.93707E+01	2.06474E+01	2.06057E+01	2.02082E+01
		Std	4.65021E−01	2.05660E+00	**3.53055E−01**	1.36756E+00	1.25775E+00
	5	Avg	2.21595E+01	2.00757E+01	**2.24948E+01**	2.20799E+01	2.19791E+01
		Std	5.39185E−01	1.84746E+00	**3.30191E−01**	9.10483E−01	1.34239E+00
			SSA	DE	AVOA	CLPSO	HHO
	2	Avg	1.45286E+01	1.49970E+01	1.46195E+01	**1.60130E+01**	1.49850E+01
		Std	5.66635E−01	8.73408E−01	7.46065E−01	1.04355E+00	1.12196E+00
	3	Avg	1.81688E+01	1.82611E+01	1.81509E+01	1.75218E+01	**1.86593E+01**
		Std	1.13356E+00	1.13843E+00	1.18533E+00	1.61658E+00	1.25812E+00
	4	Avg	2.07175E+01	2.04677E+01	2.04961E+01	1.92015E+01	2.05249E+01
		Std	1.15129E+00	7.59324E−01	1.09095E+00	1.34249E+00	1.36550E+00
	5	Avg	2.15348E+01	2.21433E+01	2.24324E+01	2.07806E+01	2.11170E+01
		Std	1.21543E+00	4.53304E−01	8.56399E−01	1.11948E+00	1.61204E+00

Table 23 Results for each algorithm on SSIM

Image	Thresholds	Item	RDMVO	MVO	ACOR	BA	WOA
35070	2	Avg	5.82458E−01	4.69236E−01	4.35705E−01	3.48059E−01	5.13570E−01
		Std	1.06807E−01	2.27811E−01	2.22217E−01	2.45689E−01	1.89909E−01
	3	Avg	**6.70272E−01**	6.10478E−01	6.29304E−01	5.94455E−01	5.94452E−01
		Std	**4.74704E−02**	1.14219E−01	5.53033E−02	1.50092E−01	1.75342E−01
	4	Avg	**6.96250E−01**	6.35169E−01	6.77580E−01	5.98576E−01	6.01862E−01
		Std	3.82026E−02	1.28073E−01	4.70200E−02	1.05372E−01	1.93099E−01
	5	Avg	**7.05683E−01**	6.41129E−01	7.04192E−01	6.68358E−01	6.49082E−01
		Std	2.84673E−02	1.39820E−01	3.26758E−02	1.42962E−01	1.86903E−01
			SSA	DE	AVOA	CLPSO	HHO
	2	Avg	4.34318E−01	**6.12753E−01**	4.12451E−01	5.77049E−01	4.52703E−01
		Std	2.44440E−01	**2.75036E−02**	2.23887E−01	1.11963E−01	2.40684E−01
	3	Avg	5.73813E−01	6.12224E−01	6.02477E−01	6.05675E−01	6.29744E−01
		Std	1.42954E−01	7.61610E−02	1.27115E−01	1.04517E−01	7.78595E−02
	4	Avg	6.72734E−01	6.94237E−01	6.68294E−01	6.16722E−01	6.69773E−01
		Std	6.00625E−02	**3.69421E−02**	4.55969E−02	1.72364E−01	5.91850E−02
	5	Avg	6.80089E−01	6.99481E−01	6.83375E−01	6.68692E−01	7.01170E−01
		Std	3.33777E−02	**2.61114E−02**	4.88234E−02	5.26131E−02	5.26053E−02
Image	Thresholds	Item	RDMVO	MVO	ACOR	BA	WOA
38092	2	Avg	**5.81106E−01**	5.54831E−01	5.62056E−01	5.50393E−01	5.78827E−01
		Std	**3.26665E−03**	4.51874E−02	5.56053E−02	7.86473E−02	4.04128E−03
	3	Avg	**6.96135E−01**	6.37586E−01	6.82541E−01	6.70714E−01	6.84428E−01
		Std	**2.15613E−03**	4.24723E−02	1.66516E−02	3.16809E−02	3.54471E−02
	4	Avg	**7.46590E−01**	6.73369E−01	7.42540E−01	7.09139E−01	7.21338E−01
		Std	**4.10756E−03**	6.91246E−02	8.98803E−03	8.42539E−02	2.80614E−02
	5	Avg	**7.98782E−01**	7.39516E−01	7.97016E−01	7.83391E−01	7.72962E−01
		Std	8.53817E−03	5.17737E−02	**3.99880E−03**	3.29883E−02	2.32505E−02
			SSA	DE	AVOA	CLPSO	HHO
	2	Avg	5.70080E−01	5.69814E−01	5.74868E−01	5.59638E−01	5.56804E−01
		Std	3.68272E−02	3.27000E−02	1.46853E−02	4.26657E−02	7.23257E−02
	3	Avg	6.64895E−01	6.65868E−01	6.71907E−01	6.55801E−01	6.75777E−01
		Std	2.90419E−02	2.99855E−02	2.68223E−02	3.49942E−02	4.06068E−02
	4	Avg	7.29917E−01	7.37534E−01	7.22087E−01	7.01669E−01	6.94601E−01
		Std	3.00925E−02	1.12737E−02	1.81987E−02	2.60537E−02	6.91072E−02
	5	Avg	7.76592E−01	7.85841E−01	7.79448E−01	7.32407E−01	7.56116E−01
		Std	2.69575E−02	1.47684E−02	1.98778E−02	3.94748E−02	4.18123E−02
Image	Thresholds	Item	RDMVO	MVO	ACOR	BA	WOA
61060	2	Avg	**7.23358E−01**	6.63423E−01	6.89739E−01	6.58243E−01	6.56746E−01
		Std	**5.70258E−03**	4.50840E−02	4.12771E−02	1.16086E−01	6.82090E−02
	3	Avg	**7.73461E−01**	7.24893E−01	7.18052E−01	7.13724E−01	7.17861E−01
		Std	2.92704E−02	4.56598E−02	**2.48077E−02**	7.94144E−02	3.33883E−02
	4	Avg	**7.90666E−01**	7.69187E−01	7.74063E−01	7.55301E−01	7.59108E−01
		Std	2.81497E−02	4.01223E−02	**2.66666E−02**	3.87458E−02	4.10301E−02
	5	Avg	**8.21290E−01**	7.74410E−01	8.10197E−01	8.10458E−01	7.84315E−01
		Std	**2.36482E−02**	5.09315E−02	3.92915E−02	2.59066E−02	3.48654E−02

Table 23 (continued)

			SSA	DE	AVOA	CLPSO	HHO
	2	Avg	6.90304E−01	7.03016E−01	6.87757E−01	6.84948E−01	6.50821E−01
		Std	2.64404E−02	2.43392E−02	2.51872E−02	3.50589E−02	7.00513E−02
	3	Avg	7.11706E−01	7.18986E−01	7.28545E−01	7.11778E−01	7.12811E−01
		Std	2.62413E−02	3.38088E−02	3.14018E−02	4.37929E−02	4.64758E−02
	4	Avg	7.75253E−01	7.75591E−01	7.76077E−01	7.68524E−01	7.45672E−01
		Std	3.96822E−02	3.03157E−02	3.85826E−02	4.45424E−02	4.60820E−02
	5	Avg	7.91693E−01	7.95047E−01	7.99813E−01	7.91034E−01	7.88178E−01
		Std	3.93137E−02	3.75672E−02	4.74277E−02	3.51399E−02	3.05523E−02
Image	Thresholds	Item	RDMVO	MVO	ACOR	BA	WOA
100080	2	Avg	**6.48150E−01**	4.80738E−01	5.33696E−01	4.91541E−01	5.24477E−01
		Std	6.45867E−02	2.04191E−01	9.62743E−02	1.26704E−01	1.86027E−01
	3	Avg	6.67078E−01	5.74375E−01	6.58841E−01	5.71467E−01	6.38962E−01
		Std	7.12438E−02	1.23708E−01	**5.86022E−02**	1.89038E−01	1.05692E−01
	4	Avg	7.37452E−01	6.89014E−01	**7.54136E−01**	6.36445E−01	6.39092E−01
		Std	6.26707E−02	1.25551E−01	**5.00229E−02**	1.87983E−01	1.25631E−01
	5	Avg	7.62333E−01	6.94221E−01	**7.82829E−01**	7.14665E−01	6.80710E−01
		Std	7.12061E−02	9.94098E−02	**4.53228E−02**	1.21486E−01	1.85030E−01
			SSA	DE	AVOA	CLPSO	HHO
	2	Avg	4.84632E−01	5.41478E−01	4.67513E−01	5.13253E−01	5.35195E−01
		Std	1.61461E−01	**4.71825E−02**	1.44787E−01	1.04757E−01	1.40204E−01
	3	Avg	6.03017E−01	**6.96713E−01**	6.23705E−01	6.39143E−01	6.39289E−01
		Std	1.77969E−01	8.23299E−02	1.10244E−01	1.27813E−01	1.17112E−01
	4	Avg	6.72732E−01	6.97989E−01	6.91727E−01	6.97154E−01	6.71087E−01
		Std	9.94391E−02	8.01619E−02	1.03964E−01	8.16534E−02	1.37119E−01
	5	Avg	7.17031E−01	7.46513E−01	7.40234E−01	7.06265E−01	7.33878E−01
		Std	1.15596E−01	6.44613E−02	7.96074E−02	1.02643E−01	8.79443E−02
Image	Thresholds	Item	RDMVO	MVO	ACOR	BA	WOA
108005	2	Avg	4.08903E−01	3.88695E−01	4.08488E−01	3.75426E−01	**4.18838E−01**
		Std	3.49155E−03	4.11799E−02	**3.01125E−03**	5.21718E−02	2.06468E−02
	3	Avg	4.88635E−01	5.29207E−01	5.14318E−01	5.16540E−01	5.22090E−01
		Std	**1.20139E−02**	7.68177E−02	3.56677E−02	8.47329E−02	4.20295E−02
	4	Avg	**6.84747E−01**	6.10814E−01	6.59319E−01	6.39286E−01	6.63144E−01
		Std	**4.58962E−03**	1.01147E−01	3.26189E−02	7.78044E−02	5.00997E−02
	5	Avg	**7.55903E−01**	6.99006E−01	7.34316E−01	7.21210E−01	7.24933E−01
		Std	**1.34612E−02**	6.70313E−02	2.76551E−02	4.81291E−02	3.20552E−02
			SSA	DE	AVOA	CLPSO	HHO
	2	Avg	4.09338E−01	4.07133E−01	4.04374E−01	4.03890E−01	4.04027E−01
		Std	1.65840E−02	8.33258E−03	1.19272E−02	4.71494E−02	2.77325E−02
	3	Avg	**5.39350E−01**	5.00022E−01	5.12861E−01	5.09079E−01	5.14234E−01
		Std	5.16993E−02	3.59112E−02	4.08208E−02	5.91204E−02	7.27443E−02
	4	Avg	6.51603E−01	6.60462E−01	6.77221E−01	6.22289E−01	6.32101E−01
		Std	4.86429E−02	3.43335E−02	3.41944E−02	7.81949E−02	9.86491E−02
	5	Avg	7.32285E−01	7.28106E−01	7.31344E−01	6.49648E−01	7.07620E−01
		Std	2.27032E−02	3.69407E−02	4.36396E−02	9.77104E−02	7.24425E−02

Table 23 (continued)

Image	Thresholds	Item	RDMVO	MVO	ACOR	BA	WOA
253027	2	Avg	4.46795E−01	4.32115E−01	5.34750E−01	5.23006E−01	4.69344E−01
		Std	**1.52891E−02**	1.73799E−01	7.02233E−02	9.38568E−02	1.24885E−01
	3	Avg	6.36349E−01	5.83712E−01	**6.64747E−01**	6.02270E−01	6.14161E−01
		Std	**2.13466E−02**	1.05822E−01	3.83127E−02	1.26031E−01	1.23459E−01
	4	Avg	**7.30680E−01**	6.75521E−01	7.19265E−01	6.91064E−01	6.85199E−01
		Std	**6.17018E−03**	5.42707E−02	3.21652E−02	9.03587E−02	6.60271E−02
	5	Avg	**7.69413E−01**	6.88633E−01	7.58773E−01	7.53670E−01	6.88058E−01
		Std	**1.19464E−02**	6.02141E−02	3.01257E−02	5.95944E−02	9.58146E−02
			SSA	DE	AVOA	CLPSO	HHO
	2	Avg	4.90921E−01	**5.39745E−01**	5.11097E−01	4.75396E−01	4.62836E−01
		Std	1.32526E−01	4.85048E−02	8.93665E−02	7.04740E−02	1.51175E−01
	3	Avg	6.31972E−01	6.59437E−01	5.46960E−01	6.03123E−01	6.34035E−01
		Std	9.12138E−02	3.51190E−02	1.27639E−01	9.47740E−02	5.44976E−02
	4	Avg	7.05092E−01	7.20018E−01	6.97387E−01	6.81322E−01	6.71941E−01
		Std	4.67451E−02	1.52104E−02	4.55363E−02	8.64394E−02	6.13281E−02
	5	Avg	7.28150E−01	7.51714E−01	7.38645E−01	7.17908E−01	7.25136E−01
		Std	5.22119E−02	2.17400E−02	4.02500E−02	4.76061E−02	5.29094E−02
Image	Thresholds	Item	RDMVO	MVO	ACOR	BA	WOA
291000	2	Avg	6.08396E−01	5.77687E−01	**6.15340E−01**	6.10515E−01	6.12159E−01
		Std	**5.26691E−03**	5.05115E−02	1.12490E−02	1.87413E−02	1.29102E−02
	3	Avg	**7.52809E−01**	7.24613E−01	7.52304E−01	7.49722E−01	7.24454E−01
		Std	4.31051E−03	3.59781E−02	**2.40736E−03**	7.66247E−03	5.96453E−02
	4	Avg	8.19919E−01	7.56075E−01	8.22844E−01	**8.26649E−01**	7.95327E−01
		Std	**5.62644E−03**	7.47802E−02	6.05612E−03	9.73529E−03	3.14059E−02
	5	Avg	8.68349E−01	8.04532E−01	**8.68807E−01**	8.62939E−01	8.33577E−01
		Std	6.87293E−03	4.56219E−02	**4.30136E−03**	1.83892E−02	3.17810E−02
			SSA	DE	AVOA	CLPSO	HHO
	2	Avg	5.97525E−01	6.09684E−01	6.10436E−01	5.91531E−01	5.96259E−01
		Std	2.94696E−02	7.01137E−03	1.70211E−02	3.18653E−02	3.26043E−02
	3	Avg	7.44741E−01	7.51282E−01	7.48167E−01	7.00673E−01	7.14694E−01
		Std	1.94115E−02	4.69371E−03	1.01169E−02	4.05839E−02	3.72257E−02
	4	Avg	8.04776E−01	8.20318E−01	8.19113E−01	7.75737E−01	7.87257E−01
		Std	1.91485E−02	6.47797E−03	1.39386E−02	4.49436E−02	2.72753E−02
	5	Avg	8.43163E−01	8.57072E−01	8.54673E−01	8.20146E−01	8.21750E−01
		Std	2.95221E−02	1.40499E−02	1.58043E−02	2.77740E−02	3.66466E−02
Image	Thresholds	Item	RDMVO	MVO	ACOR	BA	WOA
314016	2	Avg	**4.80013E−01**	4.69456E−01	4.78609E−01	4.15657E−01	4.68320E−01
		Std	**7.49083E−04**	1.00233E−02	2.89272E−03	1.16705E−01	1.15230E−02
	3	Avg	**6.16863E−01**	5.68216E−01	5.83702E−01	5.80985E−01	6.03291E−01
		Std	**2.26887E−03**	4.62627E−02	4.49783E−02	4.44358E−02	1.90775E−02
	4	Avg	**6.54529E−01**	6.13744E−01	6.50693E−01	6.52505E−01	6.36124E−01
		Std	**3.81747E−03**	5.02278E−02	1.00712E−02	3.08432E−02	2.90607E−02
	5	Avg	**7.38898E−01**	6.53836E−01	7.34575E−01	7.02610E−01	7.09029E−01
		Std	**4.60055E−03**	6.55131E−02	8.02500E−03	1.48159E−01	4.20708E−02

Table 23 (continued)

			SSA	DE	AVOA	CLPSO	HHO
	2	Avg	4.77515E−01	4.79749E−01	4.76767E−01	4.59531E−01	4.60662E−01
		Std	4.04006E−03	1.91614E−03	3.82535E−03	1.95845E−02	2.27774E−02
	3	Avg	5.80860E−01	6.03408E−01	5.89722E−01	5.68245E−01	6.00407E−01
		Std	4.10639E−02	2.33710E−02	3.78817E−02	5.33743E−02	2.15538E−02
	4	Avg	6.48661E−01	6.45955E−01	6.47579E−01	6.10069E−01	6.46510E−01
		Std	2.18596E−02	1.23669E−02	1.50932E−02	4.48866E−02	4.09525E−02
	5	Avg	7.02802E−01	7.13122E−01	7.18268E−01	6.77407E−01	6.98232E−01
		Std	3.48042E−02	2.11998E−02	3.50233E−02	5.06536E−02	4.73992E−02
Image	Thresholds	Item	RDMVO	MVO	ACOR	BA	WOA
317080	2	Avg	2.31619E−01	2.35213E−01	1.89080E−01	1.99383E−01	2.17397E−01
		Std	3.83475E−02	4.70316E−02	**1.51122E−02**	4.81209E−02	5.63780E−02
	3	Avg	3.43525E−01	3.29026E−01	3.08507E−01	3.19539E−01	3.47544E−01
		Std	6.68349E−02	5.26053E−02	4.63807E−02	4.93404E−02	5.73701E−02
	4	Avg	4.47594E−01	4.08273E−01	4.32898E−01	4.15201E−01	**4.50603E−01**
		Std	**1.42048E−02**	9.69734E−02	1.62293E−02	4.43785E−02	6.70434E−02
	5	Avg	4.77015E−01	4.32855E−01	**4.84346E−01**	4.63341E−01	4.71692E−01
		Std	1.69782E−02	7.97934E−02	**9.03930E−03**	1.99150E−02	2.57531E−02
			SSA	DE	AVOA	CLPSO	HHO
	2	Avg	1.98880E−01	2.19574E−01	2.02215E−01	**2.64646E−01**	2.25614E−01
		Std	2.66950E−02	4.24877E−02	3.29275E−02	4.52553E−02	5.75534E−02
	3	Avg	3.32639E−01	**3.53908E−01**	3.34469E−01	3.40290E−01	3.49076E−01
		Std	4.12490E−02	**3.79628E−02**	5.27159E−02	4.10847E−02	4.60895E−02
	4	Avg	4.17540E−01	4.24422E−01	4.17309E−01	3.85172E−01	4.21867E−01
		Std	3.76825E−02	1.66197E−02	3.94602E−02	4.03082E−02	4.72162E−02
	5	Avg	4.58362E−01	4.74231E−01	4.73438E−01	4.34017E−01	4.48801E−01
		Std	3.03336E−02	1.45753E−02	2.40673E−02	2.99589E−02	3.36943E−02

Table 24 Results for each algorithm on FSIM

Image	Thresholds	Item	RDMVO	MVO	ACOR	BA	WOA
35070	2	Avg	7.31182E−01	7.31722E−01	7.07795E−01	6.96731E−01	7.31591E−01
		Std	2.37137E−02	3.72835E−02	4.08731E−02	4.35840E−02	4.03283E−02
	3	Avg	**7.55981E−01**	7.50863E−01	7.40892E−01	7.38592E−01	7.47010E−01
		Std	**1.92801E−02**	3.16836E−02	2.21564E−02	2.98506E−02	3.19935E−02
	4	Avg	7.58252E−01	7.58078E−01	7.55780E−01	7.37511E−01	7.42520E−01
		Std	**1.07060E−02**	2.55677E−02	1.63303E−02	2.64421E−02	2.89947E−02
	5	Avg	7.68958E−01	7.54192E−01	7.62451E−01	7.53363E−01	7.55088E−01
		Std	**9.37589E−03**	3.66705E−02	1.14727E−02	2.78523E−02	3.46634E−02
			SSA	DE	AVOA	CLPSO	HHO
	2	Avg	7.18886E−01	7.36791E−01	7.05961E−01	**7.41882E−01**	7.28808E−01
		Std	3.43372E−02	**1.27180E−02**	3.83945E−02	2.88396E−02	3.94377E−02
	3	Avg	7.43476E−01	7.40056E−01	7.35858E−01	7.42824E−01	7.46567E−01
		Std	2.23615E−02	2.53067E−02	2.81420E−02	2.85183E−02	3.26806E−02
	4	Avg	7.61598E−01	**7.64871E−01**	7.54780E−01	7.47630E−01	7.52670E−01
		Std	2.32560E−02	1.57399E−02	1.73162E−02	3.35783E−02	2.36701E−02
	5	Avg	7.56213E−01	7.63691E−01	7.58653E−01	7.58365E−01	**7.70441E−01**
		Std	1.72506E−02	1.22232E−02	1.66355E−02	2.03332E−02	2.09682E−02
Image	Thresholds	Item	RDMVO	MVO	ACOR	BA	WOA
38092	2	Avg	**6.80846E−01**	6.54693E−01	6.56812E−01	6.50183E−01	6.66647E−01
		Std	**1.17562E−03**	2.84607E−02	3.29232E−02	4.50107E−02	5.14490E−03
	3	Avg	**7.78812E−01**	7.30571E−01	7.70473E−01	7.60339E−01	7.61520E−01
		Std	**1.03108E−03**	3.61815E−02	9.37642E−03	2.58241E−02	2.47545E−02
	4	Avg	**8.29093E−01**	7.56098E−01	8.24380E−01	8.01699E−01	8.01478E−01
		Std	**2.53551E−03**	5.58201E−02	6.16244E−03	6.21975E−02	2.77199E−02
	5	Avg	8.64332E−01	8.01598E−01	**8.64732E−01**	8.53236E−01	8.41778E−01
		Std	1.23137E−02	5.05249E−02	**7.69118E−03**	3.88108E−02	2.38331E−02
			SSA	DE	AVOA	CLPSO	HHO
	2	Avg	6.61983E−01	6.65776E−01	6.67209E−01	6.53614E−01	6.51005E−01
		Std	2.14838E−02	1.93516E−02	6.72447E−03	2.54515E−02	4.50977E−02
	3	Avg	7.55265E−01	7.55696E−01	7.60510E−01	7.32561E−01	7.55587E−01
		Std	1.89333E−02	2.23843E−02	1.88053E−02	4.05397E−02	2.86832E−02
	4	Avg	8.08541E−01	8.20454E−01	8.08729E−01	7.77094E−01	7.80932E−01
		Std	2.84323E−02	9.58958E−03	1.61298E−02	2.98630E−02	5.84309E−02
	5	Avg	8.43382E−01	8.51616E−01	8.54003E−01	8.04722E−01	8.17341E−01
		Std	2.65109E−02	1.33243E−02	1.34154E−02	3.34324E−02	4.87639E−02
Image	Thresholds	Item	RDMVO	MVO	ACOR	BA	WOA
61060	2	Avg	7.03504E−01	6.92102E−01	7.01761E−01	6.85544E−01	6.87037E−01
		Std	3.25241E−03	2.32673E−02	1.28518E−02	6.50290E−02	2.49551E−02
	3	Avg	**7.65471E−01**	7.29689E−01	7.26492E−01	7.14316E−01	7.29484E−01
		Std	2.39965E−02	2.91258E−02	**2.23232E−02**	5.71342E−02	2.94568E−02
	4	Avg	**7.78343E−01**	7.68884E−01	7.67995E−01	7.54560E−01	7.59045E−01
		Std	**2.02467E−02**	3.70528E−02	2.89071E−02	2.63390E−02	2.97874E−02
	5	Avg	**8.10135E−01**	7.80379E−01	8.07443E−01	8.07048E−01	7.86448E−01
		Std	**1.69602E−02**	5.07180E−02	3.30711E−02	2.54442E−02	2.76923E−02

Table 24 (continued)

			SSA	DE	AVOA	CLPSO	HHO
	2	Avg	7.01524E−01	**7.06921E−01**	7.03330E−01	7.02496E−01	6.94769E−01
		Std	1.47198E−02	**2.77508E−03**	1.31878E−02	8.16317E−03	1.65351E−02
	3	Avg	7.13933E−01	7.18265E−01	7.29760E−01	7.15721E−01	7.13440E−01
		Std	2.62212E−02	2.32411E−02	2.99032E−02	3.67286E−02	3.60777E−02
	4	Avg	7.63319E−01	7.67581E−01	7.71395E−01	7.63438E−01	7.52051E−01
		Std	3.08393E−02	3.00707E−02	3.32733E−02	3.52791E−02	3.21043E−02
	5	Avg	7.87928E−01	7.94801E−01	7.98560E−01	7.93933E−01	7.86943E−01
		Std	3.56529E−02	3.05379E−02	3.93536E−02	3.14542E−02	2.73337E−02
Image	Thresholds	Item	RDMVO	MVO	ACOR	BA	WOA
100080	2	Avg	**7.55577E−01**	7.48375E−01	7.44240E−01	7.41594E−01	7.33062E−01
		Std	2.18228E−02	3.12504E−02	2.67419E−02	3.63353E−02	2.79886E−02
	3	Avg	7.59590E−01	7.50936E−01	7.50956E−01	7.38543E−01	7.60388E−01
		Std	**2.93079E−02**	3.65270E−02	2.93321E−02	3.59699E−02	3.80297E−02
	4	Avg	7.64189E−01	7.65672E−01	7.65661E−01	7.59598E−01	**7.70601E−01**
		Std	3.51293E−02	3.25738E−02	**2.80824E−02**	2.84630E−02	3.94648E−02
	5	Avg	7.74368E−01	7.58034E−01	7.82257E−01	7.64154E−01	7.68477E−01
		Std	2.18726E−02	3.25070E−02	**1.49731E−02**	4.17994E−02	4.33122E−02
			SSA	DE	AVOA	CLPSO	HHO
	2	Avg	7.43183E−01	7.22700E−01	7.42283E−01	7.40069E−01	7.48445E−01
		Std	3.90345E−02	**1.74010E−02**	3.35023E−02	3.51116E−02	3.48039E−02
	3	Avg	7.57295E−01	**7.62866E−01**	7.49733E−01	7.52270E−01	7.57746E−01
		Std	4.06571E−02	2.93696E−02	3.26872E−02	3.95824E−02	3.09553E−02
	4	Avg	7.69413E−01	7.59644E−01	7.67936E−01	7.65203E−01	7.68755E−01
		Std	3.39893E−02	3.26116E−02	3.02243E−02	3.69267E−02	3.45340E−02
	5	Avg	7.77109E−01	7.69404E−01	7.69027E−01	**7.86182E−01**	7.74842E−01
		Std	3.26172E−02	2.43131E−02	3.34734E−02	3.78993E−02	4.40260E−02
Image	Thresholds	Item	RDMVO	MVO	ACOR	BA	WOA
108005	2	Avg	6.66446E−01	6.62949E−01	**6.67009E−01**	6.60244E−01	6.64687E−01
		Std	**8.72452E−04**	7.72871E−03	1.66154E−03	1.07575E−02	4.90602E−03
	3	Avg	7.16304E−01	7.18127E−01	7.22722E−01	7.21234E−01	7.06011E−01
		Std	**3.43582E−03**	1.21378E−02	6.64546E−03	1.78904E−02	2.67910E−02
	4	Avg	**7.88058E−01**	7.53175E−01	7.81443E−01	7.74102E−01	7.77582E−01
		Std	**1.16428E−03**	2.38167E−02	8.90375E−03	1.94926E−02	9.59936E−03
	5	Avg	**8.26963E−01**	7.90951E−01	8.21960E−01	8.10796E−01	8.13879E−01
		Std	**4.51468E−03**	2.46998E−02	9.57340E−03	2.40104E−02	1.46440E−02
			SSA	DE	AVOA	CLPSO	HHO
	2	Avg	6.66992E−01	6.66935E−01	6.66778E−01	6.62084E−01	6.62744E−01
		Std	2.33289E−03	1.90945E−03	2.89820E−03	8.28580E−03	8.06928E−03
	3	Avg	**7.23258E−01**	7.19027E−01	7.22196E−01	7.12436E−01	7.15871E−01
		Std	9.22652E−03	6.48706E−03	6.62379E−03	1.45442E−02	1.77030E−02
	4	Avg	7.73286E−01	7.80201E−01	7.82211E−01	7.56132E−01	7.63012E−01
		Std	1.65159E−02	9.82396E−03	8.65340E−03	2.22123E−02	3.59741E−02
	5	Avg	8.13171E−01	8.15384E−01	8.20655E−01	7.61981E−01	8.02839E−01
		Std	1.25113E−02	1.26041E−02	1.23260E−02	3.39498E−02	2.67958E−02

Table 24 (continued)

Image	Thresholds	Item	RDMVO	MVO	ACOR	BA	WOA
253027	2	Avg	**6.98503E−01**	6.46653E−01	6.72047E−01	6.78562E−01	6.66423E−01
		Std	**5.07505E−03**	1.84662E−02	1.81990E−02	2.59182E−02	2.65416E−02
	3	Avg	7.30916E−01	7.11102E−01	**7.44589E−01**	7.32431E−01	7.20719E−01
		Std	1.19745E−02	3.48320E−02	**9.63655E−03**	2.65548E−02	3.76514E−02
	4	Avg	**7.99145E−01**	7.64451E−01	7.91029E−01	7.84359E−01	7.74953E−01
		Std	**2.62620E−03**	3.01868E−02	2.01962E−02	2.93049E−02	3.00701E−02
	5	Avg	**8.26060E−01**	7.81927E−01	8.20414E−01	8.15015E−01	7.84402E−01
		Std	**7.12548E−03**	2.23030E−02	1.49913E−02	4.02374E−02	4.79938E−02
			SSA	DE	AVOA	CLPSO	HHO
	2	Avg	6.62633E−01	6.70262E−01	6.70009E−01	6.79602E−01	6.65333E−01
		Std	2.41794E−02	2.59682E−02	2.25172E−02	2.33517E−02	2.52402E−02
	3	Avg	7.34673E−01	7.41435E−01	7.26340E−01	7.18856E−01	7.27691E−01
		Std	2.78381E−02	1.51939E−02	2.94436E−02	3.34622E−02	2.74066E−02
	4	Avg	7.84331E−01	7.94611E−01	7.85530E−01	7.73137E−01	7.65344E−01
		Std	2.27051E−02	8.40208E−03	1.91503E−02	3.11365E−02	2.98235E−02
	5	Avg	8.01679E−01	8.15123E−01	8.08482E−01	7.87837E−01	7.96683E−01
		Std	3.39646E−02	1.45593E−02	1.70319E−02	2.98059E−02	2.68716E−02
Image	Thresholds	Item	RDMVO	MVO	ACOR	BA	WOA
291000	2	Avg	7.11084E−01	6.91029E−01	7.24428E−01	**7.29392E−01**	7.23583E−01
		Std	**7.73960E−03**	4.47801E−02	1.31996E−02	9.56584E−03	1.00122E−02
	3	Avg	7.92712E−01	7.82485E−01	7.93748E−01	**8.00853E−01**	7.76924E−01
		Std	**2.01211E−03**	2.52816E−02	6.63151E−03	1.51954E−02	4.38480E−02
	4	Avg	**8.55333E−01**	8.02496E−01	8.48659E−01	8.46864E−01	8.34573E−01
		Std	9.63846E−03	5.24363E−02	9.28322E−03	**8.97306E−03**	2.47327E−02
	5	Avg	**8.91763E−01**	8.47055E−01	8.76665E−01	8.77119E−01	8.55173E−01
		Std	9.27602E−03	3.28727E−02	**3.85984E−03**	1.48022E−02	2.64921E−02
			SSA	DE	AVOA	CLPSO	HHO
	2	Avg	7.07537E−01	7.12328E−01	7.18176E−01	6.99995E−01	7.12340E−01
		Std	3.05526E−02	1.02931E−02	2.09608E−02	2.62393E−02	3.49724E−02
	3	Avg	7.87891E−01	7.91553E−01	7.94799E−01	7.63500E−01	7.74977E−01
		Std	1.63817E−02	3.79308E−03	1.22413E−02	2.89502E−02	2.88069E−02
	4	Avg	8.36535E−01	8.47145E−01	8.43087E−01	8.21519E−01	8.25407E−01
		Std	1.50340E−02	1.04929E−02	1.42770E−02	3.61367E−02	2.07984E−02
	5	Avg	8.66671E−01	8.77695E−01	8.70236E−01	8.55058E−01	8.47627E−01
		Std	2.10049E−02	1.16135E−02	1.19524E−02	2.48009E−02	2.67951E−02
Image	Thresholds	Item	RDMVO	MVO	ACOR	BA	WOA
314016	2	Avg	5.96619E−01	5.91438E−01	5.96139E−01	5.64776E−01	5.89186E−01
		Std	**1.35622E−03**	6.74571E−03	1.45617E−03	5.06164E−02	9.54889E−03
	3	Avg	**7.00340E−01**	6.71553E−01	6.82847E−01	6.81713E−01	6.91880E−01
		Std	**9.29288E−04**	2.67990E−02	2.53976E−02	2.54400E−02	1.26641E−02
	4	Avg	**7.51403E−01**	7.13514E−01	7.48694E−01	7.47421E−01	7.33495E−01
		Std	**2.28921E−03**	3.30620E−02	5.30369E−03	1.88971E−02	2.18038E−02
	5	Avg	**8.15315E−01**	7.43692E−01	8.12002E−01	7.93994E−01	7.90048E−01
		Std	**2.72747E−03**	4.57983E−02	5.76489E−03	8.16950E−02	3.19082E−02

Table 24 (continued)

			SSA	DE	AVOA	CLPSO	HHO
	2	Avg	5.95120E−01	**5.96831E−01**	5.94947E−01	5.86569E−01	5.84067E−01
		Std	3.34306E−03	1.82531E−03	2.72235E−03	1.01383E−02	1.67097E−02
	3	Avg	6.80922E−01	6.93716E−01	6.84975E−01	6.69751E−01	6.90603E−01
		Std	2.30546E−02	1.29523E−02	2.21687E−02	3.25873E−02	1.30016E−02
	4	Avg	7.43987E−01	7.45106E−01	7.43999E−01	7.10206E−01	7.36410E−01
		Std	1.34386E−02	7.86485E−03	1.06646E−02	3.19927E−02	2.70715E−02
	5	Avg	7.86321E−01	7.94767E−01	7.98126E−01	7.57682E−01	7.74321E−01
		Std	2.53930E−02	1.52947E−02	2.36531E−02	3.51521E−02	3.34112E−02
Image	Thresholds	Item	RDMVO	MVO	ACOR	BA	WOA
317080	2	Avg	6.37878E−01	6.40160E−01	6.20649E−01	6.22955E−01	6.34812E−01
		Std	1.39513E−02	2.07143E−02	**4.71234E−03**	2.73716E−02	2.17535E−02
	3	Avg	7.12023E−01	7.00571E−01	6.86611E−01	6.96492E−01	7.09263E−01
		Std	4.15671E−02	3.29807E−02	2.68288E−02	3.18807E−02	3.57534E−02
	4	Avg	**7.93975E−01**	7.47789E−01	7.83320E−01	7.77762E−01	7.72371E−01
		Std	1.10059E−02	5.03110E−02	**8.69077E−03**	3.36105E−02	3.29090E−02
	5	Avg	8.31823E−01	7.73531E−01	**8.40432E−01**	8.25973E−01	8.26310E−01
		Std	1.49647E−02	4.56542E−02	**6.88022E−03**	1.90267E−02	2.69715E−02
			SSA	DE	AVOA	CLPSO	HHO
	2	Avg	6.23863E−01	6.34124E−01	6.25607E−01	**6.52353E−01**	6.35622E−01
		Std	1.04900E−02	2.02693E−02	1.18434E−02	2.14371E−02	2.04453E−02
	3	Avg	7.04749E−01	7.10597E−01	7.03611E−01	7.03478E−01	**7.13078E−01**
		Std	2.66392E−02	2.66570E−02	3.20146E−02	**2.39357E−02**	3.29881E−02
	4	Avg	7.79846E−01	7.78161E−01	7.77646E−01	7.45675E−01	7.77749E−01
		Std	2.80084E−02	1.71525E−02	2.85307E−02	3.33416E−02	3.51355E−02
	5	Avg	8.16124E−01	8.32630E−01	8.34582E−01	7.89168E−01	8.05288E−01
		Std	2.83279E−02	1.34200E−02	1.93250E−02	2.91323E−02	3.40555E−02

Table 25 Friedman test results for each algorithm on PSNR of each image

image	Thresholds	RDMVO	MVO	ACOR	BA	WOA	SSA	DE	AVOA	CLPSO	HHO
35070	2	7.73	5.15	4.95	3.90	5.40	5.05	7.00	4.98	6.40	4.45
	3	7.15	4.70	5.85	5.55	5.85	4.10	5.20	5.25	5.80	5.55
	4	7.90	4.90	5.40	4.30	3.65	4.90	6.15	5.50	5.70	6.60
	5	8.40	4.70	5.45	5.25	6.20	4.50	5.70	5.25	4.25	5.30
38092	2	9.45	5.70	5.05	4.50	4.38	5.35	6.60	5.03	4.50	4.45
	3	5.65	5.20	6.75	7.20	3.95	5.75	6.45	6.40	3.93	3.73
	4	5.30	3.05	7.63	7.38	5.00	6.30	6.60	6.50	3.45	3.80
	5	4.95	3.15	8.10	7.75	5.25	5.90	6.60	6.10	2.90	4.30
61060	2	9.10	4.33	5.40	4.95	5.23	5.25	6.48	5.60	4.88	3.80
	3	9.85	4.55	4.70	5.68	5.05	4.83	4.60	5.50	5.20	5.05
	4	9.00	5.10	4.25	5.10	4.35	6.60	5.75	5.50	5.15	4.20
	5	8.30	4.55	6.55	5.40	4.75	5.05	5.90	5.75	3.70	5.05
100080	2	8.30	4.55	5.43	3.30	6.65	4.05	7.28	3.95	6.15	5.35
	3	7.35	4.00	6.25	4.75	4.35	4.65	7.75	4.40	5.65	5.85
	4	7.00	5.00	7.80	4.55	4.70	4.30	6.25	5.45	4.60	5.35
	5	7.15	4.55	7.50	5.25	3.95	4.95	6.50	5.75	4.20	5.20
108005	2	5.90	4.15	5.95	3.85	8.03	5.73	5.53	5.13	5.10	5.65
	3	3.85	6.10	5.68	5.98	5.70	6.90	4.75	5.40	5.10	5.55
	4	7.85	3.85	5.50	6.00	5.40	5.50	5.40	6.85	3.75	4.90
	5	8.10	4.10	6.50	5.65	5.20	5.50	6.00	6.90	2.25	4.80
253027	2	3.28	4.55	7.35	6.30	4.55	6.03	6.83	5.83	4.40	5.90
	3	6.40	4.10	7.05	5.90	5.05	6.20	7.55	4.05	4.05	4.65
	4	6.45	3.80	6.40	5.85	5.25	6.50	5.75	5.80	5.20	4.00
	5	8.00	2.85	7.20	7.45	3.85	5.30	6.25	6.00	3.75	4.35
291000	2	4.95	4.05	7.03	6.88	6.70	5.38	5.55	6.70	3.90	3.88
	3	6.63	4.30	6.95	6.58	5.25	6.60	6.20	7.00	2.20	3.30
	4	6.25	3.30	6.40	8.15	5.00	4.90	6.20	7.60	3.70	3.50
	5	7.65	2.75	7.65	7.65	4.95	5.35	5.80	6.05	3.30	3.85
314016	2	7.78	4.38	7.13	3.70	4.58	6.03	7.58	6.00	3.85	4.00
	3	8.78	3.75	5.75	5.68	5.45	4.80	5.65	5.65	3.80	5.70
	4	7.83	3.40	6.15	6.93	5.00	5.65	5.60	5.50	3.25	5.70
	5	8.90	2.35	7.75	7.40	5.25	4.70	4.70	6.30	3.05	4.60
317080	2	7.15	6.05	3.93	4.58	4.45	4.30	6.20	4.65	8.25	5.45
	3	6.45	4.85	3.90	5.15	6.10	5.70	6.05	5.60	4.65	6.55
	4	7.05	4.00	5.55	6.65	4.80	6.60	5.20	6.10	3.05	6.00
	5	6.20	2.90	7.60	6.35	6.75	4.90	5.90	7.25	3.20	3.95

Table 26 Friedman test results for each algorithm on SSIM of each image

Image	Thresholds	RDMVO	MVO	ACOR	BA	WOA	SSA	DE	AVOA	CLPSO	HHO
35070	2	6.80	4.95	4.80	4.15	6.00	5.15	6.70	4.60	6.55	5.30
	3	7.40	5.40	5.30	5.35	5.60	4.60	4.75	5.30	5.65	5.65
	4	6.75	5.40	6.05	3.50	4.90	5.80	6.55	5.00	5.50	5.55
	5	5.95	4.95	6.00	5.70	6.55	4.40	5.50	4.95	4.70	6.30
38092	2	7.00	5.00	5.35	4.98	4.93	5.98	6.20	5.18	4.95	5.45
	3	7.95	3.10	5.95	4.90	7.50	4.60	4.80	5.35	4.08	6.78
	4	8.75	3.35	7.63	5.93	5.50	6.15	6.75	4.65	2.90	3.40
	5	8.50	3.45	8.20	7.30	4.90	5.00	5.90	5.45	2.35	3.95
61060	2	8.20	4.03	6.08	5.65	3.93	5.35	6.80	5.23	5.65	4.10
	3	8.90	6.00	5.25	5.63	5.15	4.53	4.90	5.35	4.75	4.55
	4	7.30	5.55	5.65	4.55	4.50	6.25	5.60	6.10	5.40	4.10
	5	7.15	4.70	6.20	6.70	4.10	4.90	5.35	6.00	4.90	5.00
100080	2	8.90	5.05	4.88	4.55	6.45	5.00	5.43	3.65	5.00	6.10
	3	6.25	3.80	5.80	4.50	5.80	5.20	7.55	4.95	5.75	5.40
	4	6.35	5.40	7.05	4.65	4.50	5.05	5.45	5.35	5.75	5.45
	5	6.80	3.85	7.30	5.40	4.85	5.20	5.70	5.55	4.95	5.40
108005	2	6.00	4.30	6.00	3.75	7.98	5.75	5.63	4.90	5.10	5.60
	3	3.75	6.25	5.63	5.93	6.00	6.80	4.60	5.20	5.20	5.65
	4	7.00	4.35	4.90	5.50	6.30	5.60	5.10	6.85	4.55	4.85
	5	7.95	4.65	5.90	5.40	5.10	5.65	5.50	6.50	3.25	5.10
253027	2	2.98	5.00	6.90	6.15	4.95	5.83	7.33	6.03	4.55	5.30
	3	5.55	4.05	7.15	5.65	5.85	6.50	6.95	3.35	4.65	5.30
	4	7.50	3.90	6.90	5.80	4.65	6.00	6.10	5.35	4.80	4.00
	5	7.95	3.05	7.10	7.20	4.20	4.60	6.10	5.95	4.15	4.70
291000	2	4.90	3.85	7.40	7.18	6.30	5.03	5.38	6.30	3.50	5.18
	3	7.63	4.30	7.20	7.03	4.15	6.35	6.85	6.30	2.00	3.20
	4	6.55	2.80	7.50	8.40	3.95	4.85	6.80	7.20	3.55	3.40
	5	8.20	2.70	8.15	7.70	4.45	5.45	5.90	6.25	3.05	3.15
314016	2	8.03	3.98	7.08	3.20	4.63	6.55	7.80	6.50	3.30	3.95
	3	8.63	3.55	5.55	5.18	5.70	4.85	6.00	5.75	4.05	5.75
	4	7.08	3.65	5.85	6.38	4.90	6.10	5.55	5.75	3.40	6.35
	5	8.85	2.50	7.75	7.60	4.90	4.80	4.70	6.05	3.25	4.60
317080	2	7.05	6.50	3.65	4.55	4.50	4.35	5.90	4.60	8.55	5.35
	3	6.05	5.35	4.00	4.35	6.20	5.05	6.60	5.25	5.70	6.45
	4	8.25	4.85	6.25	5.20	6.25	5.25	5.20	4.85	3.00	5.90
	5	7.05	3.00	7.95	4.80	6.60	5.30	6.35	6.60	2.95	4.40

Table 27 Friedman test results for each algorithm on FSIM of each image

Image	Thresholds	RDMVO	MVO	ACOR	BA	WOA	SSA	DE	AVOA	CLPSO	HHO
35070	2	6.33	5.70	4.50	3.75	6.05	5.10	6.30	4.28	7.20	5.80
	3	7.25	6.00	4.90	5.30	5.85	5.35	4.70	4.65	5.35	5.65
	4	5.75	6.20	5.50	3.50	4.25	6.55	6.85	5.00	5.70	5.70
	5	6.75	5.15	5.25	4.75	5.80	4.80	5.60	5.05	5.20	6.65
38092	2	9.60	4.45	5.50	5.15	4.58	5.20	6.65	4.93	4.20	4.75
	3	9.55	3.25	6.85	6.05	5.50	4.35	5.30	5.50	3.58	5.08
	4	9.15	2.95	7.68	6.78	4.95	5.80	6.55	5.05	2.70	3.40
	5	8.50	3.40	7.50	7.75	5.15	4.95	5.75	6.00	2.20	3.80
61060	2	5.00	4.08	6.50	6.80	3.53	5.90	7.28	6.35	5.68	3.90
	3	8.60	5.80	6.05	4.93	6.10	4.18	4.40	6.20	4.90	3.85
	4	6.75	5.90	6.15	4.45	4.80	5.60	5.35	6.10	5.70	4.20
	5	6.40	5.10	6.45	6.95	4.50	4.85	5.20	6.00	5.10	4.45
100080	2	7.20	5.75	5.88	5.50	4.35	6.25	3.13	5.25	5.40	6.30
	3	5.75	5.30	5.20	4.20	6.15	5.95	6.55	5.15	5.25	5.50
	4	5.20	5.85	5.55	5.05	5.85	5.85	4.80	5.80	5.50	5.55
	5	5.35	4.05	6.30	5.20	5.25	5.80	5.10	5.15	6.60	6.20
108005	2	5.60	4.85	6.00	3.60	5.38	6.73	6.13	6.68	5.00	5.05
	3	4.00	5.35	6.78	6.63	4.45	6.55	5.25	6.30	4.25	5.45
	4	8.40	2.95	6.10	5.85	5.55	5.55	6.15	6.35	3.00	5.10
	5	8.15	3.20	7.20	6.05	5.75	5.50	6.00	6.80	1.65	4.70
253027	2	8.38	2.65	5.95	6.25	5.10	4.48	5.28	5.33	6.50	5.10
	3	4.70	3.75	7.10	6.35	4.85	6.40	7.10	4.90	4.45	5.40
	4	7.50	3.40	6.80	6.25	5.15	5.80	6.65	5.60	4.10	3.75
	5	8.15	2.85	7.35	7.60	4.25	5.30	6.10	5.75	3.35	4.30
291000	2	4.10	4.20	6.88	7.73	6.35	5.23	4.55	6.20	3.90	5.88
	3	6.33	5.00	6.35	7.83	4.75	5.50	6.00	6.70	2.35	4.20
	4	8.15	3.10	7.30	6.40	5.15	4.60	6.10	6.25	4.25	3.70
	5	8.95	3.35	6.85	6.55	4.20	5.50	6.85	5.75	3.80	3.20
314016	2	7.58	4.93	7.03	3.50	4.48	6.03	7.43	6.00	3.90	4.15
	3	8.38	3.70	6.10	5.53	5.50	5.10	5.80	5.45	3.65	5.80
	4	7.93	3.20	6.55	6.98	4.85	5.70	5.65	5.70	3.15	5.30
	5	9.20	2.15	8.05	7.85	5.35	4.95	5.05	6.00	2.50	3.90
317080	2	6.95	6.40	3.23	4.93	5.60	3.75	5.70	4.25	8.45	5.75
	3	6.30	5.45	4.05	4.70	6.05	5.40	6.20	5.25	5.40	6.20
	4	7.70	3.60	6.15	6.15	4.95	6.20	5.50	5.80	2.95	6.00
	5	6.35	2.40	7.95	5.90	6.60	5.20	6.45	7.15	2.95	4.05

Table 28 Threshold for all algorithms on each test image

Image	Thresholds	RDMVO	MVO	ACOR	BA	WOA
03	2	55,103	68,100	55,103	69,125	57,103
	3	46,83,135	22,57,116	46,85,143	53,98,151	36,65,132
	4	31,65,103,157	85,116,165,180	40,72,103,156	26,55,85,136	43,74,102,131
	5	25,53,83,119,160	48,81,121,166,218	29,55,84,133,174	32,74,103,143,186	46,76,98,130,182
04	2	46,93	39,133	47,94	59,132	50,93
	3	41,91,148	25,56,95	45,94,148	43,116,166	60,114,163
	4	28,56,85,148	60,105,115,146	36,77,109,154	16,33,81,186	22,48,94,160
	5	25,54,84,126,169	35,73,137,179,223	33,72,111,148,185	33,61,94,153,191	40,63,79,102,160
05	2	60,105	112,144	80,140	60,106	58,104
	3	41,80,127	39,76,120	61,117,164	50,100,146	54,83,146
	4	41,80,132,184	40,95,147,188	36,58,101,151	52,103,152,193	41,92,144,196
	5	26,43,89,135,184	22,123,184,229,253	24,47,83,124,173	48,94,123,148,185	52,79,92,125,155
09	2	69,121	65,110	78,137	69,121	69,117
	3	52,93,147	33,67,167	66,117,164	54,92,175	55,88,137
	4	41,90,135,178	55,99,132,208	44,81,111,182	52,92,135,179	27,91,116,159
	5	32,65,93,143,184	88,129,187,204,232	32,56,100,145,183	87,134,164,188,213	29,64,99,143,180
12	2	76,134	64,91	71,142	76,134	63,111
	3	54,94,150	28,93,157	48,88,145	56,96,156	41,85,137
	4	31,63,94,153	23,53,132,174	46,89,131,175	103,141,172,201	30,69,105,156
	5	34,63,89,137,174	46,62,99,148,179	35,66,102,147,186	71,176,199,231,253	28,40,79,117,162
15	2	59,122	55,112	70,161	70,161	50,103
	3	42,86,135	48,94,169	54,98,171	109,190,253	59,89,138
	4	35,67,106,157	59,101,138,202	65,112,133,161	83,148,181,218	24,74,109,149
	5	23,45,74,127,173	69,137,187,217,229	24,55,85,118,165	22,44,69,104,146	55,89,107,138,179
20	2	81,140	132,180	81,144	76,137	90,141
	3	57,112,161	43,68,159	62,122,181	59,114,181	43,81,130
	4	54,99,141,182	47,62,99,199	68,97,129,171	57,104,141,180	33,70,97,143
	5	42,64,85,119,166	36,69,81,110,174	38,75,98,143,182	59,108,144,178,217	34,59,97,137,212
21	2	76,129	75,109	76,129	82,140	78,128
	3	57,87,145	61,77,116	56,87,144	48,78,134	60,87,144
	4	49,78,125,169	116,132,160,207	48,77,122,167	52,90,126,168	30,50,92,145
	5	31,60,87,128,172	49,64,122,143,205	31,51,91,128,168	46,75,100,136,177	45,72,99,124,153
25	2	64,115	55,93	74,135	62,138	61,110
	3	45,80,140	47,93,160	42,97,156	70,133,172	60,104,149
	4	39,74,110,157	39,61,88,164	34,68,97,129	89,156,191,226	27,51,87,139
	5	28,54,79,127,172	13,42,108,163,182	34,76,116,150,186	54,105,143,177,216	27,49,76,116,171
Image	Thresholds	SSA	DE	AVOA	CLPSO	HHO
03	2	56,122	57,98	64,115	64,111	40,72
	3	48,89,151	50,77,144	52,97,151	66,106,127	36,74,141
	4	37,59,114,178	20,48,90,129	43,74,111,160	38,58,89,185	40,85,102,127
	5	37,57,95,140,196	48,70,104,147,180	43,63,87,145,184	39,58,135,151,168	36,57,88,132,143
04	2	41,147	50,96	58,112	43,83	33,91
	3	22,90,147	43,86,146	54,118,152	79,135,177	30,60,120
	4	33,60,94,157	33,66,90,176	32,52,97,132	22,94,148,168	24,33,92,120
	5	32,61,86,105,191	17,46,86,118,185	13,43,79,122,191	25,81,96,141,185	48,84,111,125,146
05	2	47,106	76,145	55,106	46,101	44,90
	3	19,69,136	64,118,148	57,98,139	47,80,150	43,72,117
	4	20,36,96,190	45,97,141,185	30,52,101,155	51,93,108,138	42,72,102,140
	5	49,100,164,199,253	43,75,117,158,199	17,42,71,113,144	45,115,148,158,185	36,98,169,221,253

Table 28 (continued)

Image	Thresholds	RDMVO	MVO	ACOR	BA	WOA
09	2	55,81	61,107	66,117	68,108	57,113
	3	59,103,160	50,99,164	53,92,140	85,128,161	36,54,98
	4	26,61,88,144	37,77,117,175	39,73,106,157	22,69,118,166	48,64,99,131
	5	21,38,92,128,156	31,83,138,161,192	66,96,121,156,193	50,84,117,162,213	42,57,115,143,195
12	2	79,143	67,118	76,134	71,129	48,102
	3	50,118,176	64,105,167	37,79,136	51,89,138	38,79,113
	4	48,75,108,187	25,84,106,167	34,60,111,153	42,88,130,190	38,55,102,156
	5	30,53,94,142,196	24,76,107,140,177	29,57,90,141,182	3,56,103,167,184	21,55,92,107,168
15	2	81,145	56,122	59,119	62,138	60,96
	3	58,164,194	54,108,159	58,113,163	45,73,142	53,89,130
	4	61,175,207,253	62,100,136,175	67,149,191,253	32,52,76,96	18,44,104,168
	5	46,96,147,184,212	54,83,130,161,195	39,75,95,133,187	56,96,125,157,209	12,52,77,123,189
20	2	44,90	74,135	69,132	53,93	78,128
	3	71,104,152	55,107,166	48,103,143	75,141,191	24,70,167
	4	36,90,135,199	47,89,145,186	35,77,120,176	45,91,120,167	44,80,145,177
	5	57,94,125,173,218	67,93,123,160,184	30,53,82,123,159	50,80,109,137,180	51,70,93,127,199
21	2	76,132	75,136	70,111	79,140	65,109
	3	90,144,182	33,74,139	59,96,162	54,128,168	37,75,121
	4	38,72,100,165	41,60,114,158	33,51,99,146	70,99,140,161	30,51,89,169
	5	19,35,56,95,162	36,60,76,132,183	34,55,90,133,177	42,92,131,167,215	39,60,88,115,170
25	2	42,87	73,132	64,115	46,129	55,102
	3	52,109,184	52,96,138	68,122,164	64,108,153	74,127,171
	4	50,94,166,213	33,80,146,184	25,57,88,145	42,119,131,167	10,25,106,174
	5	29,69,124,146,172	27,63,117,155,203	30,62,102,138,175	6,51,91,110,191	23,42,54,128,176

Appendix 2

See Figs. 9, 10, 11, 12, 13, 14, 15, 16, 17, 18, 19, and 20.
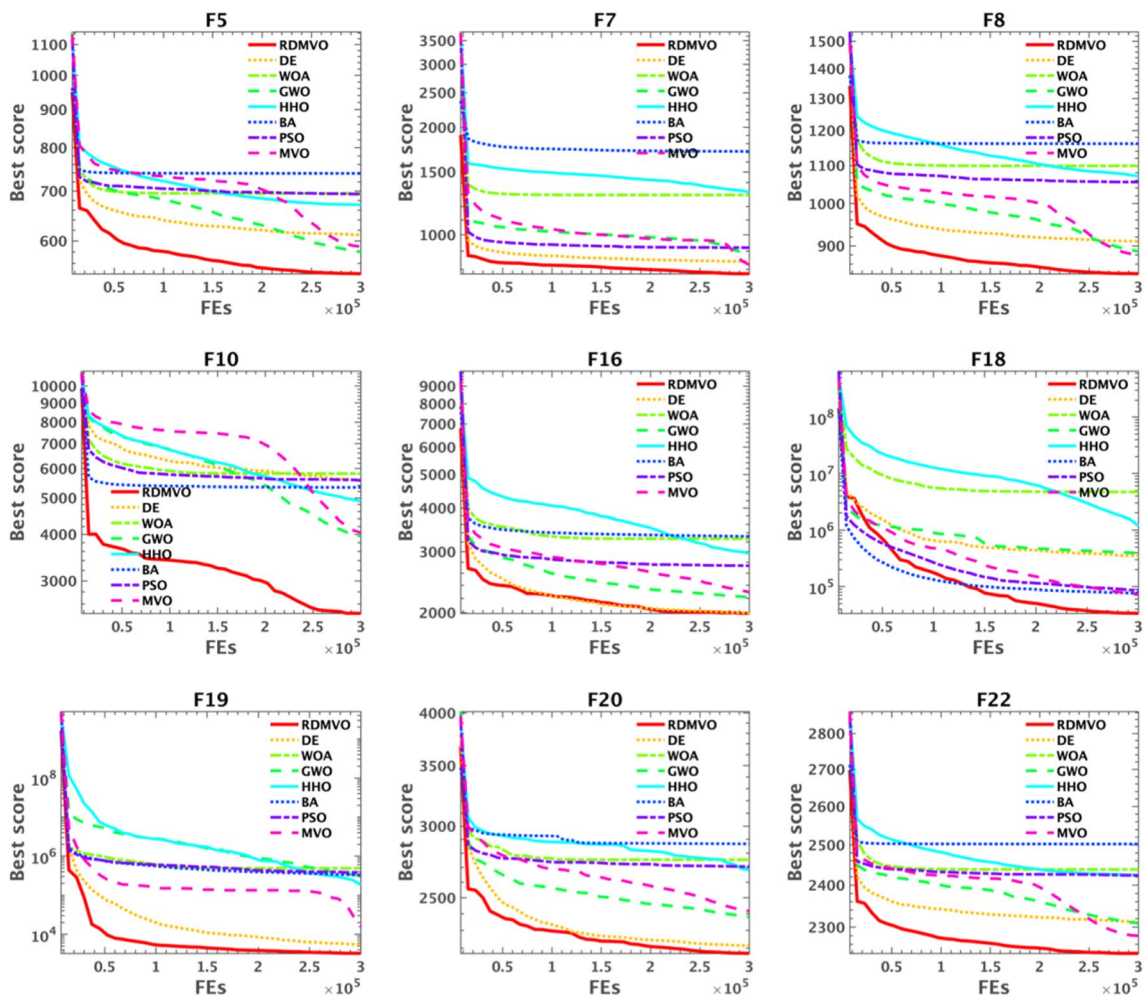
Fig. 9 Convergence curves of 9 benchmark functions

35070   38092   61060

100080   108005   253027

291000   314016   317080

Fig. 10 BKIs in the segmentation experiment
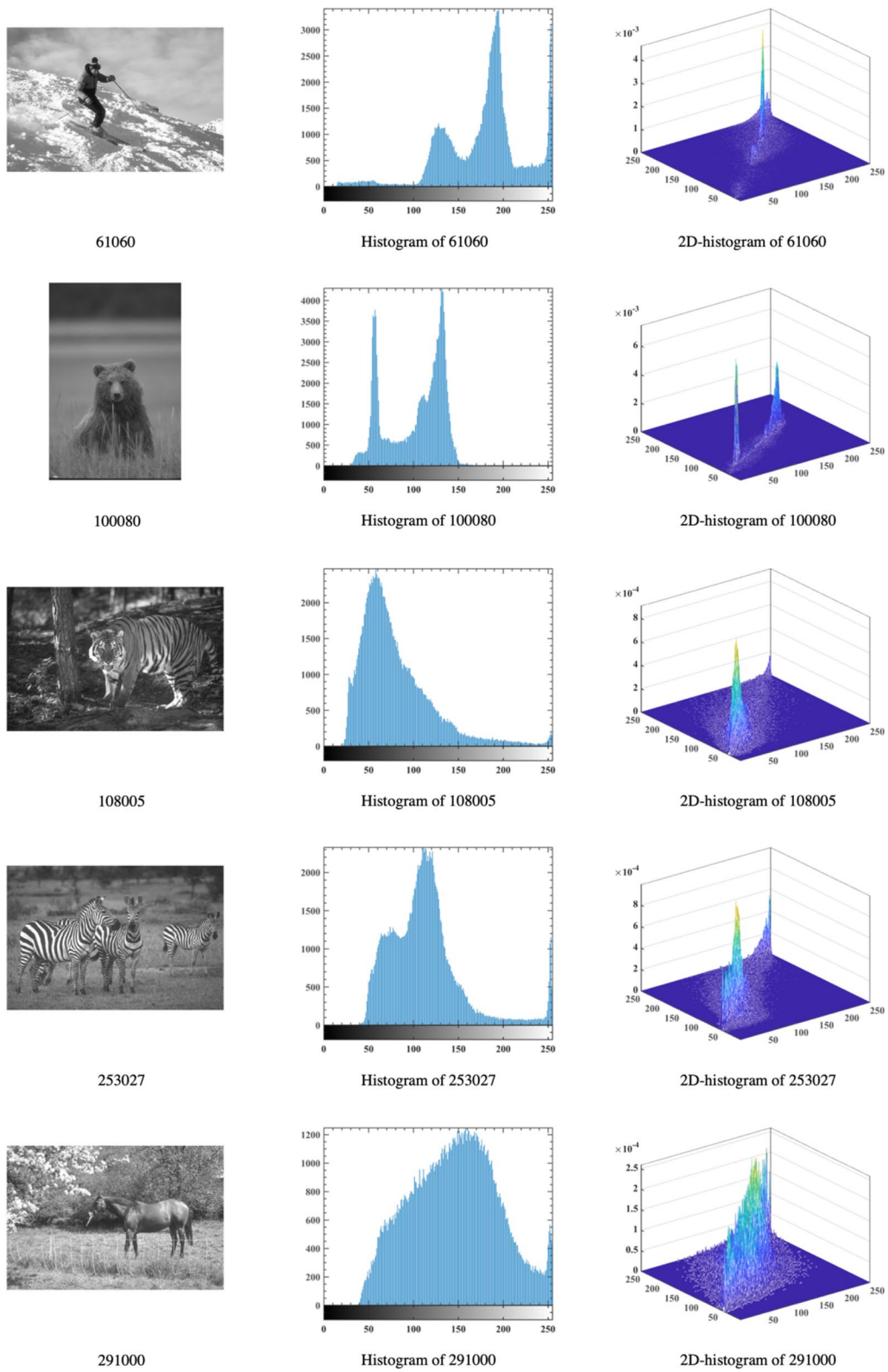
Fig. 11 Grayscale, histogram and 2D histogram of BKIs in the segmentation experiment

| 314016 | Histogram of 314016 | 2D-histogram of 314016 |

| 317080 | Histogram of 317080 | 2D-histogram of 317080 |
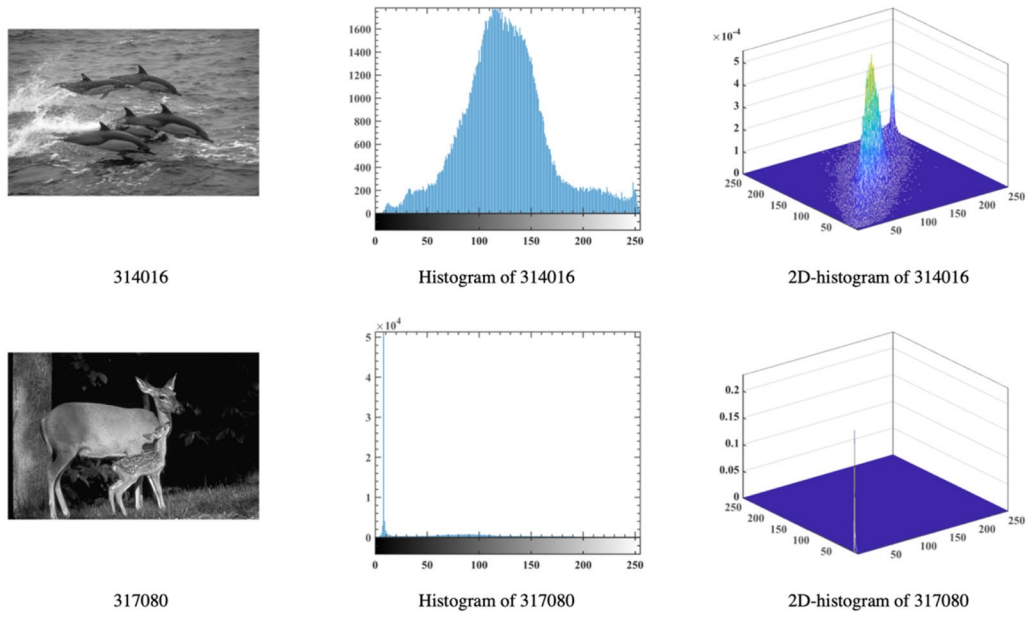
Fig. 11 (continued)
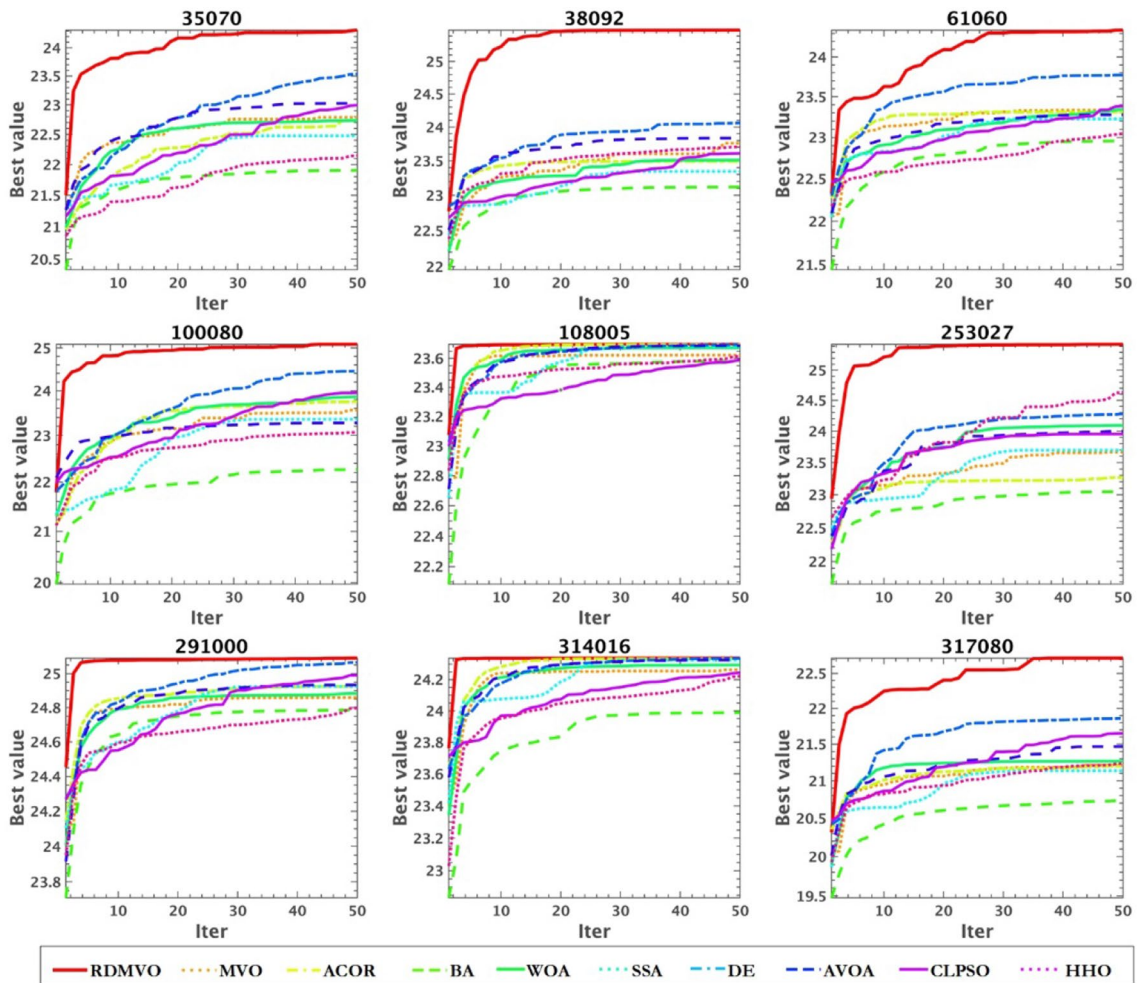
Fig. 12 Kapur's entropy convergence curve of all algorithms at threshold level 2
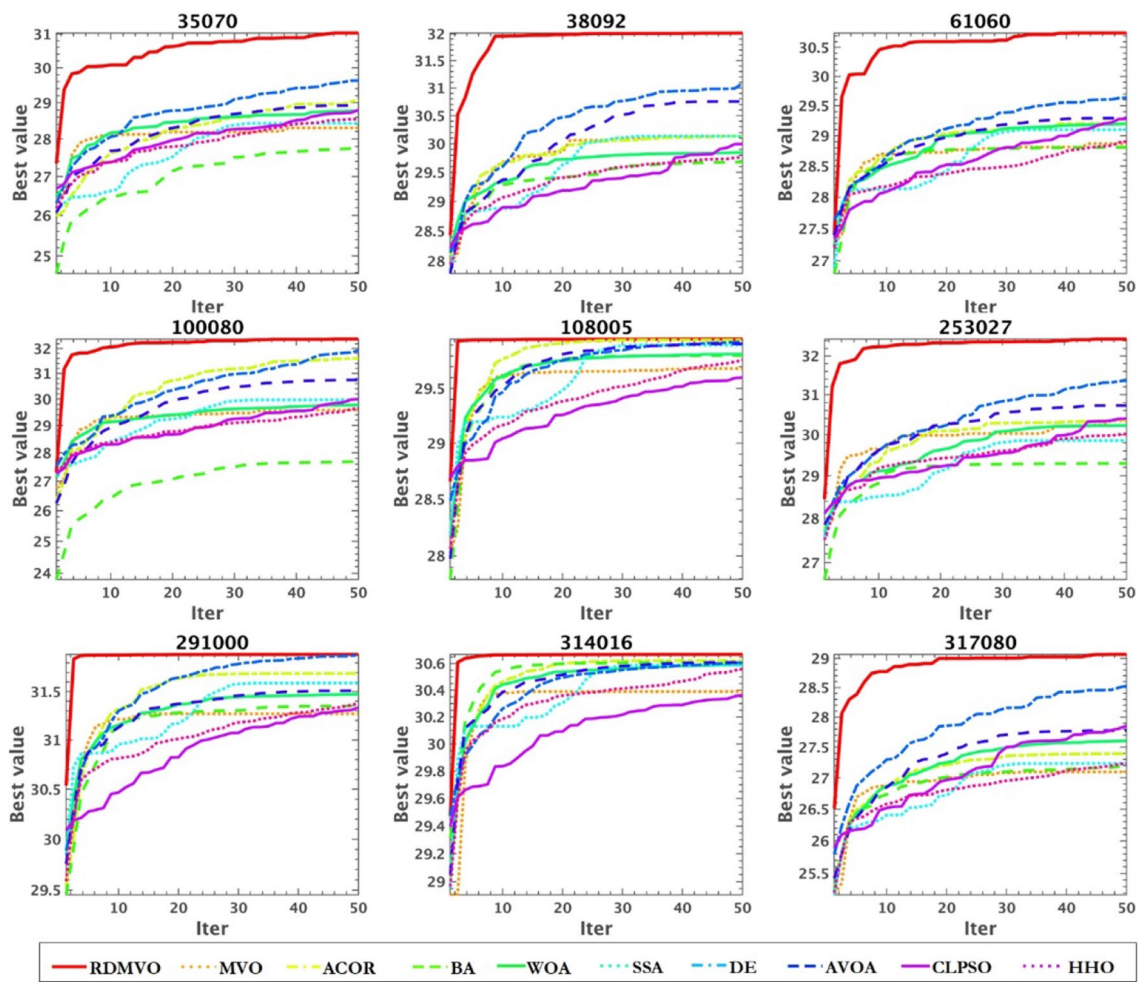
Fig. 13 Kapur's entropy convergence curve of all algorithms at threshold level 3
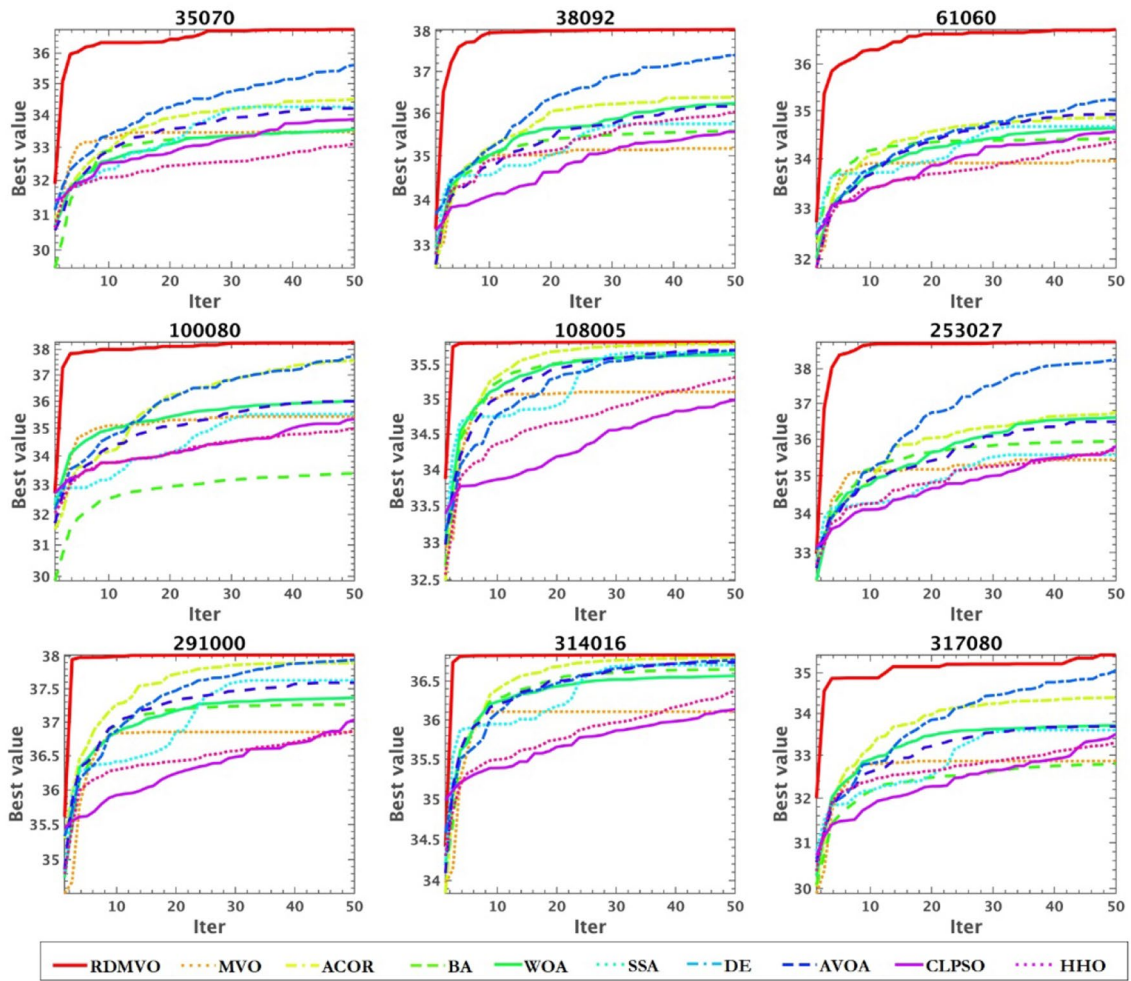
Fig. 14 Kapur's entropy convergence curve of all algorithms at threshold level 4
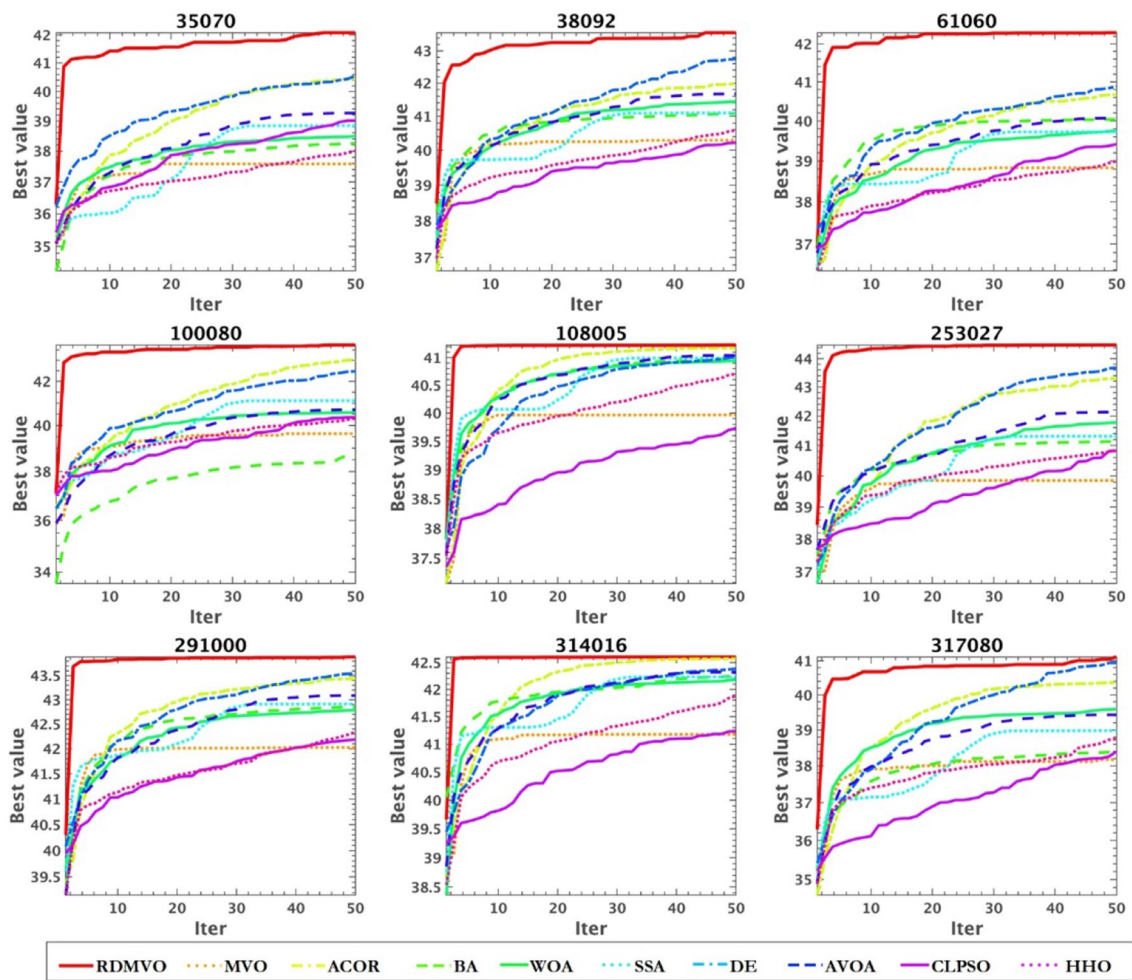
Fig. 15 Kapur's entropy convergence curve of all algorithms at threshold level 5
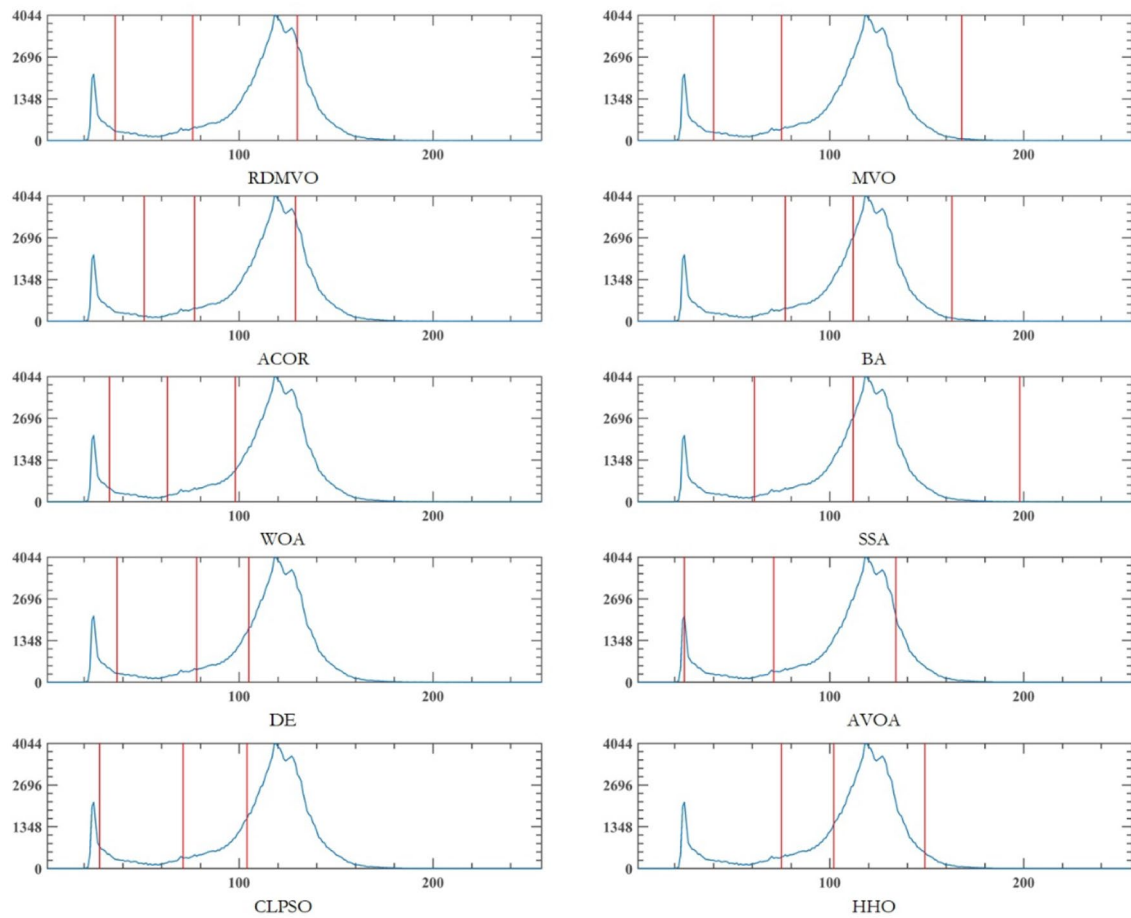
Fig. 16 Thresholds obtained of image 35,070 by all algorithms at threshold level 3
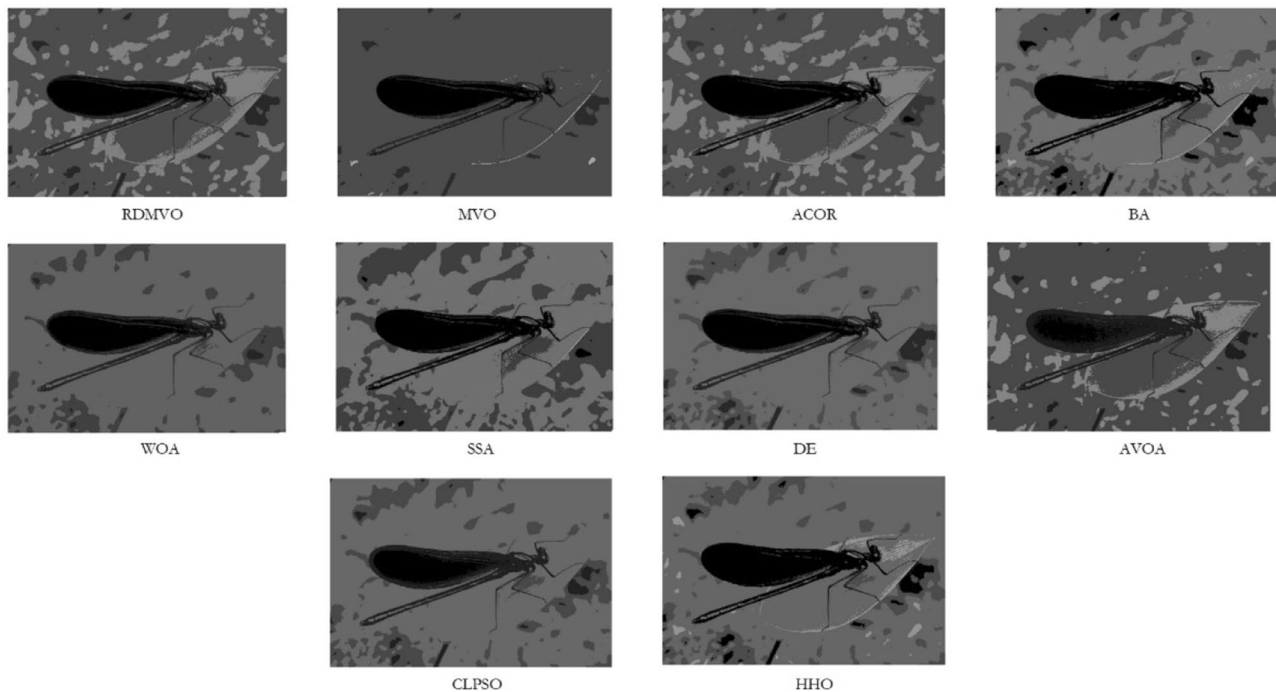
Fig. 17 Grayscale image of image 35,070 segmented by all algorithms at threshold level 3

Fig. 18 Grayscale image of all images segmented by RDMVO at different thresholds
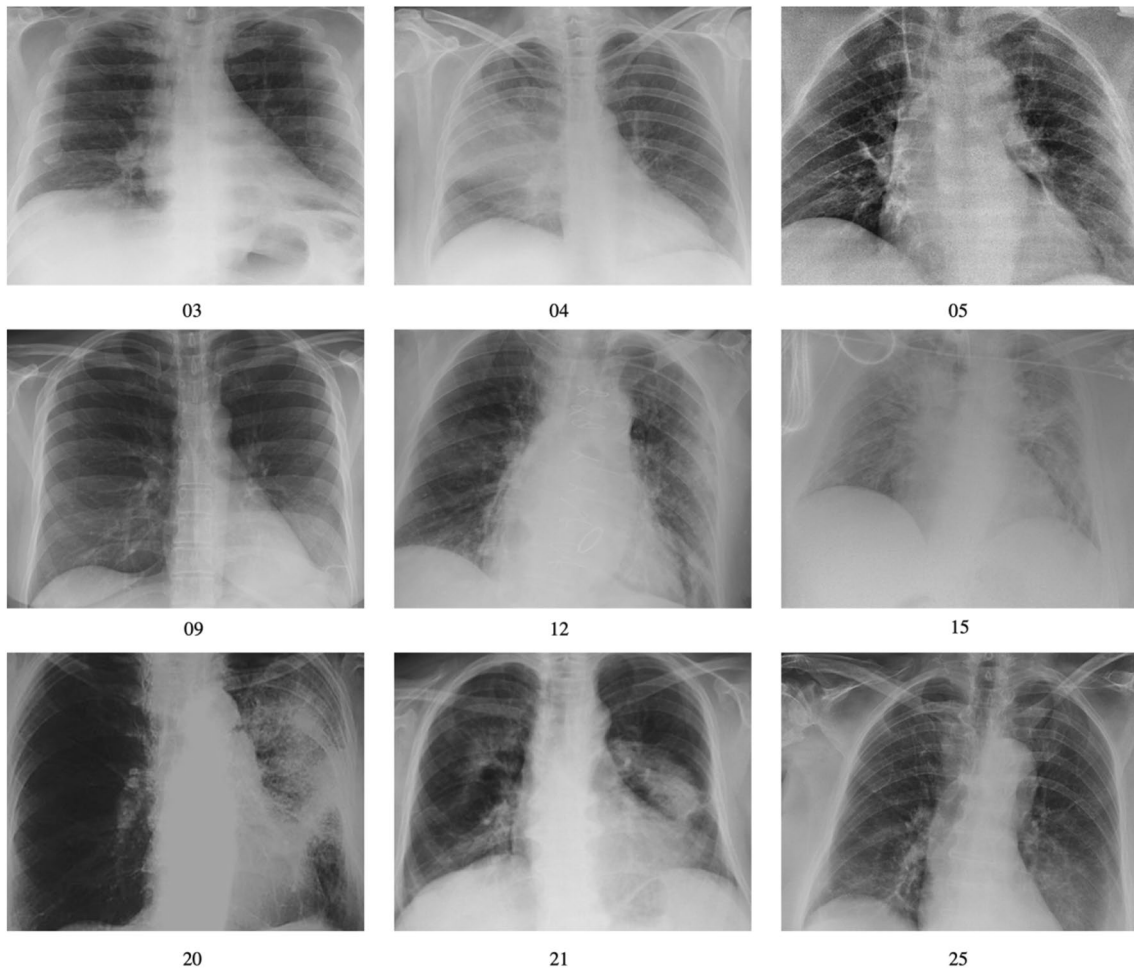
Fig. 19 COVID-19-CXIs in the segmentation experiment

Fig. 20 Grayscale, histogram and 2D histogram of COVID-19-CXIs in the segmentation experiment
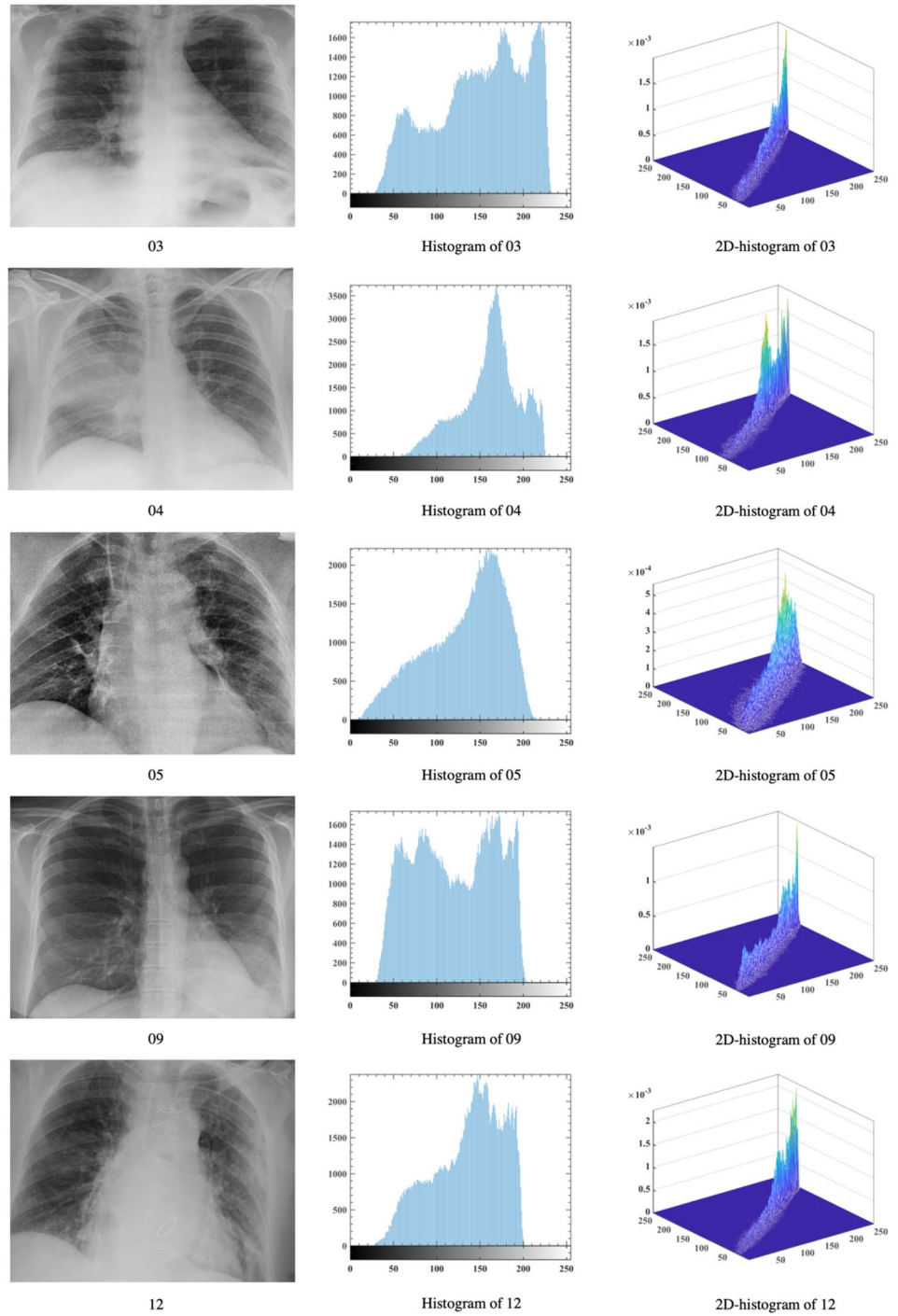
Fig. 20 (continued)
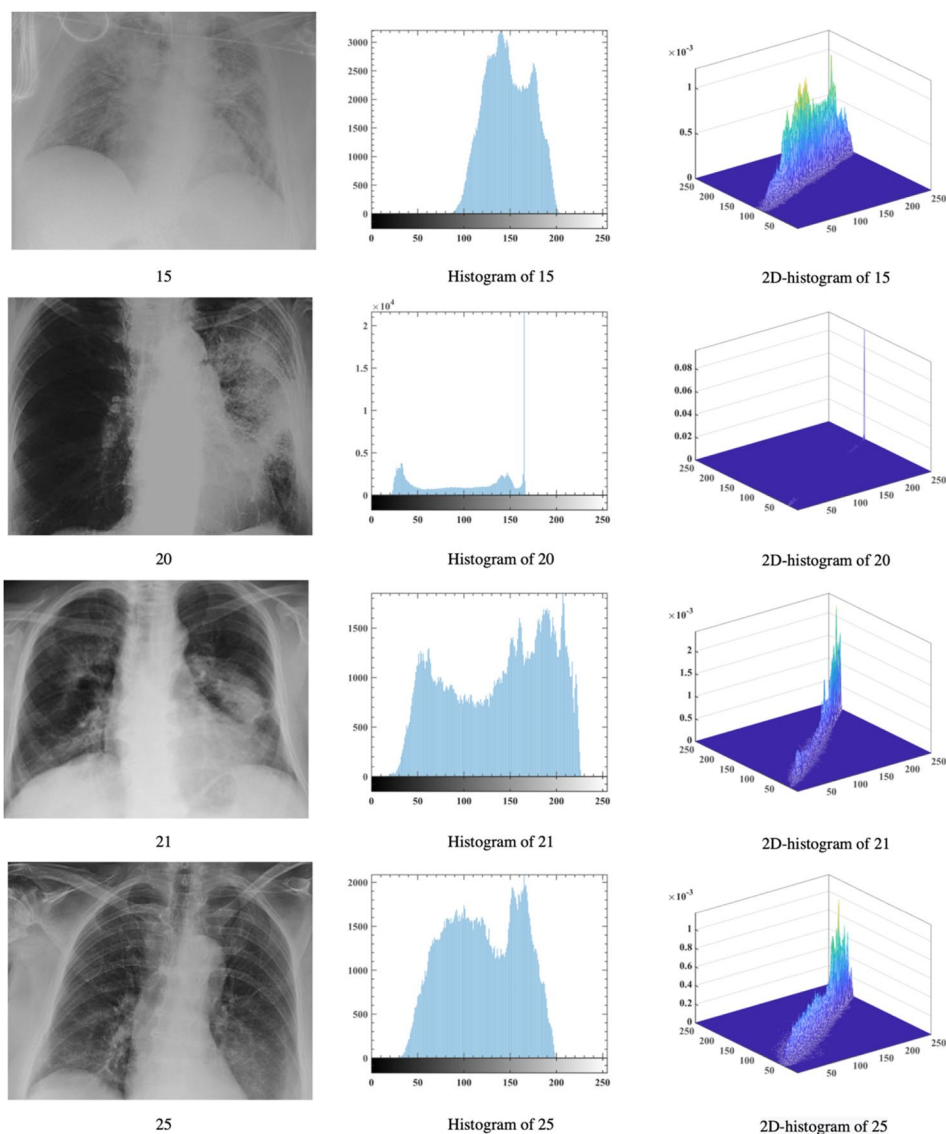
Availability of Data and Materials The data involved in this study are all public data, which can be downloaded through public channels.

Declarations

Conflict of interest The authors declare that there is no conflict of interests regarding the publication of article.

References

1. Yüce, M., Filiztekin, E., & Özkaya, K. G. (2021). COVID-19 diagnosis—A review of current methods. *Biosensors and Bioelectronics, 172*, 112752.

2. Elaziz, M. A., Ewees, A. A., Yousri, D., Alwerfali, H. S. N., Awad, Q. A., Lu, S., & Al-Qaness, M. A. A. (2020). An improved marine predators algorithm with fuzzy entropy for multi-level thresholding: Real world example of COVID-19 CT image segmentation. *IEEE Access, 8*, 125306–125330.

3. Feng, H, Liu, Y. J., Lv, M. L., & Zhong, J. Q. (2020). A case report of COVID-19 with false negative RT-PCR test: Necessity of chest CT. *Japanese Journal of Radiology, 38*(5), 409–410.

4. Ai, T., Yang, Z. L, Hou, H. Y., Zhan, C. N., Chen, C., Lv, W. Z., Tao, Q., Sun, Z. Y., & Xia, L. M. Correlation of chest CT and RT-PCR testing for coronavirus disease 2019 (COVID-19) in China: A report of 1014 cases. *Radiology, 296*(2), E32–E40.

5. American College of Radiology. *ACR recommendations for the use of chest radiography and computed tomography (CT) for suspected COVID-19 infection.* [cited March 2020]; Retrieved from https://www.acr.org/Advocacy-and-Economics/ACR-Position-Statements/Recommendations-for-Chest-Radiography-and-CT-for-Suspected-COVID19-Infection.

6. Jacobi, A., Chung, M., Bernheim, A., & Eber, C. (2020). Portable chest X-ray in coronavirus disease-19 (COVID-19): A pictorial review. *Clinical Imaging, 64*, 35–42.

7. Luo, G. Y., Yuan, Q., Li, J. L., Wang, S. G., & Yang, F. C. (2022). Artificial intelligence powered mobile networks: From cognition to decision. *IEEE Network, 36*(3), 136–144.

8. Zhang, J. Z., Zhu, C. Y., Zheng, L. T., & Xu, K. (2021). ROSEFusion: Random optimization for online dense reconstruction under fast camera motion. *ACM Transactions on Graphics (TOG), 40*(4), 1–17.

9. Li, C. Y., Dong, M. X., Li, J., Xu, G., Chen, X. B., Liu, W., & Ota, K. (2022). Efficient medical big data management with keyword-searchable encryption in healthchain. *IEEE Systems Journal*. https://doi.org/10.1109/JSYST.2022.3173538

10. Zhang, M., Chen, Y., & Lin, J. (2021). A privacy-preserving optimization of neighborhood-based recommendation for medical-aided diagnosis and treatment. *IEEE Internet of Things Journal, 8*(13), 10830–10842.

11. Liu, S., Yang, B., Wang, Y., Tian, J. W., Yin, L. R., & Zheng, W. F. (2022). 2D/3D multimode medical image registration based on normalized cross-correlation. *Applied Sciences, 12*(6), 2828.

12. Pal, N. R., & Pal, S. K. (1993). A review on image segmentation techniques. *Pattern Recognition, 26*(9), 1277–1294.

13. Chakraborty, S., Saha, A. K., Nama, S., & Debnath, S. (2021). COVID-19 X-ray image segmentation by modified whale optimization algorithm with population reduction. *Computers in Biology and Medicine, 139*, 104984.

14. Ray, S., Das, A., Dhal, K. G., Galvez, J., & Naskar, P. K. (2022). Whale optimizer-based clustering for breast histopathology image segmentation. *International Journal of Swarm Intelligence Research, 13*(1), 1–29.

15. Houssein, E. H., Emam, M. M., & Ali, A. A. (2021). An efficient multilevel thresholding segmentation method for thermography breast cancer imaging based on improved chimp optimization algorithm. *Expert Systems with Applications, 185*, 115651.

16. Choudhury, A., Samanta, S., Pratihar, S., & Bandyopadhyay, O. (2022). Multilevel segmentation of Hippocampus images using global steered quantum inspired firefly algorithm. *Applied Intelligence, 52*(7), 7339–7372.

17. Zhang, Q., Wang, Z. Y., Heidari, A. A., Gui, W. Y., Shao, Q. K., Chen, H. L., Zaguia, A., Turabieh, H., & Chen, M. Y. (2021). Gaussian Barebone Salp swarm algorithm with stochastic fractal Search for medical image segmentation: A COVID-19 case study. *Computers in Biology and Medicine, 139*, 31.

18. Liu, L., Zhao, D., Yu, F. H., Heidari, A. A., Li, C. Y., Ouyang, J. S., Chen, H. L., Mafarja, M., Turabieh, H., & Pan, J. Y. (2021). Ant colony optimization with Cauchy and greedy Levy mutations for multilevel COVID 19 X-ray image segmentation. *Computers in Biology and Medicine, 136*, 38.

19. Abdel-Basset, M., Chang, V., & Mohamed, R. (2020). HSMA_WOA: A hybrid novel Slime mould algorithm with whale optimization algorithm for tackling the image segmentation problem of chest X-ray images. *Applied Soft Computing, 95*, 19.

20. Abdel-Basset, M., Mohamed, R., Elhoseny, M., Chakrabortty, R. K., & Ryan, M. (2020). A hybrid COVID-19 detection model using an improved marine predators algorithm and a ranking-based diversity reduction strategy. *IEEE Access, 8*, 79521–79540.

21. Zhao, D., Liu, L., Yu, F. H., Heidari, A. A., Wang, M. J., Oliva, D., Muhammad, K., & Chen, H. L. (2021). Ant colony optimization with horizontal and vertical crossover search: Fundamental visions for multi-threshold image segmentation. *Expert Systems with Applications, 167*, 114122.

22. Zhao, D., Liu, L., Yu, F. H., Heidari, A. A., Wang, M. J., Liang, G. X., Muhammad, K., & Chen, H. L. (2021). Chaotic random spare ant colony optimization for multi-threshold image segmentation of 2D Kapur entropy. *Knowledge-Based Systems, 216*, 106510.

23. Su, H., Zhao, D., Yu, F. H., Heidari, A. A., Zhang, Y., Chen, H. L., Li, C. Y., Pan, J. Y, & Quan, S. C. (2022). Horizontal and vertical search artificial bee colony for image segmentation of COVID-19 X-ray images. *Computers in Biology and Medicine, 142*, 105181.

24. Horowitz, S. L., & Pavlidis, T. (1974). Picture segmentation by a directed split-and-merge procedure. proc ijcpr copenhagen.

25. Ridler, T. W., & Calvard, S. (1978). Picture thresholding using an iterative selection method. *IEEE Transactions on Systems Man and Cybernetics, 8*(8), 630–632.

26. Otsu, N. (1979). A threshold selection method from gray-level histograms. *IEEE Transactions on Systems, Man, and Cybernetics, 9*(1), 62–66.

27. Wong, A. K. C., & Sahoo, P. K. (1989). A gray-level threshold selection method based on maximum entropy principle. *Systems Man & Cybernetics IEEE Transactions on, 19*(4), 866–871.

28. Kapur, J. N., Sahoo, P. K., & Wong, A. K. C. (1985). A new method for gray-level picture thresholding using the entropy of the histogram. *Computer Vision, Graphics, and Image Processing, 29*, 273–285.

29. Peleg, S. (1980). A new probabilistic relaxation scheme. *IEEE Transactions on Pattern Analysis and Machine Intelligence, PAMI-2*(4), 362–369.

30. Derin, H., & Elliott, H. (1987). Modeling and segmentation of noisy and textured images using Gibbs random fields. *IEEE Transactions on Pattern Analysis and Machine Intelligence, PAMI-9*(1), 39–55.

31. Pao & Yohhan. (1989). Adaptive pattern recognition and neural networks United States.

32. Hoffman, R., & Jain, A. K. (1987). Segmentation and classification of range images. *IEEE Transactions on Pattern Analysis & Machine Intelligence, PAMI-9*, 608–620.

33. Rimey, R. D., & Cohen, F. S. (1988). A maximum-likelihood approach to segmenting range data. *IEEE Journal on Robotics & Automation, 4*(3), 277–286.

34. Overheim, R. D., & Wagner D. L. (1982). Light and color. New York

35. Reichenbach, S. E., Park, S. K., Alter-Gartenberg, R. (1990). Optimal small kernels for edge detection. In: Pattern recognition, 1990. Proceedings., 10th international conference on.

36. Bezdek, J. C., & Pal, S. K. (1992). Fuzzy models for pattern recognition: methods that search for structures in data. IEEE.

37. Pham, D. L., Xu, X., & Prince, J. L. (2000). Current methods in medical image segmentation. *Annual Review of Biomedical Engineering., 2*(1), 315–315.

38. Rosenfeld, A., & Torre, P. D. L. (1983). Histogram concavity analysis as an aid in threshold selection. *IEEE Transactions on Systems, Man, and Cybernetics., SMC-13*(2), 231–235.

39. Sezan, M. I. (1990). A peak detection algorithm and its application to histogram-based image data reduction. *Computer Vision, Graphics, and Image Processing, 49*(1), 36–51.

40. Yanni, M. K., & Horne, E. (1994). *A new approach to dynamic thresholding*. Boston: ScienceOpen Inc.

41. Hertz, L., & Schafer, R. W. (1988). Multilevel thresholding using edge matching. *Computer Vision, Graphics, and Image Processing, 44*(3), 279–295.

42. Rosenfeld, A. (1984). The fuzzy geometry of image subsets. *Pattern Recognition Letters, 2*(5), 311–317.

43. Kosko, B. (1986). Fuzzy entropy and conditioning. *Information Sciences, 40*(2), 165–174.

44. Tsai, W.-H. (1985). Moment-preserving thresolding: A new approach. *Computer Vision, Graphics, and Image Processing, 29*(3), 377–393.

45. Mirjalili, S., Mirjalili, S. M., & Hatamlou, A. (2016). Multi-verse optimizer: A nature-inspired algorithm for global optimization. *Neural Computing and Applications, 27*(2), 495–513.

46. Mirjalili, S., Dong, J. S., & Lewis, A. (2019). *Nature-inspired optimizers: Theories, literature reviews and applications* (Vol. 811). Berlin: Springer.

47. Heidari, A. A., Mirjalili, S., Faris, H., Aljarah, I., Mafarja, M., & Chen, H. L (2019). Harris hawks optimization: Algorithm and applications. *Future Generation Computer Systems-the International Journal of eScience, 97*, 849–872.

48. Lin, Y., Song, H., Ke, F., Yan, W. Z., Liu, Z. K., & Cai, F. M. (2022). Optimal caching scheme in D2D networks with multiple robot helpers. *Computer Communications, 181*, 132–142.

49. Yang, Y. T., Chen, H. L., Heidari, A. A., & Gandomi, A. H. (2021). Hunger games search: Visions, conception, implementation, deep analysis, perspectives, and towards performance shifts. *Expert Systems with Applications, 177*, 114864.

50. Tu, J. Z., Chen, H. L., Wang, M. J., & Gandomi, A. H. (2021). The colony predation algorithm. *Journal of Bionic Engineering, 18*(3), 674–710.

51. Li, S. M., Chen, H. L., Wang, M. J., Heidari, A. A., & Mirjalili, S. (2020). Slime mould algorithm: A new method for stochastic optimization. *Future Generation Computer Systems, 111*, 300–323.

52. Ahmadianfar, I., Asghar Heidari, A., Noshadian, S., Chen, H. L., & Gandomi, A. H. (2022). INFO: an efficient optimization algorithm based on weighted mean of vectors. *Expert Systems with Applications, 195*, 116516.

53. Ahmadianfar, I., Asghar Heidari, A., Gandomi, A. H., Chu, X. F., & Chen, H. L. (2021). RUN beyond the metaphor: an efficient optimization algorithm based on Runge–Kutta method. *Expert Systems with Applications, 181*, 115079.

54. Hussien, A. G., Heidari, A. A., Ye, X. J., Liang, G. X., Chen, H. L., & Pan, Z. F. (2022). Boosting whale optimization with evolution strategy and Gaussian random walks: an image segmentation method. *Engineering with Computers.* https://doi.org/10.1007/s00366-021-01542-0

55. Yu, H. L., Song, J. M., Chen, C. C., Heidari, A. A., Liu, J. W., Chen, H. L., Zaguia, A., & Mafarja, M. (2022). Image segmentation of Leaf Spot Diseases on Maize using multi-stage Cauchy-enabled grey wolf algorithm. *Engineering Applications of Artificial Intelligence, 109*, 104653.

56. Chen, H. L., Yang, B., Wang, S. J., Wang, G., Liu, D. Y., Li, H. Z., & Liu, W. B. (2014). Towards an optimal support vector machine classifier using a parallel particle swarm optimization strategy. *Applied Mathematics and Computation, 239*, 180–197.

57. Dong, R. Y., Chen, H. L., Heidari, A. A., Turabieh, H., Mafarja, M., & Wang, S. S. (2021). Boosted kernel search: Framework, analysis and case studies on the economic emission dispatch problem. *Knowledge-Based Systems, 233*, 107529.

58. Xia, J. F., Wang, Z. F., Yang, D. Q., Li, R. Z., Liang, G. X., Chen, H. L., Heidari, A. A., Turabieh, H., Mafarja, M., & Pan, Z. F. (2022). Performance optimization of support vector machine with oppositional grasshopper optimization for acute appendicitis diagnosis. *Computers in Biology and Medicine, 143*, 105206.

59. Xia, J. F., Yang, D. Q., Zhou, H., Chen, Y. Y., Zhang, H. L., Liu, T., Heidari, A. A., Chen, H. L., & Pan, Z. F. (2022). Evolving kernel extreme learning machine for medical diagnosis via a disperse foraging sine cosine algorithm. *Computers in Biology and Medicine, 141*, 105137.

60. Han, X., Han, Y. Y., Chen, Q. D., Li, J. Q., Sang, H. Y., Liu, Y. P., Pan, Q. K., & Nojima, Y. (2021). Distributed flow shop scheduling with sequence-dependent setup times using an improved iterated greedy algorithm. *Complex System Modeling and Simulation, 1*(3), 198–217.

61. Gao, D., Wang, G.-G., & Pedrycz, W. (2020). Solving fuzzy job-shop scheduling problem using DE algorithm improved by a selection mechanism. *IEEE Transactions on Fuzzy Systems, 28*(12), 3265–3275.

62. Wang, G.-G., Gao, D., & Pedrycz, W. (2022). Solving multi-objective fuzzy job-shop scheduling problem by a hybrid adaptive differential evolution algorithm. *IEEE Transactions on Industrial Informatics, 18*, 8519–8528.

63. Yu, H. L., Cheng, X. H., Chen, C. C., Heidari, A. A., Liu, J. W., Cai, Z. N., & Chen, H. L. (2022). Apple leaf disease recognition method with improved residual network. *Multimedia Tools and Applications, 81*, 7759–7782.

64. Chen, H. L., Wang, M. J., & Zhao, X. H. (2020). A multi-strategy enhanced sine cosine algorithm for global optimization and constrained practical engineering problems. *Applied Mathematics and Computation, 369*, 124872.

65. Yu, H. L., Qiao, S. M., Heidari, A. A., Bi, C. G., & Chen, H. L. (2022). Individual disturbance and attraction repulsion strategy enhanced seagull optimization for engineering design. *Mathematics, 10*(2), 276.

66. Ye, X. J., Liu, W., Li, H., Wang, M. J., Chi, C., Liang, G. X., Chen, H. L., & Huang, H. L. (2021). Modified whale optimization algorithm for solar cell and PV module parameter identification. *Complexity, 2021*, 8878686.

67. Hu, J., Chen, H. L., Heidari, A. A., Wang, M. J., Zhang, X. Q., Chen, Y., & Pan, Z. F. (2021). Orthogonal learning covariance matrix for defects of grey wolf optimizer: Insights, balance, diversity, and feature selection. *Knowledge-Based Systems, 213*, 106684.

68. Hu, J., Gui, W. Y., Heidari, A. A., Cai, Z. N., Liang, G. X., Chen, H. L., & Pan, Z. F. (2022). Dispersed foraging slime mould algorithm: Continuous and binary variants for global optimization and wrapper-based feature selection. *Knowledge-Based Systems, 237*, 107761.

69. Cai, Z. N., Gu, J. H., Luo, J., Zhang, Q., Chen, H. L., Pan, Z. F., Li, Y. P., & Li, C. Y. (2019). Evolving an optimal kernel extreme learning machine by using an enhanced grey wolf optimization strategy. *Expert Systems with Applications, 138*, 112814.

70. Xu, Y. T., Chen, H. L., Heidari, A. A., Luo, J., Zhang, Q., Zhao, X. H., & Li, C. Y. (2019). An efficient chaotic mutative moth-flame-inspired optimizer for global optimization tasks. *Expert Systems with Applications, 129*, 135–155.

71. Wu, S.-H., Zhan, Z.-H., & Zhang, J. (2021). SAFE: Scale-adaptive fitness evaluation method for expensive optimization problems. *IEEE Transactions on Evolutionary Computation, 25*(3), 478–491.

72. Li, J. Y., Zhan, Z. H., Wang, C., Jin, H., & Zhang, J. (2020). Boosting data-driven evolutionary algorithm with localized data generation. *IEEE Transactions on Evolutionary Computation, 24*(5), 923–937.

73. Zhao, F. Q., Di, S. L., Cao, J., Tang, J. X., & Jonrinaldi, J. (2021). A novel cooperative multi-stage hyper-heuristic for combination optimization problems. *Complex System Modeling and Simulation, 1*(2), 91–108.

74. Deng, W., Zhang, X. X., Zhou, Y. Q., Liu, Y., Zhou, X. B., Chen, H. L., & Zhao, H. M. (2022). An enhanced fast non-dominated solution sorting genetic algorithm for multi-objective problems. *Information Sciences, 585*, 441–453.

75. Hua, Y. C., Liu, Q. Q., Hao, K. G., & Jin, Y. C. (2021). A survey of evolutionary algorithms for multi-objective optimization problems with irregular Pareto fronts. *IEEE/CAA Journal of Automatica Sinica, 8*(2), 303–318.

76. Li, H. B., Zheng, G., Sun, K. J., Jiang, Z. C., Li, Y., & Jia, H. M. (2020). A logistic chaotic barnacles mating optimizer with Masi entropy for color image multilevel thresholding segmentation. *IEEE Access, 8*, 213130–213153.

77. Li, K., & Tan, Z. (2019). An improved flower pollination optimizer algorithm for multilevel image thresholding. *IEEE Access, 7*, 165571–165582.

78. Li, J. Y., Zhao, Y. D., Li, J. H., & Liu, X. J. (2015). Artificial bee colony optimizer with bee-to-bee communication and multipopulation coevolution for multilevel threshold image segmentation. *Mathematical Problems in Engineering, 2015*, 272947.

79. Li, L. G., Sun, L. J., Xue, Y., Li, S. J., Huang, X. W., & Mansour, R. (2021). Fuzzy multilevel image thresholding based on improved coyote optimization algorithm. *IEEE Access, 9*, 33595–33607.

80. Houssein, E. H., Emam, M. M., & Ali, A. A. (2021). Improved manta ray foraging optimization for multi-level thresholding using COVID-19 CT images. *Neural Computing and Applications, 33*(24), 16899–16919.

81. Khairuzzaman, A. K. M., & Chaudhury, S. (2017). Multilevel thresholding using grey wolf optimizer for image segmentation. *Expert Systems with Applications, 86*, 64–76.

82. Akay, B. (2013). A study on particle swarm optimization and artificial bee colony algorithms for multilevel thresholding. *Applied Soft Computing, 13*(6), 3066–3091.

83. Bhandari, A. K., et al. (2014). Cuckoo search algorithm and wind driven optimization based study of satellite image segmentation for multilevel thresholding using Kapur's entropy. *Expert Systems with Applications, 41*(7), 3538–3560.

84. Bhandari, A. K., Kumar, A., & Singh, G. K. (2015). Modified artificial bee colony based computationally efficient multilevel thresholding for satellite image segmentation using Kapur's, Otsu and Tsallis functions. *Expert Systems with Applications, 42*(3), 1573–1601.

85. Faris, H., Aljarah, I., & Mirjalili, S. (2016). Training feedforward neural networks using multi-verse optimizer for binary classification problems. *Applied Intelligence, 45*(2), 322–332.

86. Faris, H., Hassonah, M. A., Al-Zoubi, A. M., Mirjalili, S., & Aljarah, I. (2017). A multi-verse optimizer approach for feature selection and optimizing SVM parameters based on a robust system architecture. *Neural Computing and Applications, 30*(8), 2355–2369.

87. Ewees, A. A., El Aziz, M. A., & Hassanien, A. E. (2019). Chaotic multi-verse optimizer-based feature selection. *Neural Computing and Applications, 31*(4), 991–1006.

88. Mirjalili, S., Jangir, P., Mirjalili, S. Z., Saremi, S., & Trivedi, I. N. (2017). Optimization of problems with multiple objectives using the multi-verse optimization algorithm. *Knowledge-Based Systems, 134*, 50–71.

89. Fathy, A., & Rezk, H. (2018). Multi-verse optimizer for identifying the optimal parameters of PEMFC model. *Energy, 143*, 634–644.

90. Yilmaz, O., Altun, A. A., & Koklu, M. (2022). A new hybrid algorithm based on MVO and SA for function optimization. *International Journal of Industrial Engineering Computations, 13*(2), 237–254.

91. Shukri, S. E., Al-Sayyed, R., Hudaib, A., & Mirjalili, S. (2021). Enhanced multi-verse optimizer for task scheduling in cloud computing environments. *Expert Systems with Applications, 168*, 10.

92. Pothiraj, S., Kadambarajan, J. P., & Kadarkarai, P. (2021). Floor planning of 3D IC design using hybrid multi-verse optimizer. *Wireless Personal Communications, 118*(4), 3007–3023.

93. Wu, G., Mallipeddi, R., Suganthan, P. (2016) Problem definitions and evaluation criteria for the CEC 2017 competition and special session on constrained single objective real-parameter optimization

94. Derrac, J., Garcia, S., Molina, D., & Herrera, F. (2011). A practical tutorial on the use of nonparametric statistical tests as a methodology for comparing evolutionary and swarm intelligence algorithms. *Swarm and Evolutionary Computation, 1*(1), 3–18.

95. Alcala-Fdez, J., Sanchez, L., Garcia, S., del Jesus, M. J., Ventura, S., Garrell, J. M., Otero, J., Romero, C., Bacardit, J., Rivas, V. M., Fernandez, J. C., & Herrera, F. (2009). KEEL: A software tool to assess evolutionary algorithms for data mining problems. *Soft Computing, 13*(3), 307–318.

96. Huynh-Thu, Q., & Ghanbari, M. (2008). Scope of validity of PSNR in image/video quality assessment. *Electronics Letters, 44*(13), 800–U35.

97. Wang, Z., Bovik, A. C., Sheikh, H. R., & Simoncelli, E. P. (2004). Image quality assessment: From error visibility to structural similarity. *IEEE Transactions on Image Processing, 13*(4), 600–612.

98. Zhang, L., Zhang, L., Mou, X. Q., & Zhang, D. (2011). FSIM: A feature similarity index for image quality assessment. *IEEE Transactions on Image Processing, 20*(8), 2378–2386.

99. Weszka, J. S., & Rosenfeld, A. (1979). Histogram modification for threshold selection. *IEEE Transactions on Systems, Man, and Cybernetics, 9*(1), 38–52.

100. Ahuja, N., & Rosenfeld, A. (1978). A note on the use of second-order gray-level statistics for threshold selection. *IEEE Transactions on Systems, Man, and Cybernetics, 8*(12), 895–898.

101. Panda, & Rosenfeld. (1978). Image segmentation by pixel classification in (gray level, edge value) space. *IEEE Transactions on Computers, C–27*(9), 875–879.

102. Pun, T. (1980). A new method for grey-level picture thresholding using the entropy of the histogram. *Signal Processing, 2*(3), 223–237.

103. Buades, A., Coll, B., & Morel, J. A non-local algorithm for image denoising. In: 2005 IEEE computer society conference on computer vision and pattern recognition (CVPR'05). 2005.

104. Liu, Y., Tian, J. W., Hu, R. R., Yang, B., Liu, S., Yin, L. R., & Zheng, W. F. (2022). Improved feature point pair purification algorithm based on SIFT during endoscope image stitching. *Frontiers in Neurorobotics*. https://doi.org/10.3389/fnbot.2022.840594

105. Cao, Z. Y., Wang, Y. X., Zheng, W. F., Yin, L. R., Tang, Y. S., Miao, W., Liu, S., & Yang, B. (2022). The algorithm of stereo vision and shape from shading based on endoscope imaging. *Biomedical Signal Processing and Control, 76*, 103658.

106. Zhang, Z. Y., Wang, L. X., Zheng, W. F., Yin, L. R., Hu, R. R., & Yang, B. (2022). Endoscope image mosaic based on pyramid ORB. *Biomedical Signal Processing and Control, 71*, 103261.

107. Rosenbrock, H. H. (1960). An automatic method for finding the greatest or least value of a function. *The Computer Journal, 3*(3), 175–184.

108. Kang, F., Li, J., & Ma, Z. (2011). Rosenbrock artificial bee colony algorithm for accurate global optimization of numerical functions. *Information Sciences, 181*(16), 3508–3531.

109. Li, C. Y., Li, J., Chen, H. L., Jin, M., & Ren, H. (2021). Enhanced Harris hawks optimization with multi-strategy for global optimization tasks. *Expert Systems with Applications, 185*, 30.

110. Witten, T. A., & Sander, L. M. (1983). Diffusion-limited aggregation. *Physical Review B, 27*(9), 5686–5697.

111. Salimi, H. (2015). Stochastic fractal search: A powerful metaheuristic algorithm. *Knowledge-Based Systems, 75*, 1–18.

112. Zhao, S. W., Wang, P. J., Heidari, A. A., Chen, H. L., Turabieh, H., Mafarja, M., & Li, C. Y. (2021). Multilevel threshold image segmentation with diffusion association slime mould algorithm and Renyi's entropy for chronic obstructive pulmonary disease. *Computers in Biology and Medicine, 134*, 104427.

113. Wang, W. C., Yuan, X. H., Wu, X. J., & Liu, Y. L. (2017). Fast image dehazing method based on linear transformation. *IEEE Transactions on Multimedia, 19*(6), 1142–1155.

114. Du, P., Wang, J. Z., Hao, Y., Niu, T., & Yang, W. D. (2019). A novel hybrid model based on multi-objective Harris hawks optimization algorithm for daily PM2.5 and PM10 forecasting. *Applied Soft Computing, 96*, 106620.

115. Liu, R. J., Wang, X. S., Lu, H. M., Wu, Z. H., Fan, Q., Li, S. X., & Jin, X. (2021). SCCGAN: Style and Characters Inpainting Based on CGAN. *Mobile Networks and Applications, 26*(1), 3–12.

116. Liu, K. Q., Ke, F., Huang, X., Yu, R., Lin, F., Wu, Y. Q., & Ng, D. W. K. (2021). DeepBAN: A temporal convolution-based communication framework for dynamic WBANs. *IEEE Transactions on Communications, 69*(10), 6675–6690.

117. Li, J., Xu, K., Chaudhuri, S., Yumer, E., Zhang, H., & Guibas, L. (2017). Grass: Generative recursive autoencoders for shape structures. *ACM Transactions on Graphics (TOG), 36*(4), 1–14.

118. Zhou, W. J., Yu, L., Zhou, Y., Qiu, W. W., Wu, M. W., & Luo, T. (2018). Local and global feature learning for blind quality evaluation of screen content and natural scene images. *IEEE Transactions on Image Processing, 27*(5), 2086–2095.

119. Zhou, Y., Li, L., & Ma, M. (2015). A novel hybrid bat algorithm for the multilevel thresholding medical image segmentation. *Journal of Medical Imaging and Health Informatics, 5*, 1742–1746.

120. Abd Elaziz, M., Nabil, N., Moghdani, R., Ewees, A. A., Cuevas, E., & Lu, S. (2021). Multilevel thresholding image segmentation based on improved volleyball premier league algorithm using whale optimization algorithm. *Multimedia Tools and Applications, 80*(8), 12435–12468.

121. Alwerfali, H. S. N., Elaziz, M. A., Al-Qaness, M. A. A., Abbasi, A. A., Lu, S., Liu, F., & Li, L. (2019). A multilevel image thresholding based on hybrid Salp swarm algorithm and fuzzy entropy. *IEEE Access, 7*, 181405–181422.

122. Cuevas, E., Zaldivar, D., & Pérez-Cisneros, M. (2010). A novel multi-threshold segmentation approach based on differential evolution optimization. *Expert Systems with Applications, 37*(7), 5265–5271.

123. Bao, X. L., Jia, H. M., & Lang, C. B. (2019). A novel hybrid Harris Hawks optimization for color image multilevel thresholding segmentation. *IEEE ACCESS, 7*, 76529–76546.

124. Liang, J. J., Qin, A. K., Suganthan, P. N., & Baskar, S. (2006). Comprehensive learning particle swarm optimizer for global optimization of multimodal functions. *IEEE Transactions on Evolutionary Computation, 10*(3), 281–295.

125. Abdollahzadeh, B., Gharehchopogh, F. S., & Mirjalili, S. (2021). African vultures optimization algorithm: A new nature-inspired metaheuristic algorithm for global optimization problems. *Computers & Industrial Engineering, 158*, 107408.

126. Qiu, S., Zhao, H. K., Jiang, N., Wang, Z. L., Liu, L., An, Y., Zhao, H. Y., Miao, X., Liu, R. C., & Fortino, G. (2022). Multi-sensor information fusion based on machine learning for real applications in human activity recognition: State-of-the-art and research challenges. *Information Fusion, 80*, 241–265.

127. Wu, Z. D., Li, R. C., Zhou, Z. F., Guo, J. F., Jiang, J. H., & Xu, X. N. (2020). A user sensitive subject protection approach for book search service. *Journal of the Association for Information Science and Technology, 71*(2), 183–195.

128. Wu, Z. D., Shen, S. G., Lian, X. Z., Su, X. N., & Chen, E. H. (2020). A dummy-based user privacy protection approach for text information retrieval. *Knowledge-Based Systems, 195*, 105679.

129. Wu, Z. D., Shen, S. G., Zhou, H. P., Li, H. X., Lu, C. L., & Zou, D. D. (2021). An effective approach for the protection of user commodity viewing privacy in e-commerce website. *Knowledge-Based Systems, 220*, 106952.

130. Cao, X., Wang, J., & Zeng, B. (2022). A study on the strong duality of second-order conic relaxation of AC optimal power flow in radial networks. *IEEE Transactions on Power Systems, 37*(1), 443–455.

131. Wu, Z. D., Li, G. L., Shen, S. G., Lian, X. Z., Chen, E. H., & Xu, G. D. (2021). Constructing dummy query sequences to protect location privacy and query privacy in location-based services. *World Wide Web, 24*(1), 25–49.

132. Wu, Z. D., Wang, R. Q., Li, Q., Lian, X. Z., Xu, G. D., Chen E. H., & Liu, X. Y. (2020). A location privacy-preserving system based on query range cover-up for location-based services. *IEEE Transactions on Vehicular Technology, 69*, 5244–5254.

133. Zhang, X. Q., Fan, C. X., Xiao, Z. H., Zhao, L., Chen, H. L., & Chang, X. (2022). Random reconstructed unpaired image-to-image translation. *IEEE Transactions on Industrial Informatics*. https://doi.org/10.1109/TII.2022.3160705

134. Hu, Z. Y., Wang, J., Zhang, C. F., Luo, Z. Z., Luo, X. Q., Xiao, L., & Shi, J. (2022). Uncertainty Modeling for Multicenter Autism Spectrum Disorder Classification Using Takagi–Sugeno–Kang Fuzzy Systems. *IEEE Transactions on Cognitive and Developmental Systems, 14*(2), 730–739.

135. Tian, Y., Su, X. C., Su, Y. S., & Zhang, X. Y. (2020). EMODMI: A multi-objective optimization based method to identify disease modules. *IEEE Transactions on Emerging Topics in Computational Intelligence, 5*(4), 570–582.

136. Su, Y. S., Li, S., Zheng, C. H., & Zhang, X. Y. (2019). A heuristic algorithm for identifying molecular signatures in cancer. *IEEE Transactions on NanoBioscience, 19*(1), 132–141.

137. Li, D., Zhang, S., & Ma, X. (2021). Dynamic module detection in temporal attributed networks of cancers. *IEEE/ACM Transactions on Computational Biology and Bioinformatics*. https://doi.org/10.1109/TCBB.2021.3069441

138. Ma, X., Sun, P. G., & Gong, M. (2020). An integrative framework of heterogeneous genomic data for cancer dynamic modules based on matrix decomposition. *IEEE/ACM Transactions on Computational Biology and Bioinformatics*. https://doi.org/10.1109/TCBB.2020.3004808

139. Yin, J. Y., Sun, W., Li, F. C., Hong, J. J, Li, X. X., Zhou, Y., Lu, Y. J., Liu, M. Z., Zhang, X., Chen, N., Jin, X. P., Xue, J., Zeng, S., Yu, L. S., & Zhu, F. (2020). VARIDT 1.0: variability of drug transporter database. *Nucleic Acids Research, 48*(D1), D1042–D1050.

140. Zhu, F., Shi, Z., Qin, C., Tao, L., Liu, X., Xu, F., Zhang, L., Song, Y., Liu, X. H., Zhang, J. X., Han, B. C., Zhang, P., & Chen, Y. Z. (2012). Therapeutic target database update 2012: A resource for facilitating target-oriented drug discovery. *Nucleic Acids Research, 40*(D1), D1128–D1136.